Worcester Polytechnic Institute
Digital WPI

Masters Theses (All Theses, All Years) | Electronic Theses and Dissertations

2003-04-28

Measurement of TOA Using Frequency Domain Techniques for Indoor Geolocation

Emad Dolatshahi Zand
Worcester Polytechnic Institute

Follow this and additional works at: https://digitalcommons.wpi.edu/etd-theses

Repository Citation
Zand, Emad Dolatshahi, "*Measurement of TOA Using Frequency Domain Techniques for Indoor Geolocation*" (2003). *Masters Theses (All Theses, All Years)*. 429.
https://digitalcommons.wpi.edu/etd-theses/429

This thesis is brought to you for free and open access by Digital WPI. It has been accepted for inclusion in Masters Theses (All Theses, All Years) by an authorized administrator of Digital WPI. For more information, please contact wpi-etd@wpi.edu.

Measurement of TOA Using Frequency Domain Techniques for Indoor Geolocation

A thesis submitted to the faculty

of the

Worcester Polytechnic Institute

in partial fulfillment of the requirements for the degree of

Master of Science

in

Electrical and Computer Engineering

by

EMAD D. ZAND

Emad Dolatshahi Zand

April 21, 2003

Approved:

Dr. Kaveh Pahlavan
Thesis Advisor

Dr. John Orr
ECE Department Head

To my parents

Abstract

Frequency domain techniques have been widely used in indoor radio propagation measurements and modeling for telecommunication applications. This work addresses measurement of the time of arrival (TOA) of the first path for geolocation applications using results of frequency domain channel measurements. First, we analyze the effect upon TOA measurement accuracy due to: sampling period of the radio channel in the frequency domain, sampling period in the time domain used for detection of the TOA and the windowing filter used before transformation to the time domain. Then, we provide some results of measurement made in line of sight (LOS) and Obstructed LOS (OLOS) indoor environments in order to compare the characteristics of the measured TOA in these two important scenarios for indoor geolocation applications. Finally, we compare the measurement results with the ray tracing based model that had been developed previously for indoor geolocation applications.

Acknowledgements

The author is profoundly indebted to Professor Kaveh Pahlavan for his guidance and encouragement in regard to this work and other technical and non-technical concerns.

The author is grateful to his WPI friend and fellow doctoral candidate Bardia Alavi, for his assistance with much of the measurement collection and general support. An extra special thanks is due to Dr. Jacques Beneat and Dr. Xinrong Li for numerous discussions, help and suggestions. Thanks to friend Obi Aghogho for help with the large block of measurements performed last summer.

I am extremely grateful to members of my thesis committee, Dr. Allen Levesque and Dr. Kevin Clements for their valuable comments and encouragements.

Thanks are due to all my professors at WPI through whom I have learn a lot. In particular, I would like to thank Prof. Whitmal, Prof. Novak and Prof. Sunar through whom I was able to extend my knowledge in related areas.

The writer takes this opportunity to express thanks to National Science Foundation that provided support for this research.

Words cannot express my thanks to my parents and my sister and brother who were responsible for enabling me in reaching this point of my life.

Table of Contents

Abstract iii
Acknowledgements iv
Table of Contents v
List of Figures vii
List of Tables xi
Chapter 1 Introduction 1
1.1 Background and Motivation 1
1.2 Contribution of the Thesis 5
1.3 Outline of the Thesis 5
Chapter 2 Measurement Systems 7
2.1 Introduction 7
2.2 Overview of Characterization of Multipath Fading Channels 7
2.3 Measurement Techniques 8
2.3.1 Time Domain Measurement Techniques 8
2.3.2 Frequency Domain Measurement Technique 9
2.4 Description of the Measurement System 9
2.5 Derivation of the Channel Impulse Response 12
2.5.1 Derivation of the Impulse Response Using the Chirp Z Algorithm 14
2.6 Filtering of Frequency Response by a Window 15
2.7 Distance Estimation Using Peak Detection Algorithm 16
Chapter 3 Parameters Affecting TOA Accuracy 18
3.1 Introduction 18
3.2 Effects of Frequency Distance in the Measurement (Δf) 19
3.3 Effects of Sampling in Time 26
3.3.1 Effects of Sampling Rate on Calibration 27
3.3.2 Combined Effects of Sampling Rate and Multipath 29
3.4 Effects of Filtering 32
Chapter 4 Analysis of Measurements in Different Sites 40
4.1 Introduction 40
4.2 Description of Measurement sites 43
4.3 LOS Measurements in AK 219 44
4.4 LOS Measurements in AK 311 47
4.5 LOS Measurements in the Undergraduate Lounge 49
4.6 LOS Measurements in AK 320 52
4.7 LOS Measurements in Norton Company (indoor to indoor) 54
4.8 OLOS measurements in Fuller Laboratories 57
4.8.1 Indoor to Indoor OLOS Measurements in Fuller Laboratories 60
4.8.2 Outdoor to Indoor OLOS Measurements in Fuller Laboratories 61
4.8.3 Outdoor to Floor OLOS Measurements in Fuller Laboratories 63
4.9 OLOS measurements in the WPI Guest House 65
4.9.1 Indoor to Indoor OLOS Measurements in the Guest House 67
4.9.2 Outdoor to Indoor OLOS Measurements in the Guest House 68
4.9.3 Outdoor to floor OLOS Measurements in the Guest House 70
4.10 OLOS measurements in Norton Company 72

4.10.1 Indoor to Indoor OLOS Measurements in Norton Company 73
4.10.2 Outdoor to Indoor OLOS Measurements in Norton Company..... 75
4.11 Comparative Performance in LOS and OLOS Environments 77
4.12 Comparison of Distance Error with Gaussian Model 82
Chapter 5 Summary and Future Work..... 85
5.1 Summary 85
5.2 Future work 87
Appendix A 88
Appendix B 92
References..... 97

List of Figures

Figure 1-1 A Functional Block Diagram of Wireless Geolocation Systems 2
Figure 1-2 Important Geolocation Parameters 3
Figure 2-1 Block Diagram of the Frequency Domain Measurement System 10
Figure 2-2 Sample Frequency and Time Response of a Radio Frequency Channel 11
Figure 2-3 Monopole Quarter Wave Antenna with Ground Plane for 1 GHz Center Frequency 11
Figure 2-4 Generating the Channel Impulse Response Using IDFT 13
Figure 2-5 (a) Channel Impulse Response Filtered by Hanning Window, (b) Channel Impulse Response Without Filtering (Rectangular Window) 15
Figure 2-6 (a) Channel Impulse Response, (b) Detection of Peaks Using Peak Detection Algorithm 17
Figure 3-1 Measurement Process 19
Figure 3-2 Frequency and Time Responses of Point 7 (P7) at Four Different Values of Δf. Solid Red Lines and Dashed Black Lines in the Time Responses Represent Expected and Detected First Paths, Respectively. 20
Figure 3-3 Illustration of Tc, Td and τ on a Channel Impulse Response 22
Figure 3-4 Effects of Sampling in Frequency Domain on (a) Variance of Distance Error and (b) Mean of Distance Error 23
Figure 3-5 Log of Variance of Error around Δf=1/Tc 24
Figure 3-6 CIR Generated with Δf=1/Tc 25
Figure 3-7 Effect of Quantization in Detecting the First Path 26
Figure 3-8 Configuration of 8 Points Used in Calibration Analysis 27
Figure 3-9 Effect of Δt 32
Figure 3-10 Frequency Response after Applying Rectangular Window for the Random Point in AK320 34
Figure 3-11 Time Response Using Rectangular Window for the Random Point in AK320 34
Figure 3-12Frequency Response after Applying Bartlett Window for the Random Point in AK320 35
Figure 3-13 Time Response Using Bartlett Window for the Random Point in AK320 35
Figure 3-14Frequency Response after Applying Hanning Window for the Random Point in AK320 36
Figure 3-15 Time Response Using Hanning Window for the Random Point in AK320 36
Figure 3-16Frequency Response after Applying Hamming Window for the Random Point in AK320 37
Figure 3-17 Time Response Using Hanning Window for the Random Point in AK320 37
Figure 3-18Frequency Responses of Rectangular (solid blue), Bartlett (dotted black), Hanning (dash dot green) and Hamming Windows (dashed red) 38
Figure 3-19Time Responses of Rectangular (solid blue), Bartlett (dotted black), Hanning (dash dot green) and Hamming Windows (dashed red) 38
Figure 4-1Channel Impulse Response for a LOS Case 41
Figure 4-2Channel Impulse Response for a OLOS Case 41
Figure 4-3Undetected Direct Path (UDP) 42
Figure 4-4Non-distinguishable Direct Path (NDDP) 43

Figure 4-5 Schematic of Measurement Site in AK 219 45
Figure 4-6 Complementary CDFs of the Actual Distance (solid black), the Absolute Value of Error Based on the TOA of the first path (dashed blue) and the Absolute Value of Error Based on the TOA of the Strongest Path (dotted red) in AK 219 46
Figure 4-7 Complementary CDFs of the Relative Received Power of the First Path (dashed blue) and the Relative Received Power of the Strongest Path (dotted red) in AK 219 46
Figure 4-8 Schematic of Measurement Site in AK 311 48
Figure 4-9 Complementary CDFs of the Actual Distance (solid black), the Absolute Value of Error Based on the TOA of the first path (dashed blue) and the Absolute Value of Error Based on the TOA of the Strongest Path (dotted red) in AK 311 48
Figure 4-10 Complementary CDFs of the Relative Received Power of the First Path (dashed blue) and the Relative Received Power of the Strongest Path (dotted red) in AK 311 49
Figure 4-11 Schematic of Measurement Site in Undergraduate Lounge of ECE Dept. ... 50
Figure 4-12 Complementary CDFs of the Actual Distance (solid black), the Absolute Value of Error Based on the TOA of the first path (dashed blue) and the Absolute Value of Error Based on the TOA of the Strongest Path (dotted red) in Undergraduate Lounge..... 51
Figure 4-13 Complementary CDFs of the Relative Received Power of the First Path (dashed blue) and the Relative Received Power of the Strongest Path (dotted red) in AK 311 51
Figure 4-14 Schematic of Measurement Site in AK 320 53
Figure 4-15 Complementary CDFs of the Actual Distance (solid black), the Absolute Value of Error Based on the TOA of the first path (dashed blue) and the Absolute Value of Error Based on the TOA of the the Strongest Path (dotted red) in AK 320 54
Figure 4-16 Complementary CDFs of the Relative Received Power of the First Path (dashed blue) and the Relative Received Power of the Strongest Path (dotted red) in AK 320 54
Figure 4-17 Schematic of Measurement Site in Norton Company (indoor to indoor) 56
Figure 4-18 Complementary CDFs of the Actual Distance (solid black), the Absolute Value of Error Based on the TOA of the first path (dashed blue) and the Absolute Value of Error Based on the TOA of the Strongest Path (dotted red) in Norton Company (indoor to indoor) 57
Figure 4-19 Complementary CDFs of the Relative Received Power of First Path (dashed blue) and the Relative Received Power of the Strongest Path (dotted red) in Norton Company (indoor to indoor) 57
Figure 4-20 Schematic of Measurement Site in Fuller Laboratories. (a) shows indoor to indoor and outdoor to indoor cases.(b) shows outdoor to floor scenario..... 59
Figure 4-21 Complementary CDFs of the Actual Distance (solid black), the Absolute Value of Error Based on the TOA of the first path (dashed blue) and the Absolute Value of Error Based on the TOA of the Strongest Path (dotted red) in Fuller Laboratories (indoor to indoor)..... 61

Figure 4-22 Complementary CDFs of the Relative Received Power of the First Path (dashed blue) and the Relative Received Power of the Strongest Path (dotted red) in Fuller Laboratories (indoor to indoor) 61
Figure 4-23 Complementary CDFs of the Actual Distance (solid black), the Absolute Value of Error Based on the TOA of the first path (dashed blue) and the Absolute Value of Error Based on the TOA of the Strongest Path (dotted red) in Fuller Laboratories (outdoor to indoor)..... 63
Figure 4-24 Complementary CDFs of the Relative Received Power of the First Path (dashed blue) and the Relative Received Power of the Strongest Path (dotted red) in Fuller Laboratories (outdoor to indoor) 63
Figure 4-25 Complementary CDFs of the Actual Distance (solid black), the Absolute Value of Error Based on the TOA of the first path (dashed blue) and the Absolute Value of Error Based on the TOA of the Strongest Path (dotted red) in Fuller Laboratories (outdoor to floor) 65
Figure 4-26 Complementary CDFs of Relative Received Power of the First Path (dashed blue) and the Relative Received Power of the Strongest Path (dotted red) in Fuller Laboratories (outdoor to floor) 65
Figure 4-27 Schematic of Measurement Site in WPI Guest House. (a) shows indoor to indoor and outdoor to indoor cases.(b) shows outdoor to floor scenario..... 66
Figure 4-28 Complementary CDFs of the Actual Distance (solid black), the Absolute Value of Error Based on the TOA of the first path (dashed blue) and the Absolute Value of Error Based on the TOA of the Strongest Path (dotted red) in the Guest House (indoor to indoor)..... 68
Figure 4-29 Complementary CDFs of the Relative Received Power of the First Path (dashed blue) and the Relative Received Power of the Strongest Path (dotted red) in the Guest House (indoor to indoor) 68
Figure 4-30 Complementary CDFs of the Actual Distance (solid black), the Absolute Value of Error Based on the TOA of the first path (dashed blue) and the Absolute Value of Error Based on the TOA of the Strongest Path (dotted red) in the Guest House (outdoor to indoor)..... 69
Figure 4-31 Complementary CDFs of the Relative Received Power of First Path (dashed blue) and the Relative Received Power of the Strongest Path (dotted red) in the Guest House (outdoor to indoor) 70
Figure 4-32 Complementary CDFs of the Actual Distance (solid black), the Absolute Value of Error Based on the TOA of the first path (dashed blue) and the Absolute Value of Error Based on the TOA of the Strongest Path (dotted red) in the Guest House (outdoor to floor) 71
Figure 4-33 Complementary CDFs of the Relative Received Power of the First Path (dashed blue) and the Relative Received Power of the Strongest Path (dotted red) in the Guest House (outdoor to floor) 72
Figure 4-34 Schematic of Measurement Site in Norton Company (indoor to indoor and outdoor to indoor) 73
Figure 4-35 Complementary CDFs of the Actual Distance (solid black), the Absolute Value of Error Based on the TOA of the first path (dashed blue) and the Absolute Value of Error Based on the TOA of the Strongest Path (dotted red) in Norton Company (indoor to indoor) 74

Figure 4-36 Complementary CDFs of the Relative Received Power of the First Path (dashed blue) and the Relative Received Power of the Strongest Path (dotted red) in Norton Company (indoor to indoor) 75
Figure 4-37 Complementary CDFs of the Actual Distance (solid black), the Absolute Value of Error Based on the TOA of the first path (dashed blue) and the Absolute Value of Error Based on the TOA of the Strongest Path (dotted red) in Norton Company (outdoor to indoor) 76
Figure 4-38 Complementary CDFs of the Relative Received Power of the First Path (dashed blue) and the Relative Received Power of the Strongest Path (dotted red) in Norton Company (outdoor to indoor) 77
Figure 4-39 Comparison of Complementary CDFs of the Distance Error Based on the TOA of the First Path for LOS (dashed blue) and OLOS (dotted red) 78
Figure 4-40 Comparison of Complementary CDF of the Distance Error Based on the TOA of the Strongest Path for LOS (dashed blue) and OLOS (dotted red) 79
Figure 4-41 Comparison of Complementary CDFs of Distance Error Based on the TOA of the First Path for LOS (dashed blue), DDP (dotted red) and UDP (solid black) . 81
Figure 4-42 Comparison of Complementary CDFs of the Distance Error Based on the TOA of the Strongest Path for LOS (dashed blue), DDP (dotted red) and UDP (solid black) 81
Figure 4-43 Comparison Between Complementary CDFs of the Distance Error for LOS Measurements and the Model 82
Figure 4-44 Comparison Between Complementary CDFs of the Distance Error for OLOS Measurements and the Model 83
Figure 4-45 Comparison Between Complementary CDFs of the Distance Error for DDP Measurements and the Model 84

List of Tables

Table 1 Comparison of Performance Measures for Telecommunications..... 4
Table 2 Calibration Parameters for Point 1..... 28
Table 3 Errors in Estimation of TOA for Points Shown in Fig. 3-8..... 28
Table 4 Errors in Estimation of TOA Due to Multipath and Hand Measurement for Points Shown in Fig. 3-8..... 29
Table 5 Errors in Estimation of TOA for the Collection of Points in AK 219..... 30
Table 6 Results of Measurement for the Random Point in AK320..... 33
Table 7 Results of Measurement for a Collection of 32 Points at the Third Floor of Atwater Kent Laboratories for Four Different Types of Filters..... 39
Table 8 Measurement Results in AK 219..... 45
Table 9 Measurement Results in AK 311..... 48
Table 10 Measurement Results in Undergraduate Lounge..... 50
Table 11 Measurement Results in AK 320..... 53
Table 12 Measurement Results in Norton Company (indoor to indoor)..... 56
Table 13 Measurement Results in Fuller Laboratories (indoor to indoor)..... 60
Table 14 Measurement Results in Fuller Laboratories (outdoor to indoor)..... 62
Table 15 Measurement Results in Fuller Laboratories (outdoor to floor)..... 64
Table 16 Measurement Results in the Guest House (indoor to indoor)..... 67
Table 17 Measurement Results in the Guest House (outdoor to indoor)..... 69
Table 18 Measurement Results in the Guest House (outdoor to floor)..... 71
Table 19 Measurement Results in Norton Company (indoor to indoor)..... 74
Table 20 Measurement Results in Norton Company (outdoor to indoor)..... 76
Table 21 Mean and Variance of Distance Error for Different Scenarios..... 86
Table 22 Comparisons between the Measurement Results and the Model..... 87
Table 23 Measurement database filename strings description..... 92

Chapter 1 Introduction

1.1 Background and Motivation

Geolocation, position location and radiolocation are terms that are widely used these days to indicate the process of determining the location of a mobile station [1]. Location finding systems for indoor areas is an emerging technology that has become very important in recent years. The applications of these systems range from commercial and public safety uses to military purposes. In commercial applications for industrial areas, there is a need to locate in-demand portable equipments while for residential areas there is a great demand to keep track of people with special needs such as the elderly and children. In public safety and military applications, indoor geolocation systems are needed to find the position of policemen, fire fighters or soldiers inside a building. All these new applications involve defining the location in an indoor area where traditional GPS systems are not suitable due to the harsh multipath environment. Fig. 1-1 illustrates the functional block diagram of a wireless geolocation system. The main parts of these systems are a location-sensing block, positioning algorithm and display system. The location-sensing block measures metrics related to the position of the mobile station relative to a known reference point. These metrics could be angle of arrival (AOA) in direction-based systems while time of arrival (TOA), received signal strength (RSS), or carrier signal phase of arrival (POA) might be the metrics in distance-based systems. The positioning algorithm calculates the coordinates of the mobile station using these metrics. The poorer the accuracy of the metrics, the more complex the positioning algorithm are

required. The display could be software on a private PC or software on a LAN or a universally accessible service on the web [2].

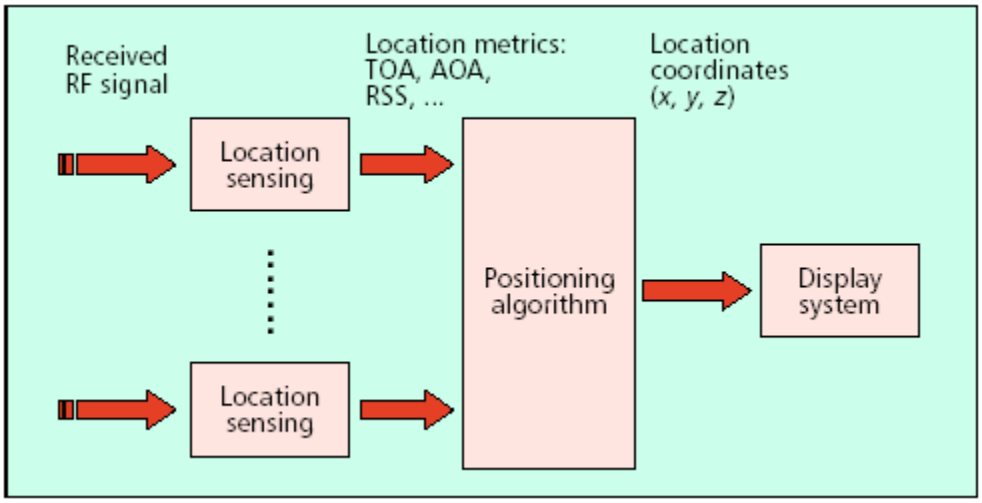

Figure 1-1 A Functional Block Diagram of Wireless Geolocation Systems

The wideband models and measurements currently available for indoor radio channels are not useful for designing new indoor geolocation systems. This is because telecommunication models deal primarily with path loss and rms delay spread in order to estimate coverage and data rate. However in indoor geolocation systems, the most significant parameters are the time of arrival (TOA) of the direct line of sight (DLOS) path and paths that arrive very close to this path as well as their relative received powers. For geolocation applications, the DLOS path is the most important parameter since its TOA is directly proportional to the physical distance between transmitting and receiving antennas. However, since the measurement system is not ideal – it has finite bandwidth, finite dynamic range and introduces noise – the DLOS path can never be extracted perfectly from a measurement. The most reasonable approximation is the first path in the profile detected above a given noise floor. The other paths are also important since they

can affect the TOA and amplitude of the first path. The most significant of these paths is the strongest path, which is commonly detected in receivers locking onto the strongest signal. Given these facts, new measurements and modeling must be done to characterize the radio channel by focusing on the amplitude and TOA/distance of the first and strongest paths as shown in Fig. 1-2 [3].

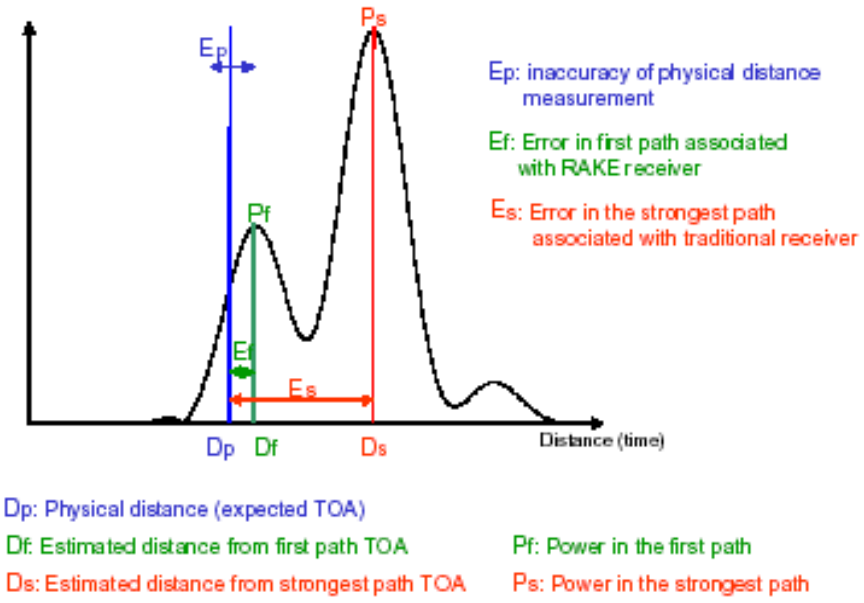

Figure 1-2 Important Geolocation Parameters

Telecommunications and geolocation require different though similar performance measures. Table 1 compares performance measures for telecommunications and geolocation systems based on [8]. In telecommunications, quality of service is typically defined as signal to noise ratio (SNR) or bit error rate (BER). Likewise in geolocation, the accuracy of service could be defined as the percentage of calls located within an accuracy of δ meters in the case of the E-911 service or distribution of distance error at a geolocation receiver. The grade of service for telecommunications is

Table 1 Comparison of Performance Measures for Telecommunications

Telecommunications Systems	**Geolocation Systems**
Quality of service ● *Signal to interference ratio* ● *Packet error rate* ● *Bit error rate*	*Accuracy of service* ● Percentage of calls located within an accuracy of δ meters ● Distribution of distance error at a geolocation receiver
Grade of service ● Call blocking probability ● Availability of resources ● Unacceptable quality	*Location Availability* ● Percentage of location requests not fulfilled ● Unacceptable uncertainty in location
Coverage area	*Coverage area*
Capacity ● Subscriber density that can be handled	*Capacity* ● Location requests/frequency that can be handled
Other system parameters ● Delay (call setup, channel assignment, etc.) ● Reliability ● Database lookup time ● Message and time complexity ● Network management system	*Other system parameters* ● Delay in location computation ● Reliability ● Database look-up table ● Management and complexity

usually the call blocking rate in the peak hour. In a similar way, location availability can be defined as percent of location requests not fulfilled perhaps because of not having enough location metrics or the measurements lead to unacceptable uncertainty in location accuracy. Coverage in telecommunication systems is related to the service area where access to the wireless network is possible. For geolocation systems, coverage corresponds to the area where there are enough location metrics to locate the mobile station. Finally, there are other issues in geolocation system in a manner similar to telecommunication systems such as end-to-end delay, reliability, management and complexity.

To help the growth of this emerging technology, there is a need to develop a scientific framework for the design and performance analysis of such systems.

1.2 Contribution of the Thesis

The contributions of this thesis can be summarized as follows:

1- The effects of sampling in frequency, sampling in time and filtering in the accuracy of TOA measurement are analyzed using results of frequency domain measurements.

2- A supplementary measurement program was conducted to augment the existing measurement database in CWINS reported by Dr. Jacques Beneat [5]. The new measurements represent exclusively the line of sight (LOS) scenarios and include 72 measurements at 1GHz with 200MHz bandwidth taken in four different areas in the Atwater Kent Laboratories at the Worcester Polytechnic Institute. The previous measurement database for 1GHz was collected in obstructed line-of-sight (OLOS) scenarios and included 80 measurements in three different buildings.

3- The ranging accuracy of the TOA based indoor geolocation systems in LOS and OLOS areas are compared and the accuracy of the ray tracing based models with the results of measurements are examined.

1.3 Outline of the Thesis

Chapter 2 starts with an overview of characterization of the radio channel and existing measurement techniques. In particular, the frequency domain measurement system and derivation of the channel profile from this kind of measurement technique are discussed. Chapter 3 discusses the parameters affecting the accuracy of the indoor geolocation system. The effect of sampling in the frequency domain is studied first. Then the effect of sampling in the time domain is analyzed. The chapter concludes by examining the effect of filtering in the frequency domain. Chapter 4 analyzes the results of measurements that were conducted at different sites. First, the statistics of

measurement results from each site are presented. Then the behavior of LOS and OLOS scenarios are compared. Finally, the results of measurements are compared with the ray tracing based model for indoor geolocation. Chapter 5 summarizes the research results and discusses the possibilities for future work.

Chapter 2 Measurement Systems

2.1 Introduction

In this chapter, we begin by providing an introduction to the radio channel characterization. Then, we explain some of the measurement techniques used for characterizing the radio channel. We focus on frequency domain techniques in particular and describe in detail the measurement system that we used throughout this work.

2.2 Overview of Characterization of Multipath Fading Channels

Multipath channels are generally considered as linear time variant systems. In order to characterize these systems, let us consider the effect of a multipath channel on a transmitted signal represented as:

$$x(t) = \mathbf{Re}[x_l(t)e^{j2\pi f_c t}] \tag{2.1}$$

The received band pass signal may be expressed in the form of

$$y(t) = \mathbf{Re}\sum_n \alpha_n(t)x[t-\tau_n(t)] \tag{2.2}$$

where $\alpha_n(t)$ and $\tau_n(t)$ represent the time variant attenuation factor and propagation delay associated with the *n*th path, respectively. Substitution for $x(t)$ from (2.1) into (2.2) yields the result:

$$y(t) = \mathbf{Re}(\{\sum_n \alpha_n(t)e^{-j2\pi f_c \tau_n(t)}x_l[t-\tau_n(t)]\}e^{j2\pi f_c t}) \tag{2.3}$$

The equivalent low pass received signal, y_l, is obtained from (2.3) as:

$$y_l = \sum_n \alpha_n(t)e^{-j2\pi f_c \tau_n(t)}x_l[t-\tau_n(t)] \tag{2.4}$$

From (2.4) it follows that the equivalent low pass channel is described by the time variant impulse response:

$$h(\tau,t) = \sum_n \alpha_n(t) e^{-j2\pi f_c \tau_n(t)} \delta_l[t - \tau_n(t)] \tag{2.5}$$

2.3 Measurement Techniques

Both narrowband and wideband measurements are used for characterization of radio channels. The definitions of narrowband and wideband measurements follow closely the definitions of narrowband and wideband communication systems. A narrowband measurement is made over a bandwidth in which the statistics at one frequency are highly correlated with the statistics at the rest of the frequencies in the band. The measurement technique is simple because a continuous wave (CW) signal is the transmitted waveform. A wideband measurement is conducted over a band in which the statistics at one frequency may be uncorrelated with the statistics of other frequencies in the band. Wideband measurements can be divided into time domain techniques and frequency domain techniques [7].

2.3.1 Time Domain Measurement Techniques

There are two major methods for time domain measurement of the channel impulse response: direct method and spread spectrum technique. In the direct method, a narrow pulse (ideally an impulse) with a low duty cycle is transmitted periodically and the received signal arriving from different paths is observed. In the spread spectrum technique a wideband spread spectrum signal is sent and then the received signal is correlated with the transmitted sequence [9] on the receiver side. In both cases, the resolution of the measurement system is inversely proportional to the bandwidth of the

measurement system. In the spread spectrum technique, the ratio of peak to average power is unity. In the pulse transmission method, the average to peak power ratio is very high because of the large duty cycle of the transmitted pulse. As a result, direct pulse transmission systems suffer from inefficient use of transmitter power and provide less coverage with respect to spread spectrum techniques, which have amplifiers designed for identical peak power operation. However, spread spectrum measurement systems are more complex than pulse transmission measurement systems.

2.3.2 Frequency Domain Measurement Technique

In frequency domain measurements of channel propagation characteristics, the frequency response of the channel is measured directly. In indoor areas these measurement are performed conveniently with the aid of a network analyzer [1]. In this kind of measurement system, which is basically the frequency sweep system, the frequency is normally incremented by a constant amount and held for a fixed time while one sample of frequency response is measured [7]. Then by taking the inverse Fourier transform of the frequency response channel, the impulse response is obtained. The resolution of the impulse response is proportional to the bandwidth of the measurement system. The indoor radio channel measurements presented in this thesis were collected using the frequency sweep measurement system.

2.4 Description of the Measurement System

The block diagram of the measurement system used for frequency domain measurements of the radio channel is shown in Fig. 2-1 The main component of the measurement system is a network analyzer with the Fourier option that measures the

frequency response of the channel. The transmitter portion of the frequency domain measurement system consists of the network analyzer's synthesized source, a long cable to provide mobility to the transmitter, a power amplifier and an antenna. The receiver portion of the frequency domain measurement system consists of the receiving antenna, an attenuator and the receiver portion of the network analyzer. The receiving antenna is of the same design as that used for the transmitter.

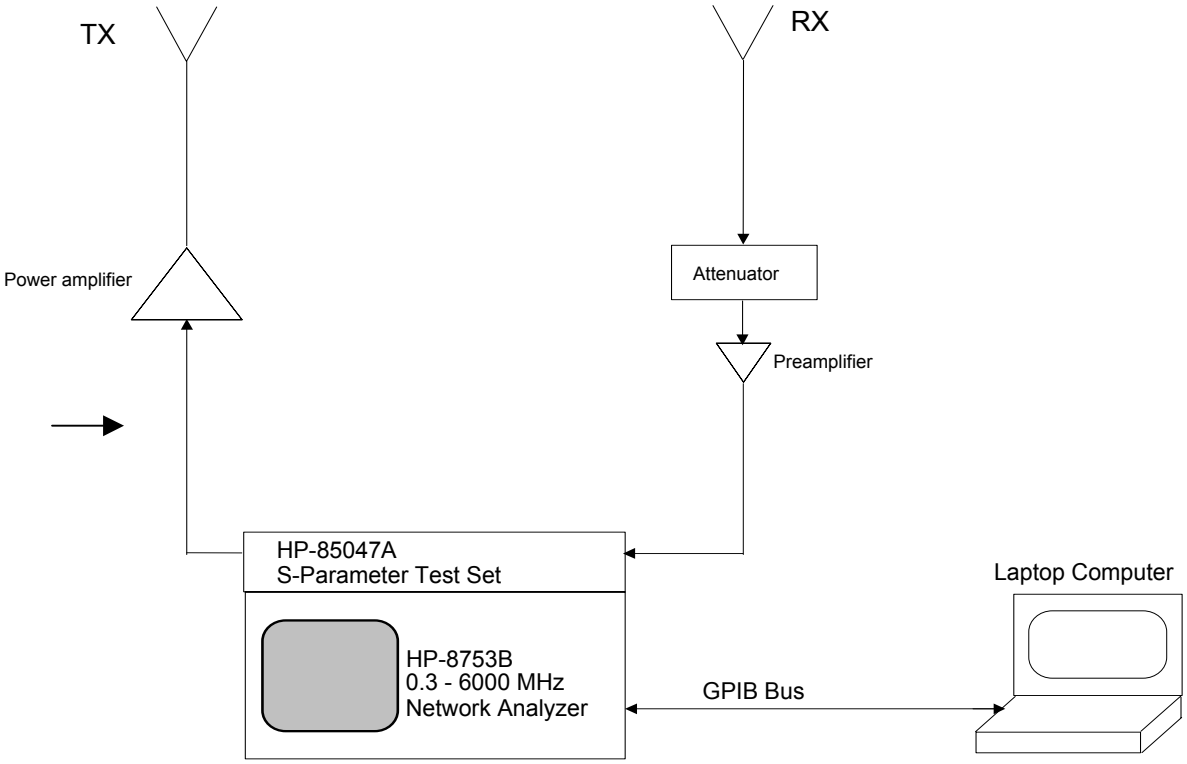

Figure 2-1 Block Diagram of the Frequency Domain Measurement System

The network analyzer is controlled by a laptop through Hewlett Packard's version of a general-purpose instrumentation bus (GPIB). The laptop initializes the network analyzer preceding each measurement and collects the data at the completion of each measurement. The magnitude and phase of the measured frequency response and the amplitude of the time response are stored for each measurement. Sample frequency and

time responses are given in Fig. 2-2. The data can later be transferred to a desktop computer for further analysis.

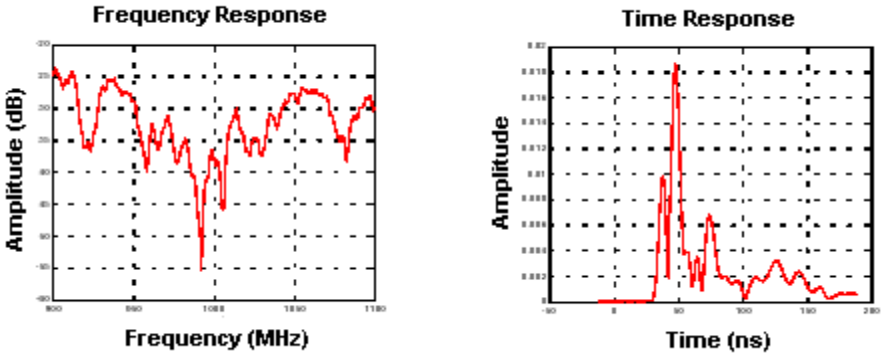

Figure 2-2 Sample Frequency and Time Response of a Radio Frequency Channel

For a 1 GHz center frequency, a monopole quarter wave antenna with rectangular ground plane is used. The dimensions of the monopole correspond to $\lambda/4$, where λ is the wavelength of the signal. The side of the ground plane corresponds to $\lambda/2$. A picture of the antenna is given in Fig. 2-3. This type of antenna is typically described as omnidirectional with a -0.85dBi gain in the direction of the horizontal plane.

Figure 2-3 Monopole Quarter Wave Antenna with Ground Plane for 1 GHz Center Frequency

2.5 Derivation of the Channel Impulse Response

The channel impulse response of a communications channel described by (2.5) for a selected frequency band is retrieved by taking the inverse Fourier transform of the frequency response of the channel at that band. If BW represents the bandwidth of the measurement system and the network analyzer sweeps the frequency spectrum with a resolution of Δf , then the number of samples of the frequency spectrum, N_f , is:

$$N_f = \left\lfloor \frac{BW}{\Delta f} \right\rfloor \tag{2.6}$$

If $X[k]$ represents the kth sample of the frequency response, the time response is obtained by taking the IDFT of the frequency response as follows:

$$x[n] = \frac{1}{N_f} \sum_{k=0}^{N_f-1} X[k] e^{j2\pi kn/N_f} \quad , 0 \le n \le N_f - 1 \tag{2.7}$$

where $x[n]$ represents the nth sample of the channel impulse response. The time response that is generated by getting IDFT is a periodic waveform that has a period of:

$$T_s = 1/\Delta f \tag{2.8}$$

Also, the resolution of the time response (sampling period) would be:

$$\Delta t = \frac{T_s}{N_f} \tag{2.9}$$

Fig. 2-4 illustrates this transformation. As shown in Fig. 2.4 (b), the channel impulse response becomes approximately zero after a certain amount of time, which implies that the value of the time response after a certain time does not have a major impact on the frequency response. Therefore, we do not lose any valuable information by cutting the

impulse response into pieces of T_s seconds. We will discuss this issue in more detail in Chapter 3 when we discuss parameters affecting the accuracy .

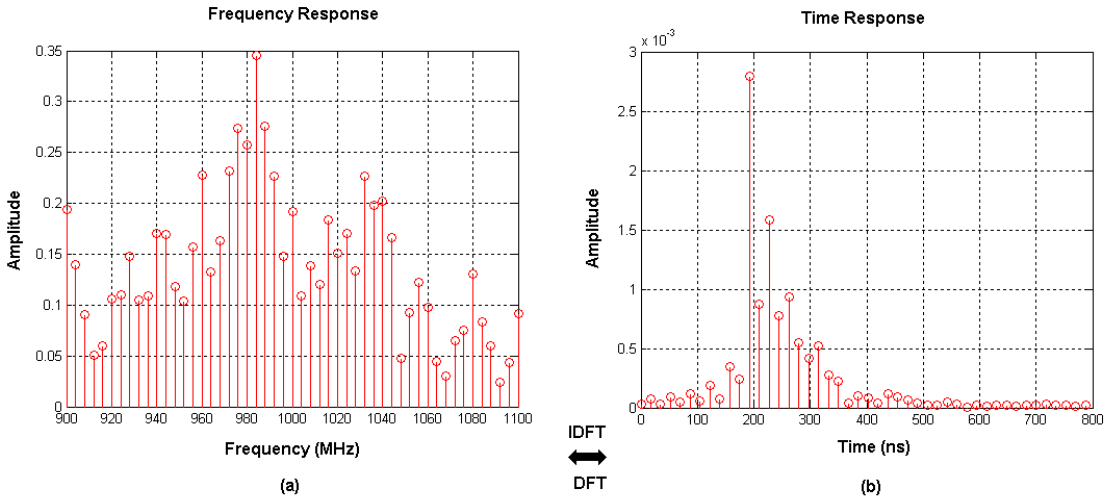

Figure 2-4 Generating the Channel Impulse Response Using IDFT

Most of the time in geolocation applications, we are only interested in part of the channel impulse response. This part is usually from the beginning up to the TOA of the first path or the strongest path. Furthermore, we might want to make the sampling period, Δt, very small to have better accuracy in estimation of the TOA of the first path or the strongest path. If the time response is generated over the interval $0 < t < t_1$ with N_t samples, then the sampling period must be:

$$\Delta t = \frac{t_1}{N_t} \tag{2.10}$$

Based on (2.9) the only way to achieve this resolution with a fixed frequency sampling period is to increase the number of samples of the frequency response. This can be done by zero padding outside the desired bandwidth. The overall number of frequency samples that is needed after zero padding must be:

$$N = \frac{T_s}{\Delta t} = \frac{1}{\Delta f \times \Delta t} \tag{2.11}$$

Finally, the time response can be obtained as follows:

$$x[n] = \frac{1}{N_f}\left(\sum_{k=0}^{N-1} X[k] e^{j2\pi kn/N}\right) = \frac{1}{N_f}\left(\sum_{k=0}^{N_f-1} X[k] e^{j2\pi kn \cdot \Delta f \cdot \Delta t}\right), 0 < n < N_t \tag{2.12}$$

The procedure described above cannot be implemented through a direct IDFT algorithm. Therefore we utilize a method called the Chirp Z Algorithm, which gives us more flexibility in calculating the channel impulse response. The Chirp Z Algorithm is described in the next section.

2.5.1 Derivation of the Impulse Response Using the Chirp Z Algorithm

The Chirp Z-transform of a signal x is the Z-transform of x along a spiral contour defined by m, ω and a. The scalar m is a specifies the length of the transform, ω is the ratio between points along the z-plane spiral contour of interest and scalar a is the complex starting point on that contour. In fact

$$CZT(x[n], a, \omega, m) = X(z)\Big|_{z = a.\omega^{-k}}, 0 \le k \le m-1 \tag{2.13}$$

If $a = 1, \omega = e^{-j2\pi/N}$ and $m = N$ then we have:

$$CZT(x[n], 1, e^{-j2\pi/N}, N) = \sum_{n=0}^{N-1} x[n] e^{-j2\pi kn/N} = X[k] \tag{2.14}$$

which is essentially N point DFT of $x[n]$.

In order to calculate CIR for the range $0 \le t \le t_1$, we take the complex conjugate of the right hand side of (2.12) twice and we have:

$$x[n] = \frac{1}{N_f}\left(\sum_{k=0}^{N-1} X[k]^* e^{-j2\pi kn/N}\right)^* =$$

$$\frac{1}{N_f}\left(CZT(X[k]^*, 1, e^{-j2\pi/N}, N)\right)^* \quad 0 \le n \le N_t \tag{2.15}$$

2.6 Filtering of Frequency Response by a Window

In geolocation applications, we are interested in isolating the received path to the fullest extent possible. Therefore, before applying the IDFT we use a digital filter such as a Hanning or Hamming window to reduce the effects of side lobes. If $W[k]$ represents kth sample of the digital filter then from (2.12) we have:

$$x[n] = \frac{1}{N_f}\left(\sum_{k=0}^{N_f-1} X[k]\cdot W[k] e^{j2\pi kn\cdot\Delta f\cdot\Delta t}\right), 0 < n < N_t \tag{2.16}$$

Fig. 2-5 illustrates the effect of filtering. Both case (a) and (b) have been obtained from the same frequency response. It is clear that for case (a) which has been filtered with a Hanning window has lower side lobes than case (b), which does not utilize any filtering.

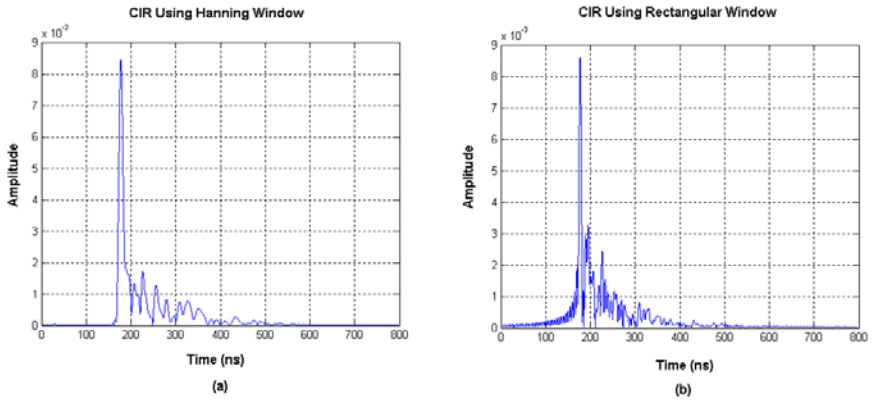

Figure 2-5 (a) Channel Impulse Response Filtered by Hanning Window, (b) Channel Impulse Response Without Filtering (Rectangular Window)

2.7 Distance Estimation Using Peak Detection Algorithm

Detecting the peaks in the channel impulse response (CIR) is of a great concern for indoor geolocation applications, especially for those that are based on TOA techniques. We associate a tap with each peak and then estimate the distance based on the TOA of the first path. If τ is the TOA of the first path and c is the speed of radio propagation in air the distance can be estimated as follows:

$$d = \tau \,.\, c \tag{2.17}$$

In this research, we are applying a very simple algorithm for detecting the peaks. First, we detect local maxima in the channel profile and then choose the ones that are above a certain threshold as our peaks. We use a threshold for two reasons. First, we want to make sure that detected peaks are above the sensitivity level of the network analyzer, which in this case happens to be –100dBm. Second, we want to avoid detecting the side lobes that are generated in the process of windowing as peaks. In order to fulfill both of these conditions we set the threshold as follows:

$$Threshold = Max\,(\text{-}100dBm,\ \beta \times P_s) \tag{2.18}$$

where P_s is the maximum value of the CIR and β is a constant that has a value of $\beta = 10\%$ unless otherwise stated. Fig. 2.6 (a) and (b) illustrates the peak detection algorithm.

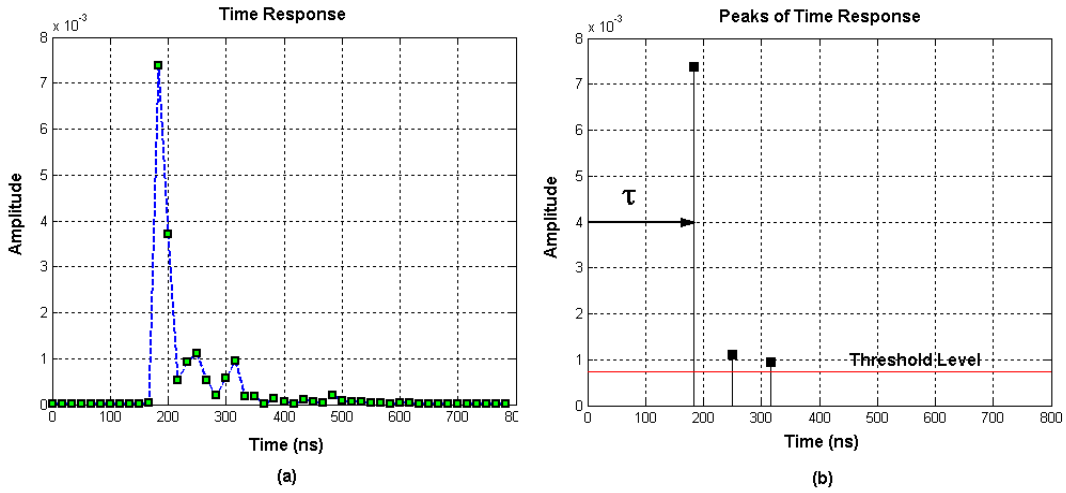

Figure 2-6 (a) Channel Impulse Response, (b) Detection of Peaks Using Peak Detection Algorithm

Chapter 3 Parameters Affecting TOA Accuracy

3.1 Introduction

As described in [3], the first problem limiting the ranging ability is the effect of multipath. Since the system has limited bandwidth, it cannot differentiate between the first path and first few other paths. Therefore, the detected TOA of the first path is somewhere between the TOA of the first path and the paths close to this path. This error in the detection of the first path is caused by multipath and is a function of the bandwidth of the measurement system. Generally, the objective of the measurement program is to collect a database of channel impulse responses from which error statistics for the TOA of the first path can be defined and later used for channel modeling purposes.

As shown in Fig.3-1, there are a number of detailed parameters besides multipath affecting the accuracy of the measurement of the TOA of the first path. These parameters are the sampling period in the frequency domain measurements, Δf, and sampling period in the time domain,Δt, as well as the type of filter used in the frequency domain before applying the inverse Fourier transform.

In this chapter, we begin by analyzing the relationship between Δf and the accuracy of TOA measurement. Then, we describe the effect of Δt along with multipath on the calibration and the measurement of TOA. Finally, we explain the effect of filtering on the overall accuracy of the measurement system.

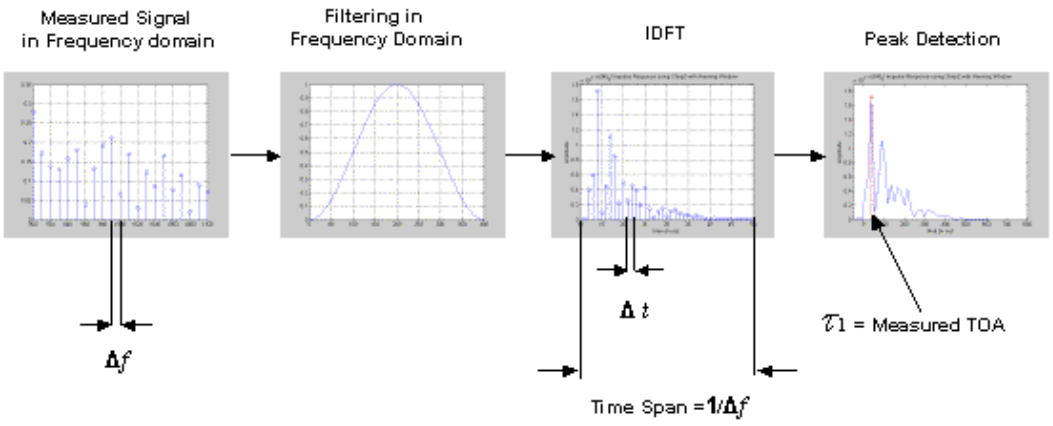

Figure 3-1 Measurement Process

3.2 Effects of Frequency Distance in the Measurement (Δf)

The overall frequency band that we measure is $N_f \times \Delta f$, where N_f is the number of samples in the frequency domain and Δf is the distance between two measured samples of the channel response. After taking the inverse discrete Fourier transform, the time response is a periodic function in time with a period of $1/\Delta f$ as follows:

$$x[n] = \frac{1}{N_f}\left(\sum_{k=0}^{N_f-1} X[k] \cdot W[k] e^{j2\pi kn \cdot \Delta f \cdot \Delta t} \right), \; 0 < n < N_t \qquad (3.1)$$

For the derivation of this equation refer to sections 2.5 and 2.6.

In order to analyze the effect of sampling in the frequency domain, Δf, we collected a set of 16 LOS points measured inside Room AK 320 within an approximate range of 1 to 5 meters. We then increase Δf, while keeping Δt fixed at 0.0625 ns in the entire process. Fig. 3-2 is a set of figures showing the frequency and time responses for point 7 (P7) at four different values of Δf.

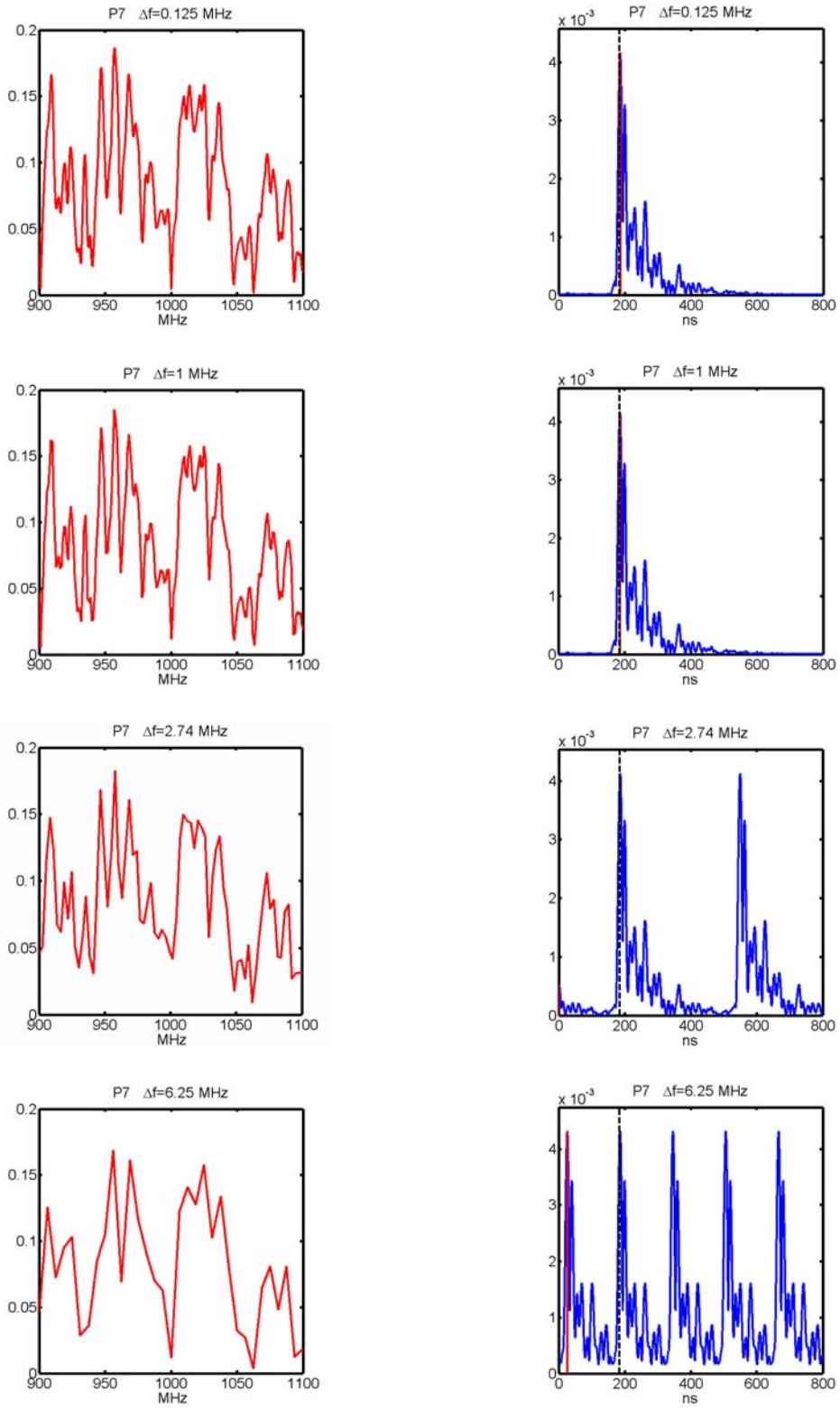

Figure 3-2 Frequency and Time Responses of Point 7 (P7) at Four Different Values of Δf. Solid Red Lines and Dashed Black Lines in the Time Responses Represent Expected and Detected First Paths, Respectively.

The reader can refer to Appendix A for the complete list of time and frequency responses for point 7 at every single Δf. As illustrated in Fig. 3-2, the detected first path and the expected first path are very close to each other for Δf=0.125 MHz and Δf=1 MHz but they are relatively far apart for Δf =2.74 MHz and Δf= 6.25 MHz due to the effect of aliasing. After taking the inverse discrete Fourier transform, the time response is in fact a periodic function that covers a span of time given by $1/\Delta f$. What we see in the last two time responses of Fig. 3-2 is actually several periods of the channel impulse response.

Figs 3-4(a) and 3-4(b) show the mean and the variance of distance error associated with each Δf for the 16 LOS measurements that we conducted in AK 320. In order to interpret the results in Fig.3-4, we define three parameters: Td, Tc and τ. Td is the delay in the measurement system due to cables and antennas. This parameter is a fixed value for a set of measurements. Tc is the TOA of the first path, which is a function of actual distance and τ is the delay between the first and the final path in the CIR. These parameters are depicted in Fig.3-3, which shows a CIR generated with the following values: N_t =12801 points, 0ns<t<600ns, Δf=0.125 MHz and BW=200 MHz. As we see in Fig.3-3, in order to avoid aliasing in a collection of points, the maximum value acceptable for Δf, Δf_{td}, is such that it can accommodate the maximum time span in the measurement set in one period. As a result:

$$\Delta f_{td} = \frac{1}{\mathrm{Tc} + (\mathrm{Td} + \tau)\mathrm{max}} \tag{3.2}$$

We have the following set of data for the described collection of points:

Maximum of TOA plus delay spread in the collection, $(\mathrm{Td}+\tau)\,\mathrm{max}$ =195ns

Delay in the measurement system, Tc=169 ns

Therefore we have:

$$\Delta f_{td} = \frac{1}{\mathrm{Tc} + (\mathrm{Td} + \tau)\mathrm{max}} = \frac{1}{364\mathrm{ns}} = 2.74 \text{ MHz} \tag{3.3}$$

Now if we look at Fig. 3-4 we notice that initially the mean and variance of distance error remains almost constant. However, as Δf approaches 2.74 MHz, there is a sudden jump in the mean and variance. This is due to the aliasing effect. As we further increase Δf we notice that the variance of error in distance goes up and down randomly and average error remains high. This is because of the fact that, after reaching the aliasing threshold we can no longer extract the first path and what we are detecting is just a random aliased path. As we see in Fig. 3-4, as long as Δf is kept below threshold level, variation of that does not change the distance error significantly.

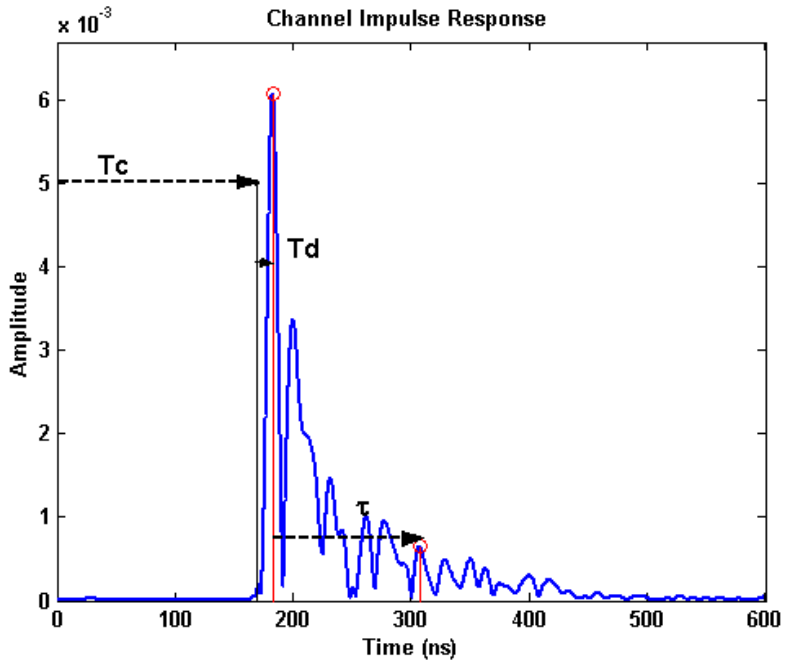

Figure 3-3 Illustration of Tc, Td and τ on a Channel Impulse Response

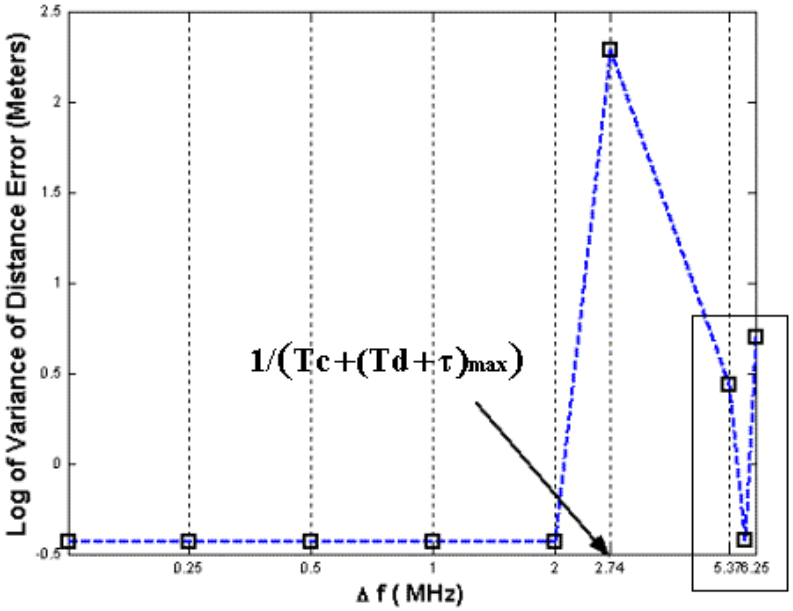

(a)

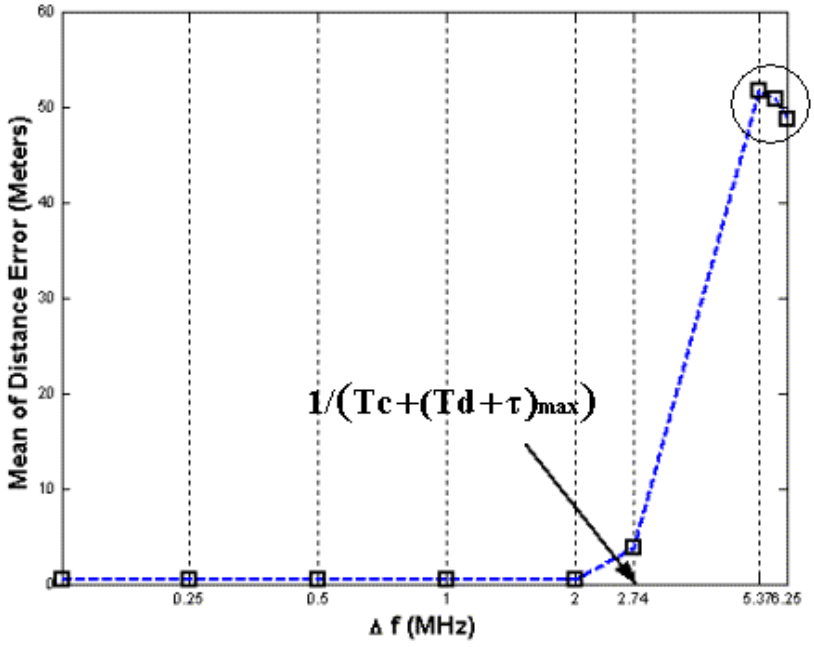

(b)

Figure 3-4 Effects of Sampling in Frequency Domain on (a) Variance of Distance Error and (b) Mean of Distance Error

There is a special point in Fig. 3-4 (a), which is affected by aliasing but has a very low variance of error. This particular point along with its neighboring points is surrounded by a rectangle. The corresponding points in Fig. 3-4 (b) are shown inside a circle. If we enlarge that rectangular region in Fig.3-4 (a), as shown in Fig.3-5, we realize that the decrease in variance of error happens at Δf=1/Tc**.** In order to explain this sharp decrease in variance of error, the CIR of a point in the measurement set is depicted in Fig.3-6. As shown in the figure when Δf=1/Tc the path that is detected by the algorithm is seperated from the real path by about Tc seconds. As a result, although the mean error as shown in Fig.3-4 (b) is high, the variance of error is very low.

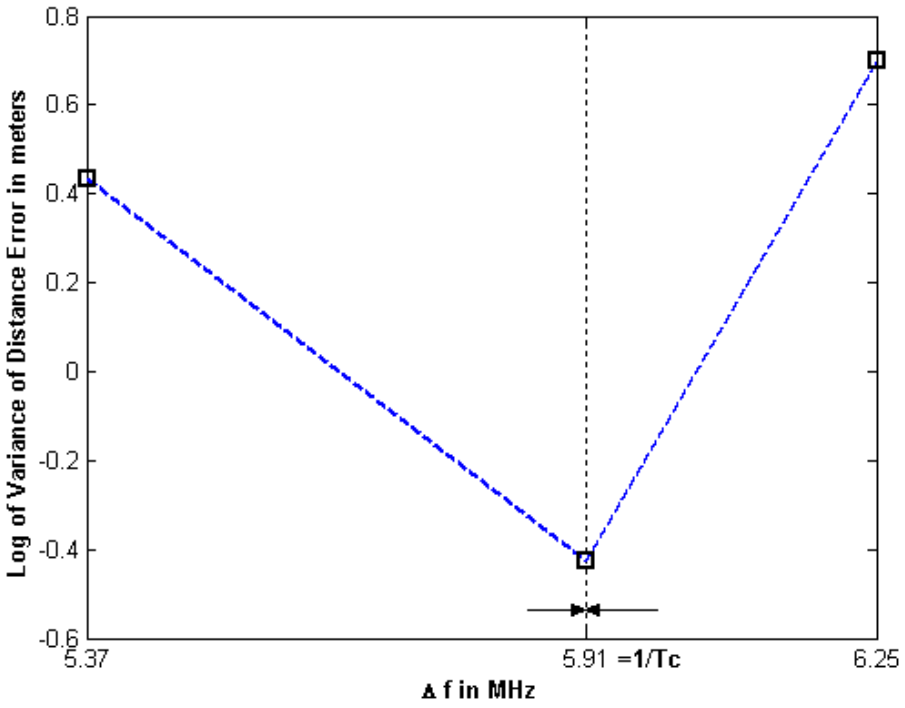

Figure 3-5 Log of Variance of Error around Δf=1/Tc

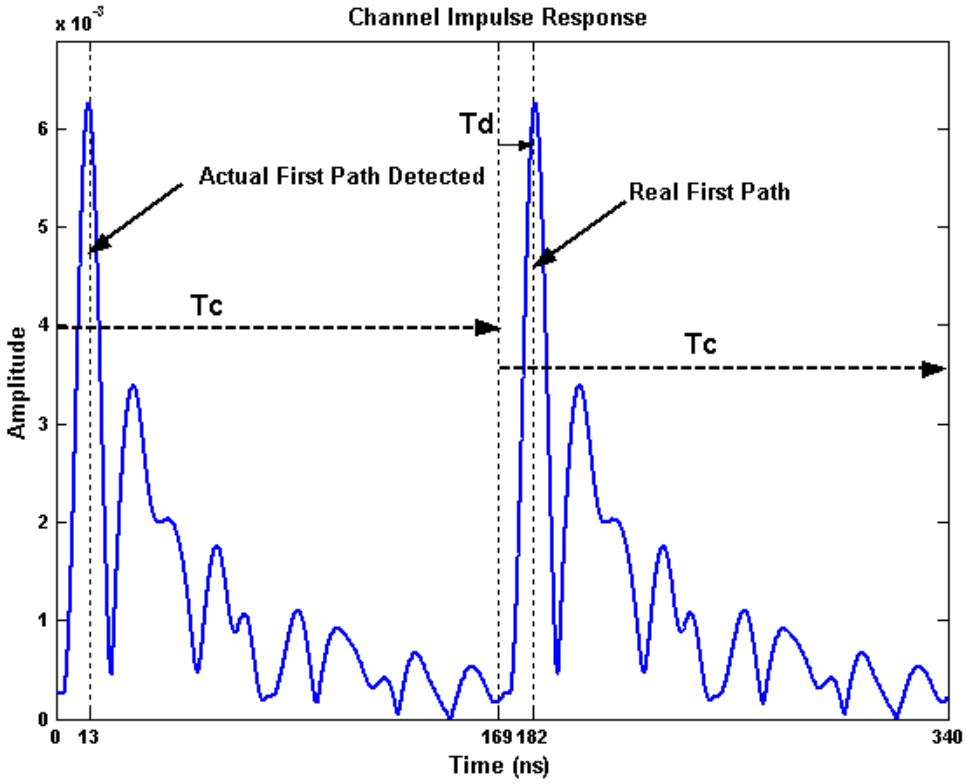

Figure 3-6 CIR Generated with Δf=1/Tc

3.3 Effects of Sampling in Time

As described in section 2.4, time response is a periodic waveform with the period of $1/\Delta f$ and the sampling period of Δt. Since samples of the time response are seperated from one another by Δt, the TOA of the first path that is detected by the peak detection algorithm is always quantized to the nearest time sample. Fig.3-7 illustrates the quantization effect on a CIR. In Fig. 3-7 the red curves represents the CIR that is generated with Δt =10 ns. Notice that the actual time of arrival of first path is at 172.6 ns but due to quantization effect first path is detected at 170 ns causing error of 2.6 ns in estimation of TOA. In the next two subsections we provide an analytical discussion of the effect of sampling in time on the accuracy of the measurement system.

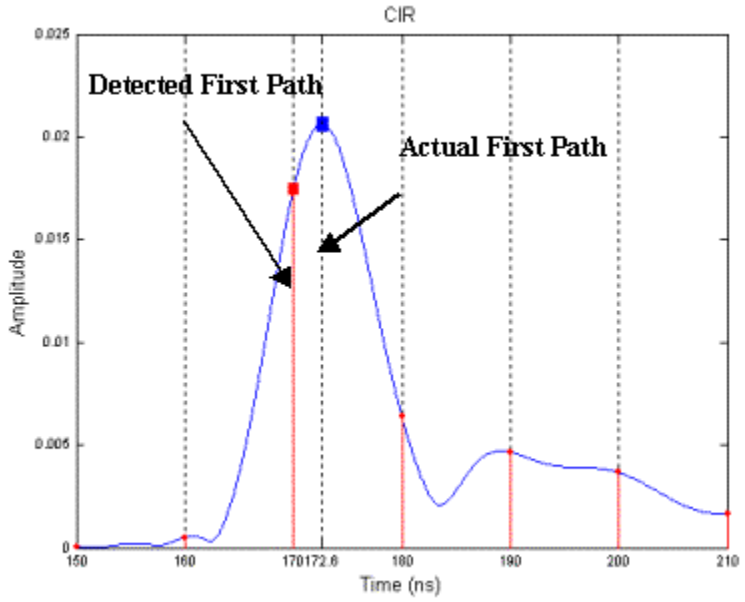

Figure 3-7 Effect of Quantization in Detecting the First Path

3.3.1 Effects of Sampling Rate on Calibration

In order to calibrate the measurement set, an LOS point in one meter that has minimal effect of multipath is selected. We then fix the sampling rate Δt at very small value, in this study to 0.0625 ns. Given the TOA of the first path to be in $\frac{10}{3} \cong 3.333333$ ns, we set the delay in the measurement system so that estimated TOA matches the actual TOA and as a result, the error associated with estimation becomes zero. Now as we increase Δt we expect the error in estimation of TOA to be in the range of

$$\frac{-\Delta t}{2} < error_{TOA} < \frac{\Delta t}{2} \tag{3.4}$$

In order to verify this assumption we selected eight points on the circumference of a circle with radius of 1.00 meter and calibrated the measurement system with respect to first point and observed the error of estimation on the set by changing sampling rate Δt from 0.0625ns to 4.00 ns. Table 2 shows the result of calibration for the first point and Table 3 reflects the results of measurements for entire collection of points.

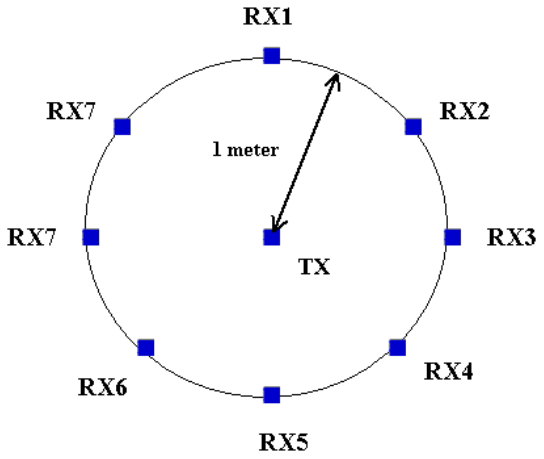

Figure 3-8 Configuration of 8 Points Used in Calibration Analysis.

Table 2 Calibration Parameters for Point 1.

Δt (ns)	Measured TOA (ns)	Delay in the Measurement System (ns)	Calibrated TOA (ns)	Actual Distance (meters)
0.0625	172.625	169.2916666667	3.333333	1

Table 3 Errors in Estimation of TOA for Points Shown in Fig. 3-8

Δt (ns) / $error_{TOA}$ (ns)	0.0625	0.125	0.250	0.50	1.00	2.00	2.5	3.0075	4.00
Point1	0	0	-0.125	-0.125	0.375	-0.625	-0.125	-1.1964	-0.625
Point 2	**-0.125**	**-0.125**	-0.125	-0.125	0.375	-0.625	-0.125	-1.1964	-0.625
Point 3	**-0.25**	**-0.25**	-0.125	-0.125	**-0.625**	-0.625	-0.125	-1.1964	-0.625
Point 4	**-0.0625**	**-0.125**	-0.125	-0.125	0.375	-0.625	-0.125	-1.1964	-0.625
Point 5	**0.375**	**0.375**	**0.375**	**0.375**	0.375	-0.625	-0.125	**1.8111**	-0.625
Point 6	**-0.3125**	**-0.375**	**-0.375**	-0.125	**-0.625**	-0.625	-0.125	-1.1964	-0.625
Point 7	**0.0625**	**0.125**	0.125	-0.125	0.375	-0.625	-0.125	-1.1964	-0.625
Point 8	**-0.125**	**-0.125**	-0.125	-0.125	0.375	-0.625	-0.125	-1.1964	-0.625

Notice that the error in estimation of TOA is always in the range of $\frac{-\Delta t}{2} < error_{TOA} < \frac{\Delta t}{2}$ for the first point which is our point of calibration. This is also the case for most of the other points in the set. Those errors that are not in the range of quantization error are marked by red bold font. In the first two columns the Δt is set to 0.0625ns and 0.125 ns respectively. If we consider the speed of light to be $3\times10^{8} m/s$, then Δt=0.125ns and Δt=0.0625ns corresponds to 3.75 centimeter and 1.875 centimeters, respectively. For these two values of Δt the error in measurement with hands and also effect of multipath overshadows the quantization error. The remaining six points in the table that show errors greater than the quantization error are suffering from multipath effect; five of them

belong to Point 5 and Point 6 on the circle. Table 4 reflects the error in estimation of TOA after removing the quantization error for this collection of points.

Table 4 Errors in Estimation of TOA Due to Multipath and Hand Measurement for Points Shown in Fig. 3-8

Δt (ns) / $error_{TOA}$ (ns)	0.0625	0.125	0.250	0.50	1.00	2.00	2.5	3.0075	4.00
Point1	0	0	0	0	0	0	0	0	0
Point 2	-0.125	-0.125	0	0	0	0	0	0	0
Point 3	-0.25	-0.25	0	0	-1	0	0	0	0
Point 4	-0.0625	-0.125	0	0	0	0	0	0	0
Point 5	0.375	0.375	0.25	0.5	0	0	0	-3	0
Point 6	-0.3125	-0.375	-0.25	0	-1	0	0	0	0
Point 7	0.0625	0.125	0	0	0	0	0	0	0
Point 8	-0.125	-0.125	0	0	0	0	0	0	0

The results in Table 3 lead us to consider the effect of changing the sampling rate, Δt, while we have multipath effect. In the next section we discuss this issue in more detail.

3.3.2 Combined Effects of Sampling Rate and Multipath

In the previous section we noticed that as we change the Δt for a calibrated point the error in estimation of time of arrival always remain in the range of $\frac{-\Delta t}{2} < error_{TOA} < \frac{\Delta t}{2}$. However, as we change Δt for other points, sometimes the error exceeds the quantization error. In order to investigate this effect more comprehensively, we collected a set of 26 LOS points in Room AK 219 and calibrated the measurement system with respect to the first point and then varied Δt from 0.0625 ns up to 4 ns. Notice that the sampling period of the frequency spectrum, Δf, is fixed at 500 KHz for this measurement set. Table 4 shows the results of the observation.

Table 5 Errors in Estimation of TOA for the Collection of Points in AK 219

Δt (ns) / $error_{TOA}$ (ns)	0.0625	0.125	0.250	0.50	1.00	2.00	3.0075	4.00
Point 1	0.0143	0.0143	0.0143	0.2643	0.2643	-0.7357	0.7229	1.2643
Point 2	0.8151	0.7526	0.8776	0.8776	0.8776	-0.1224	0.3438	1.8776
Point 3	-2.2289	-2.1664	-2.1664	-2.4164	-1.9164	-2.9164	-2.4502	-0.9164
Point 4	-0.4462	-0.5087	-0.3837	-0.6337	-0.1337	-0.1337	0.3475	-0.1337
Point 5	-1.5344	-1.5344	-1.4094	-1.4094	-1.4094	-2.4094	-0.9207	-0.4094
Point 6	-1.2431	-1.2431	-1.2431	-0.9931	-1.4931	-0.4931	-2.0269	-0.4931
Point 7	-0.8102	-0.7477	-0.7477	-0.9977	-0.4977	-1.4977	-0.0391	0.5023
Point 8	-1.2511	-1.2511	-1.2511	-1.0011	-1.0011	-1.0011	-2.5349	-1.0011
Point 9	-2.1174	-2.1174	-2.2424	-2.2424	-1.7424	-1.7424	-1.2612	-1.7424
Point 10	-1.0404	-1.0404	-1.0404	-0.7904	-0.7904	-0.7904	-1.3017	-0.7904
Point 11	-2.2492	-2.1867	-2.3117	-2.0617	-2.5617	-1.5617	-1.0956	-3.5617
Point 12	-1.0549	-0.9924	-1.1174	-0.8674	-0.8674	-1.8674	-0.4238	-1.8674
Point 13	-1.2276	-1.2901	-1.2901	-1.0401	-1.5401	-1.5401	-0.0814	0.4599
Point 14	-0.4407	-0.4407	-0.5657	-0.3157	-0.8157	0.1843	-1.3496	0.1843
Point 15	-0.4906	-0.5531	-0.5531	-0.3031	-0.3031	-0.3031	0.1781	-0.3031
Point 16	0.0758	0.0133	0.0133	0.2633	0.2633	-0.7367	-1.263	1.2633
Point 17	-1.7256	-1.6631	-1.6631	-1.9131	-1.4131	-1.4131	-2.9619	-3.4131
Point 18	-0.8749	-0.9374	-0.8124	-0.8124	-1.3124	-0.3124	-1.8613	-2.3124
Point 19	-0.5727	-0.5727	-0.5727	-0.8227	-0.3227	-0.3227	0.1284	-0.3227
Point 20	-0.5704	-0.5704	-0.5704	-0.3204	-0.8204	-0.8204	0.6382	1.1796
Point 21	-0.1461	-0.1461	-0.2711	-0.2711	-0.2711	-0.2711	-0.7974	1.7289
Point 22	-0.9961	-0.9961	-0.9961	-1.2461	-0.7461	-0.7461	-0.2949	-0.7461
Point 23	-0.7844	-0.7844	-0.7844	-1.0344	-0.5344	-0.5344	-0.0833	-0.5344
Point 24	-0.5764	-0.5764	-0.7014	-0.7014	-0.2014	-1.2014	0.2572	0.7986
Point 25	0.3418	0.2793	0.2793	0.2793	0.2793	0.2793	-0.247	2.2793
Point 26	0.3321	0.2696	0.2696	0.5196	0.0196	1.0196	-0.4992	-0.9804
Variance (meters)	0.0561	0.0522	0.0551	0.0623	0.057	0.0675	0.0948	0.2019

If we assume the error due to quantization and multipath to be independent, and consider these two sources as the major sources of error, then we have:

$$\sigma^2_{error_TOA} = \sigma^2_{error_TOA_Q} + \sigma^2_{error_TOA_M} \quad (3.5)$$

where $\sigma^2_{error_TOA_Q}$ and $\sigma^2_{error_TOA_M}$ are variances of estimation error due to quantization and multipath, respectively. Additionally, if we assume error due to quantization is uniformly distributed in the range of $\frac{-\Delta t}{2} < error_{TOA_Q} < \frac{\Delta t}{2}$ then the variance of error due to quantization is:

$$\sigma^2_{error_TOA_Q} = \frac{\Delta t^2}{12} \tag{3.6}$$

This value is actually the lower bound for the variance of error as we vary Δt. We can easily write (3.5) in terms of distance rather than time because distance is proportional to time of arrival.

$$\sigma^2_{error_dist} = \sigma^2_{error_dist_Q} + \sigma^2_{error_dist_M} = \frac{\Delta d^2}{12} + \sigma^2_{error_dist_M} \tag{3.7}$$

where, $$\Delta d = \Delta t \times 0.3 \tag{3.9}$$

assuming that light travels at the speed of $0.3\ {}^{m}\!/_{ns}$ in air.

Fig.3-9 illustrates the variance of distance error for the collection of points described above. Notice that as we increase Δ*t* the variance of error increases and it is always above the lower bound determined by the quantization.

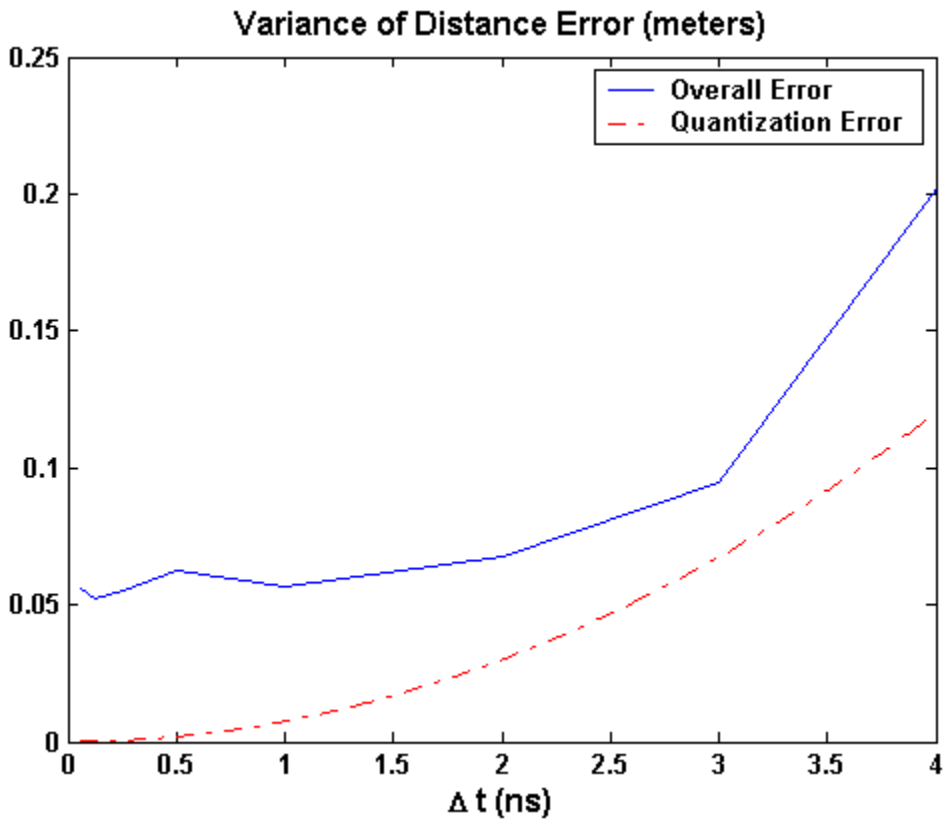

Figure 3-9 Effect of Δ*t*

3.4 Effects of Filtering

In this section, we analyze the effect of filtering on the accuracy of the measurement of the distance error. As described in section 3.1, the sampled measured signal in the frequency domain is first passed through a frequency domain digital filter. The effect of filtering can be examined by changing the filter type while keeping the sampling period in frequency and time domains fixed. Fig. 3-10 to Fig. 3-17 illustrate the frequency and time response of a random point in AK 320 using different type of windows. For all of these figures, Δf=500KHz and Δt 0.0624 ns. Table 6 shows the distance error associated to each filter type for this random point. Note that the accuracy

of distance error changes as we apply different filters. In order to perform statistical analysis on the effect of filtering we collected 32 points that represent LOS and OLOS scenarios, on the third floor of Atwater-Kent Laboratories. We fixed the values of Δf and Δt to 500 KHz and 0.0624 ns, respectively and applied four different filters for each measurement. Table 7 shows the distance error (**E**) for each point due to different type of filters. From Table 7 we see that the variance of error decreases from Rectangular to Bartlett and from Bartlett to Hanning. This phenomenon could be associated to the reduction of the side lobe peak in these filters. However the variance of error is greater with the Hamming window than with the Hanning window, though the Hamming window has a smaller first side lobe. From Fig.3-19, which shows the time responses of the windows, we see that except for the first two side lobes, the Hanning window has smaller side lobes than the Hamming window. This comparison justifies the smaller value in the variance of error for the Hanning window.

Table 6 Results of Measurement for the Random Point in AK320

Filter Type / E (meters)	Rectangular Window	Bartlett Window	Hanning Window	Hamming Window
Random Point	5.38	0.0268	0.008	0.0269

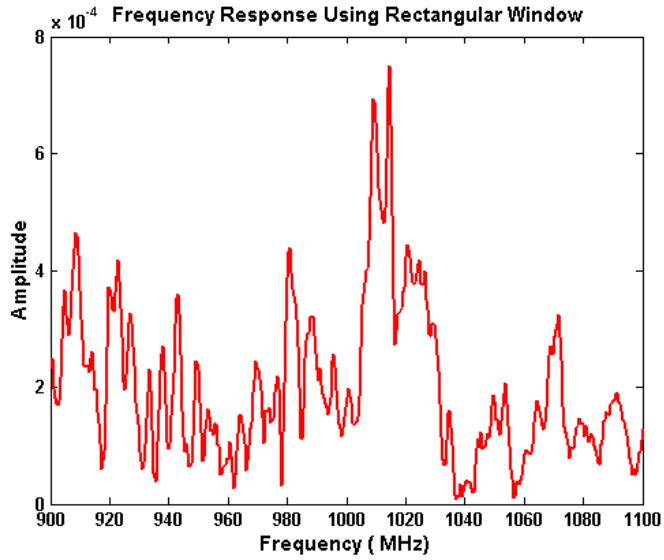

Figure 3-10 Frequency Response after Applying Rectangular Window for the Random Point in AK320

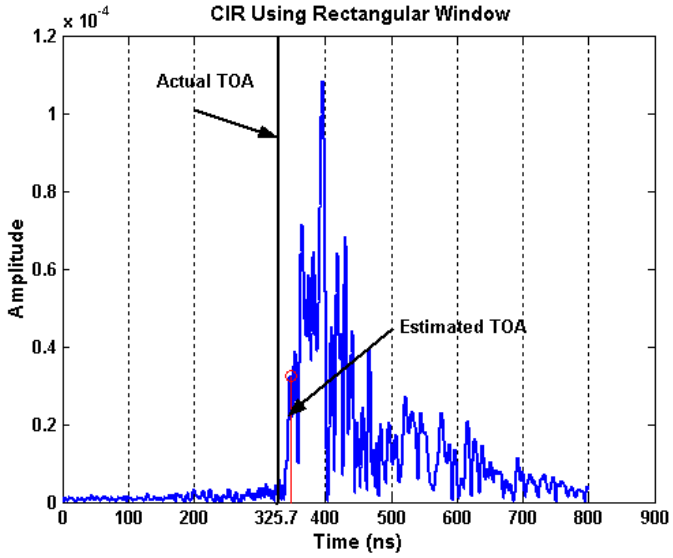

Figure 3-11 Time Response Using Rectangular Window for the Random Point in AK320

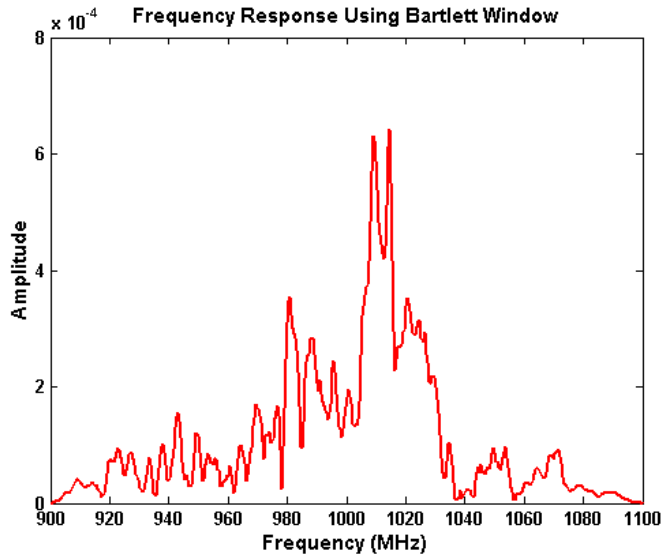

Figure 3-12Frequency Response after Applying Bartlett Window for the Random Point in AK320

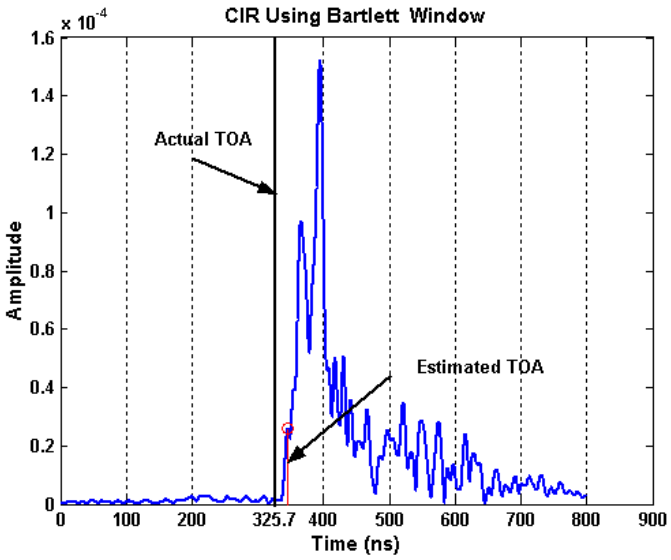

Figure 3-13 Time Response Using Bartlett Window for the Random Point in AK320

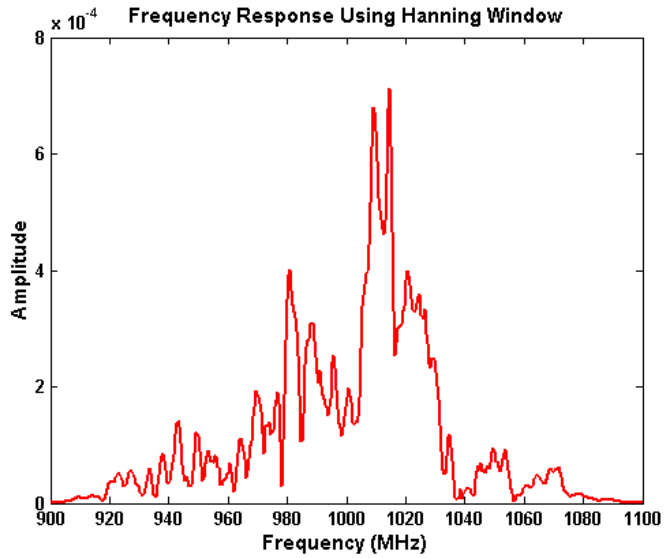

Figure 3-14Frequency Response after Applying Hanning Window for the Random Point in AK320

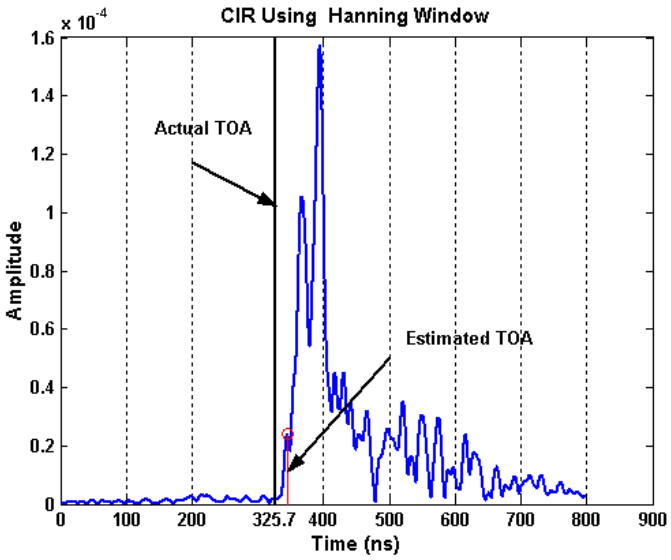

Figure 3-15 Time Response Using Hanning Window for the Random Point in AK320

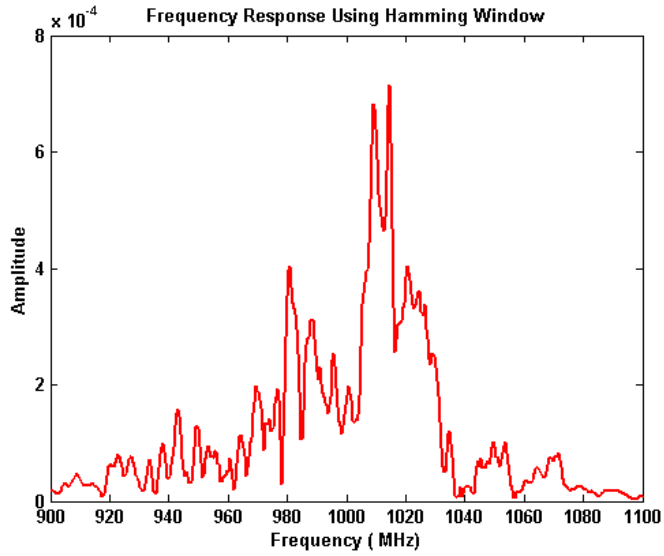

Figure 3-16Frequency Response after Applying Hamming Window for the Random Point in AK320

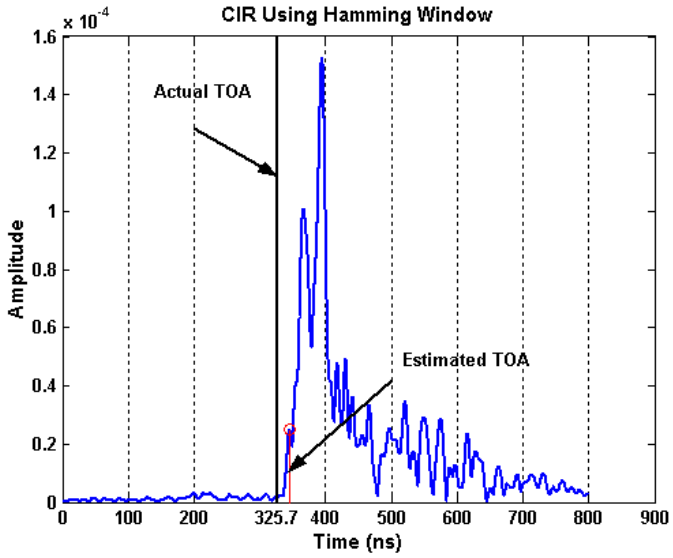

Figure 3-17 Time Response Using Hanning Window for the Random Point in AK320

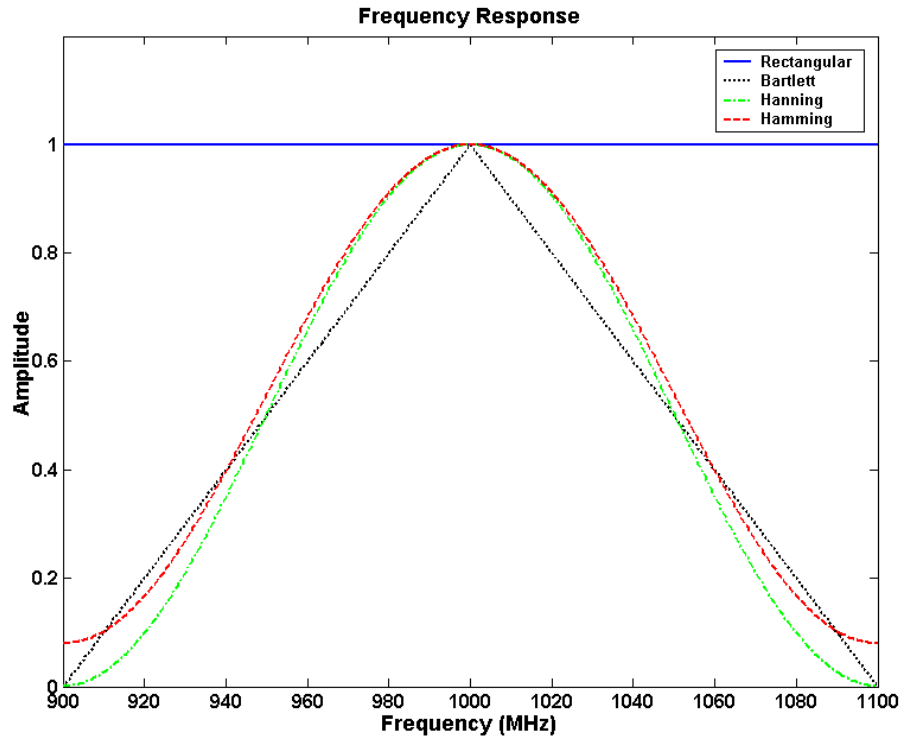

Figure 3-18Frequency Responses of Rectangular (solid blue), Bartlett (dotted black), Hanning (dash dot green) and Hamming Windows (dashed red)

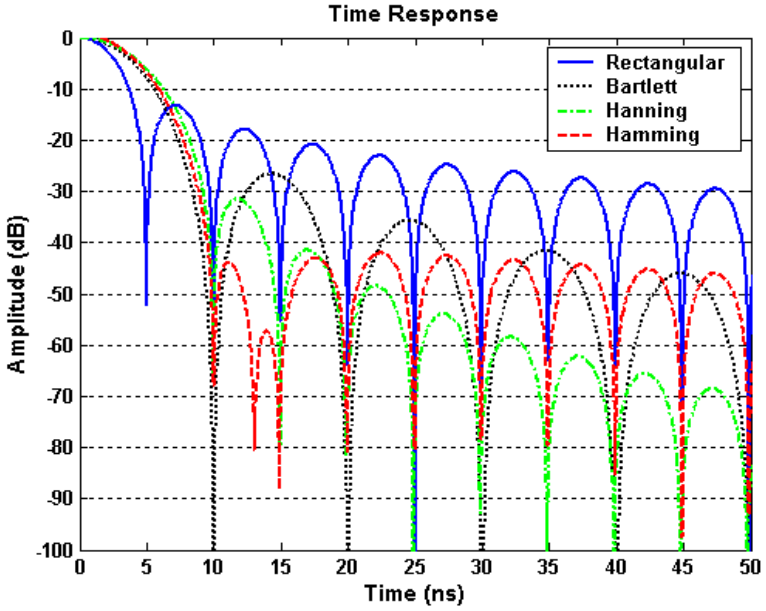

Figure 3-19Time Responses of Rectangular (solid blue), Bartlett (dotted black), Hanning (dash dot green) and Hamming Windows (dashed red)

Table 7 Results of Measurement for a Collection of 32 Points at the Third Floor of Atwater Kent Laboratories for Four Different Types of Filters

Filter Type / E (meters)	Rectangular Window	Bartlett Window	Hanning Window	Hamming Window
Point 1	-6.313	-6.1817	-5.9192	-6.0505
Point 2	-3.7469	-3.2969	-3.1844	-3.2969
Point 3	0.1158	-4.1404	-4.0279	-4.1404
Point 4	-1.4353	-4.5478	-4.3978	-4.5478
Point 5	-1.835	-4.61	-4.1412	-4.9475
Point 6	-1.9432	-4.0807	-3.9307	-4.0432
Point 7	-0.7069	-0.9694	-3.8756	-3.9319
Point 8	-1.723	-1.6667	-1.6105	-1.648
Point 9	-2.7942	-2.888	-2.813	-2.8505
Point 10	-0.8619	-5.8119	-5.5869	-5.6619
Point 11	-3.9073	-6.1011	-6.0261	-6.1011
Point 12	-2.461	-2.3673	-2.5173	-2.5173
Point 13	-2.0687	-1.7312	-1.4312	-1.6187
Point 14	-2.1274	-1.7899	-1.6399	-1.7524
Point 15	-0.7784	-4.3596	-4.4721	-4.4346
Point 16	3.51	-0.077	-0.077	-0.0958
Point 17	3.6	-0.0794	-0.0981	-0.0981
Point 18	5.14	0.0388	0.02	0.02
Point 19	3.54	-0.0414	-0.0789	-0.0976
Point 20	3.47	-0.212	-0.212	-0.212
Point 21	3.64	-0.2625	-0.375	-0.3
Point 22	5.16	0.2449	0.2824	0.2262
Point 23	11.33	0.5453	0.5266	0.5078
Point 24	8.27	0.5392	0.4829	0.4829
Point 25	5.64	0.5184	0.5559	0.5184
Point 26	5.38	0.0268	0.008	0.0269
Point 27	5.32	-0.2127	-0.269	-0.2127
Point 28	8.7	0.1682	0.0932	0.1682
Point 29	5.05	0.1135	0.1135	0.0572
Point 30	3.76	-0.1865	-0.299	-0.224
Point 31	3.77	0.1075	0.1262	0.0887
Point 32	2.1	-0.1563	-0.1938	-0.1751
Variance (meters)	17.6761	4.856442	4.657846	4.951794

Chapter 4 Analysis of Measurements in Different Sites

4.1 Introduction

In indoor positioning environments, we sometimes face a scenario where there is an obstruction between the transmitter and the receiver. The obstructions could be due to the inherent architecture of the indoor environment, such as walls and partitions, which are fixed for the entire period of the measurement process, or due to the temporal movements of objects, such as people walking between the transmitter and the receiver. We refer to these cases as OLOS scenarios. As the signal goes through an obstruction, the signal strength reduces significantly and the direct line of sight (DLOS) path received at the receiver may be weaker than paths arriving from other directions. On the other hand, we have LOS cases in which there is no obstruction between the transmitter and the receiver. In LOS cases, the DLOS path does not face any reflection or diffraction and is only affected by free space path loss. As a result, the DLOS path is always the strongest path in LOS cases. Notice that the DLOS path is always the first path in both OLOS and LOS cases because it reaches the receiver via the shortest route. However, detection of the DLOS path is usually more difficult in OLOS cases due to stronger multipath effects. As a result, we expect more error in distance estimation for OLOS cases. Fig.4-1 and Fig. 4-2 illustrate two sample CIRs for LOS and OLOS cases. The DLOS path is marked by a solid red line in each figure.

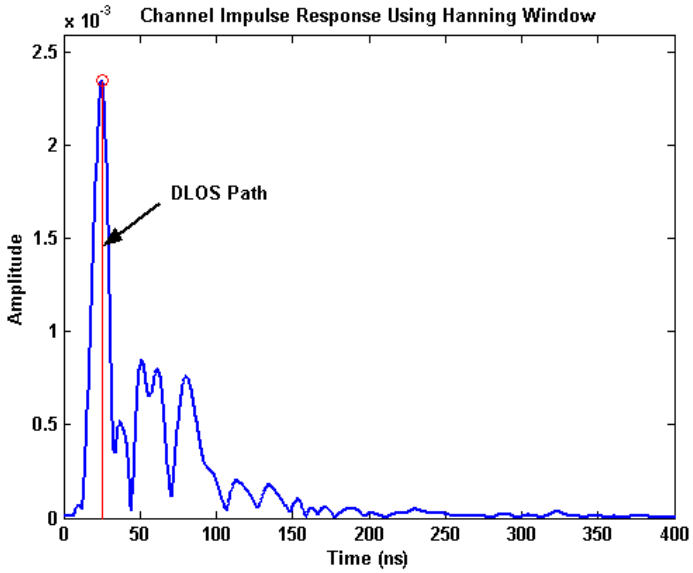

Figure 4-1Channel Impulse Response for a LOS Case

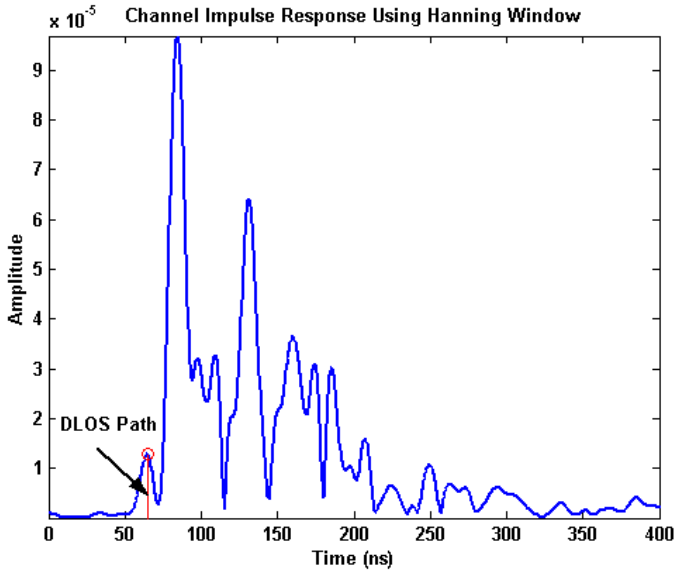

Figure 4-2Channel Impulse Response for a OLOS Case

The main problems limiting the ranging accuracy of an OLOS scenario are illustrated in Figs. 4-3 and 4-4. These figures show two main situations in which the detected first path is not the DLOS path. The first situation is referred to as the undetected direct path

(UDP). In UDP cases, the path joining the transmitting and receiving antennas must cross many obstacles, such as walls and metallic objects, which makes the resulting DLOS path so attenuated that it falls below the measurement system threshold level and it cannot be detected. In this situation, the detected first path will correspond to the shortest indirect path in which several bounces have occurred before reaching the receiver. This case can produce large errors since the TOA of this first detected multipath has no apparent relation to the direct LOS path. The second situation is referred to as non-distinguishable direct path (NDDP). In a NDDP situation, the limited bandwidth of the system makes it impossible to distinguish the LOS path from the first few other paths arriving at the receiver. In this case, the detected TOA of the first path will correspond to a combination of the TOAs of the DLOS path and the first few other paths. The errors in this case should be reasonable since the TOA detected is strongly dependent on the DLOS path [3].

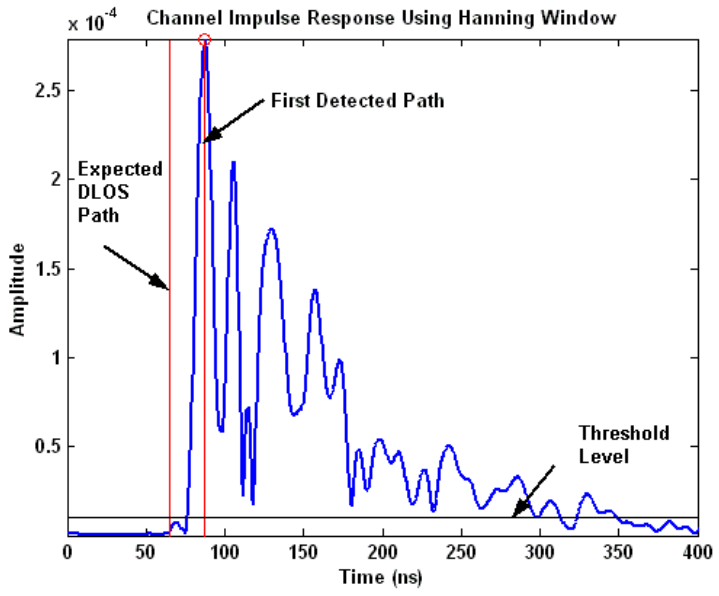

Figure 4-3Undetected Direct Path (UDP)

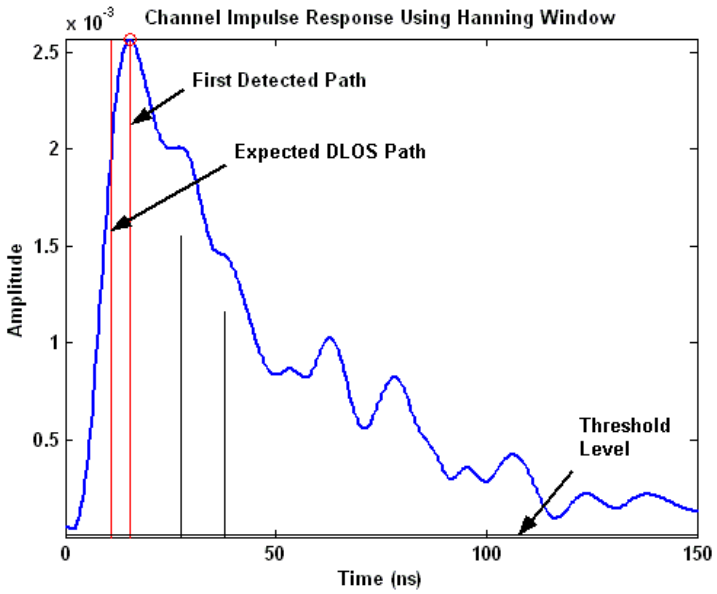

Figure 4-4Non-distinguishable Direct Path (NDDP)

In this chapter, we begin by providing the statistics of measurement results in different environments. These measurements are categorized into two subclasses: LOS and OLOS. We then compare the accuracy of our indoor positioning system in the LOS and OLOS scenarios. Finally, we compare the results of measurements with the ray tracing based model that has been developed previously for indoor geolocation.

4.2 Description of Measurement sites

In order to study the performance of our measurement system, we created a measurement database composed of the measurements that were reported in [5] and the additional measurements that were collected in Atwater Kent Laboratories at 1GHz center frequency with 200MHz of bandwidth. The total number of measurements is 152. 72 of these measurements represent LOS scenarios and the rest correspond to OLOS scenarios. We chose a diverse group of measurement sites so that different indoor positioning scenarios can be represented. LOS measurements were conducted in rooms

219, 311, 320 and the undergraduate lounge of Atwater Kent Laboratories and inside Norton Company. OLOS measurements were taken in Fuller Laboratories, Norton Company and the WPI Guest House. Before giving the results of measurements, we must define some parameters. The parameter E_f is the absolute value of the distance error based on the TOA of the first path while E_s is the absolute value of distance error based on TOA of the strongest path and d is the actual distance. The normalized error E_n is defined as follows:

$$E_n = \frac{error}{d} \tag{4.1}$$

The parameters P_f and P_s are the relative received power of the first path and the strongest path in the receiver, respectively.

4.3 LOS Measurements in AK 219

Room AK 219 is located on the second floor of Atwater Kent Laboratories. It is surrounded by brick walls and metallic windows. The floor is also covered by carpet. The room includes several rows of desks and chairs for students, a large blackboard and a podium. A total of 26 LOS measurements were conducted in Room AK 219 with Δf and Δt set to 500 KHz and 0.5 ns, respectively. Fig.4-5 illustrates the schematic of the measurement site. All the points are within 8 meters of the transmitter, which is located in the center of the hall. Table 8 shows the results of the measurements. It is interesting to see that the values of P_f and Ps are not the same for measurement points at 3,4,5,6, and 9 although there is no obstruction. The reason could be due to the change in the antenna pattern caused by structures around the antenna, such as walls and metallic objects. As

the antenna pattern changes, the DLOS path may be received with lower gain than other paths and thus the first path may not be the strongest path any longer.

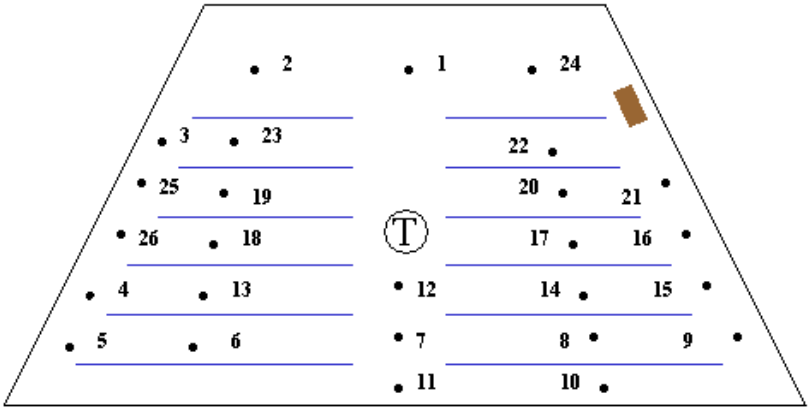

Figure 4-5 Schematic of Measurement Site in AK 219

Table 8 Measurement Results in AK 219

Points	d (meters)	E_n	E_f (meters)	E_s (meters)	P_f (dB)	P_s (dB)
1	3.7084	-0.0214	0.0793	0.0793	-43.1929	-43.1929
2	4.7244	-0.0557	0.2633	0.2633	-43.492	-43.492
3	5.5626	0.1303	0.7249	4.3751	-55.7858	-54.8429
4	6.5278	0.0291	0.1901	4.0099	-52.7899	-52.5571
5	7.8105	0.0541	0.4228	6.0272	-55.7182	-55.6296
6	5.4356	0.0548	0.2979	8.2521	-52.9462	-49.9679
7	3.937	0.076	0.2993	0.2993	-47.3132	-47.3132
8	5.588	0.0537	0.3003	0.3003	-51.1065	-51.1065
9	7.0104	0.096	0.6727	5.9273	-56.0799	-52.695
10	7.9248	0.0299	0.2371	0.2371	-52.6814	-52.6814
11	5.1562	0.12	0.6185	0.6185	-49.7958	-49.7958
12	2.2479	0.1158	0.2602	0.2602	-44.0216	-44.0216
13	3.9497	0.079	0.312	0.312	-48.3764	-48.3764
14	5.2324	0.0181	0.0947	0.0947	-50.7826	-50.7826
15	6.5786	0.0138	0.0909	0.0909	-54.0708	-54.0708
16	6.1087	-0.0129	0.079	0.079	-48.9424	-48.9424
17	3.9116	0.1467	0.5739	0.5739	-49.3752	-49.3752
18	3.5814	0.0681	0.2437	0.2437	-48.2937	-48.2937
19	2.9845	0.0827	0.2468	0.2468	-44.4596	-44.4596
20	3.7338	0.0257	0.0961	0.0961	-46.9001	-46.9001
21	5.969	0.0136	0.0813	0.0813	-49.2054	-49.2054
22	3.1115	0.1201	0.3738	0.3738	-45.5126	-45.5126
23	3.048	0.1018	0.3103	0.3103	-44.9234	-44.9234
24	3.8481	0.0547	0.2104	0.2104	-46.8751	-46.8751
25	5.8039	-0.0144	0.0838	0.0838	-50.2032	-50.2032
26	6.7818	-0.023	0.1559	0.1559	-53.0583	-53.0583

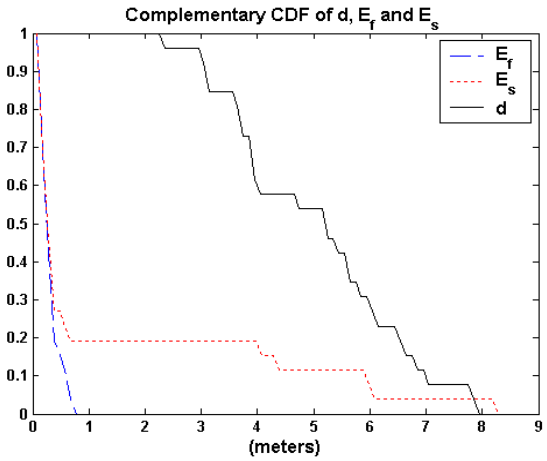

Figure 4-6 Complementary CDFs of the Actual Distance (solid black), the Absolute Value of Error Based on the TOA of the first path (dashed blue) and the Absolute Value of Error Based on the TOA of the Strongest Path (dotted red) in AK 219

Fig. 4-6 compares the complementary CDF of the distance error with the actual distance. Although the actual distance is less than 8 meters, the distance error based on the TOA of the first path is less than 1 meter while the distance error based on the TOA of the strongest path can reach up to 8.25 meters. Here, $\overline{\mathbf{E}_f}$ = 0.2815 meters and **Var**($\mathbf{E}_f$)=0.0352 meters, while $\overline{\mathbf{E}_s}$ = 1.2924 meters and **Var**($\mathbf{E}_s$)=5.3204 meters.

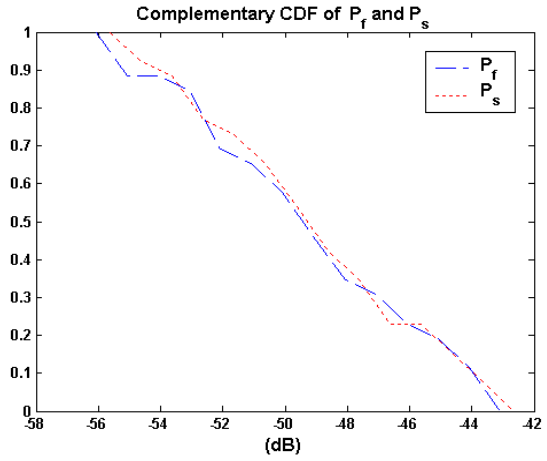

Figure 4-7 Complementary CDFs of the Relative Received Power of the First Path (dashed blue) and the Relative Received Power of the Strongest Path (dotted red) in AK 219

Fig. 4-7 shows the complementary CDFs of relative received power of the first path and the strongest path. These two curves are very close to one another and the figure shows that the relative received powers vary in the range of 43dB to 56 dB.

4.4 LOS Measurements in AK 311

Room AK 311 is located on the third floor of Atwater Kent Laboratories. It is a small conference room that includes two blackboards, one desk and several chairs around the desk. The space is surrounded by bricks wall and metallic window frames and in addition to the fluorescent lights; many utility pipes and metallic support beams hang from the ceiling. The floor is covered by carpet. Six LOS measurements were conducted in AK 311 with Δf and Δt set to 125KHz and 0.5ns, respectively. Fig. 4-8 illustrates the schematic of the measurement site. All the points are within 2.5 meters of distance from the transmitter, which is located in the center of the room. Table 9 shows the results of measurements and we see that for the entire set of points the received first path is indeed the strongest path. Fig.4-9 compares the complementary CDF of error with the actual distance. In this case the error is less than half a meter. Here, $\overline{\mathbf{E}_f} = \overline{\mathbf{E}_s} = 0.2871$ meters and $\mathbf{Var}(\mathbf{E}_f) = \mathbf{Var}(\mathbf{E}_s) = 0.0234$meters. Fig.4-10 shows the complementary CDFs of relative received power of the first path and the strongest path. In fact in this case, these two curves are identical and the measured path loss is between 41 dB and 46 dB.

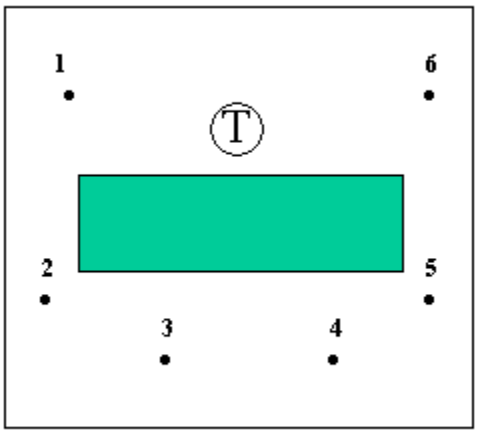

Figure 4-8 Schematic of Measurement Site in AK 311

Table 9 Measurement Results in AK 311

Points	d (meters)	E_n	E_f (meters)	E_s (meters)	P_f (dB)	P_s (dB)
1	1.6129	-0.0464	0.0748	0.0748	-42.2117	-42.2117
2	1.9812	0.1482	0.2935	0.2935	-44.2055	-44.2055
3	2.2606	0.1871	0.4229	0.4229	-45.6768	-45.6768
4	2.1082	0.1995	0.4205	0.4205	-45.648	-45.648
5	2.3114	-0.0546	0.1263	0.1263	-42.044	-42.044
6	2.2225	0.1731	0.3848	0.3848	-42.2523	-42.2523

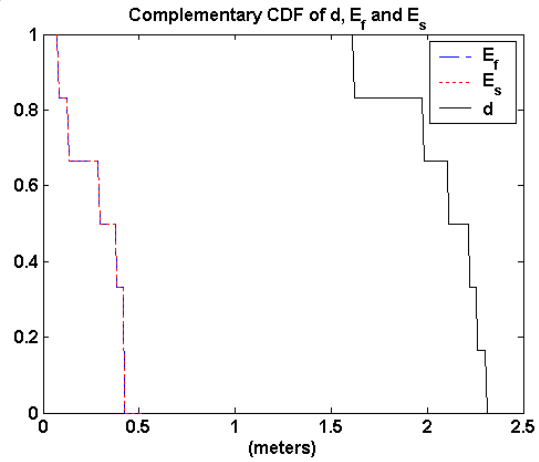

Figure 4-9 Complementary CDFs of the Actual Distance (solid black), the Absolute Value of Error Based on the TOA of the first path (dashed blue) and the Absolute Value of Error Based on the TOA of the Strongest Path (dotted red) in AK 311

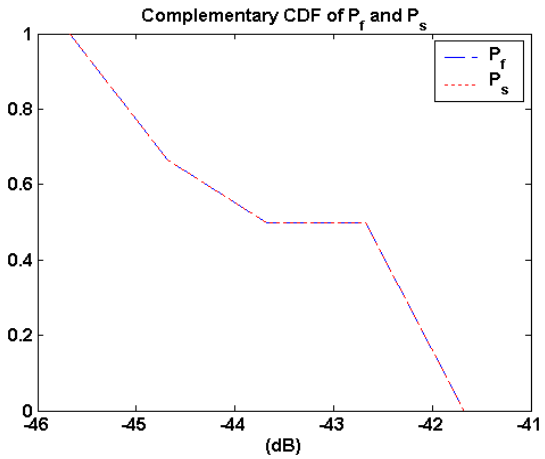

Figure 4-10 Complementary CDFs of the Relative Received Power of the First Path (dashed blue) and the Relative Received Power of the Strongest Path (dotted red) in AK 311

4.5 LOS Measurements in the Undergraduate Lounge

The Undergraduate Lounge is located on the first floor of Atwater Kent Laboratories. It is surrounded by brick walls and wooden window frames. The floor is covered by carpet. In addition to the fluorescent lights, many utility pipes and metallic support beams hang from the ceiling. The Lounge includes tables and couches for undergraduate students. 14 LOS measurements were conducted in Undergraduate Lounge with Δf and Δt set to 500KHz and 0.5ns, respectively. Fig. 4-11 illustrates the schematic of the measurement site. All the points are within 8 meters of distance from transmitter, which is located in the center of the lounge. Table 10 shows the results of measurements and we see that for this measurement set, the received first path is the strongest path. Fig. 4-12 compares the complementary CDF of error with the actual distance. In this case the error is less than 1.5 meters. Here, $\overline{\mathbf{E}_f} = \overline{\mathbf{E}_s} = 0.3430$ meters and $\mathbf{Var}(\mathbf{E}_f) = \mathbf{Var}(\mathbf{E}_s) = 0.1323$ meters.

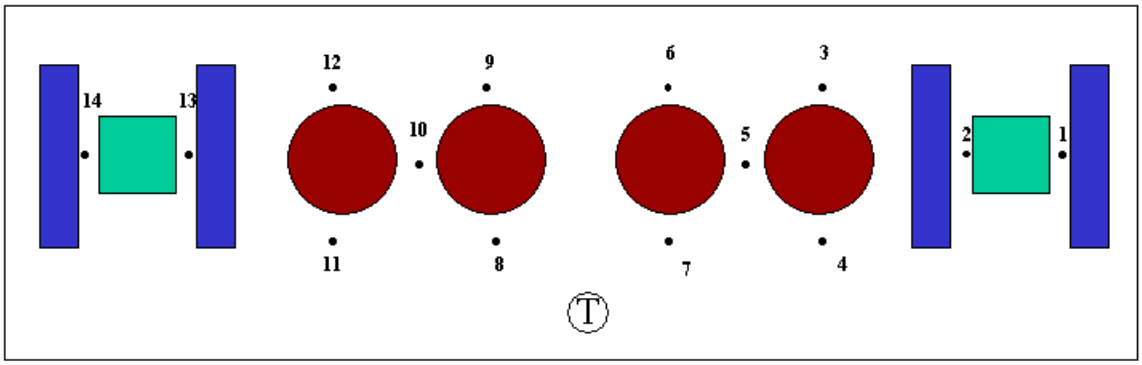

Figure 4-11 Schematic of Measurement Site in Undergraduate Lounge of ECE Dept.

Table 10 Measurement Results in Undergraduate Lounge

Points	d (meters)	E_n	E_f (meters)	E_s (meters)	P_f (dB)	P_s (dB)
1	6.8834	-0.0951	0.6543	0.6543	-52.5831	-52.5831
2	5.4864	-0.0185	0.1013	0.1013	-49.7365	-49.7365
3	3.4798	-0.0885	0.3079	0.3079	-42.91	-42.91
4	3.2639	0.0234	0.0762	0.0762	-43.9628	-43.9628
5	2.3876	0.0418	0.0999	0.0999	-42.6229	-42.6229
6	1.9939	0.1536	0.3062	0.3062	-42.944	-42.944
7	1.1811	0.0791	0.0934	0.0934	-36.1619	-36.1619
8	1.9558	0.2905	0.5681	0.5681	-43.3106	-43.3106
9	2.8067	-0.0823	0.231	0.231	-45.6188	-45.6188
10	3.0226	0.0943	0.2849	0.2849	-43.8305	-43.8305
11	4.1021	-0.0549	-0.2251	-0.2251	-42.3486	-42.3486
12	4.2926	-0.0571	0.2451	0.2451	-42.9886	-42.9886
13	6.2865	0.0157	0.0988	0.0988	-50.9107	-50.9107
14	7.6454	-0.1821	1.3923	1.3923	-53.0731	-53.0731

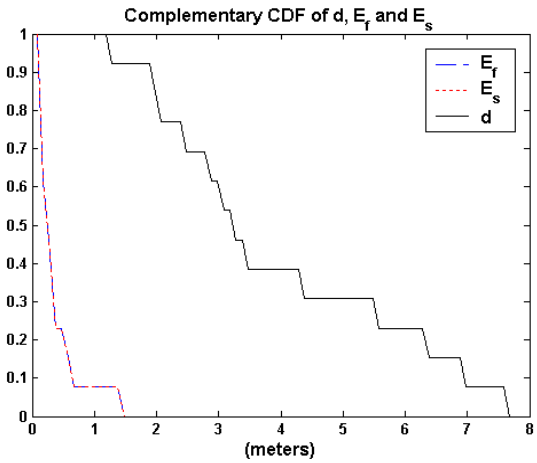

Figure 4-12 Complementary CDFs of the Actual Distance (solid black), the Absolute Value of Error Based on the TOA of the first path (dashed blue) and the Absolute Value of Error Based on the TOA of the Strongest Path (dotted red) in Undergraduate Lounge

Fig. 4-13 shows the complementary CDFs of relative received power of the first path and the strongest path. In fact in this case, these two curves are identical and it shows that the path loss measured is between 36 dB and 53 dB.

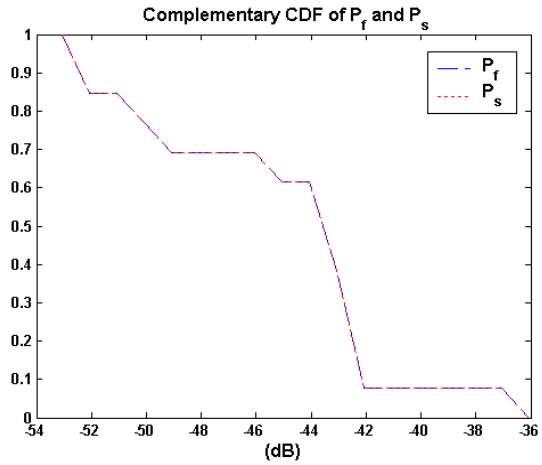

Figure 4-13 Complementary CDFs of the Relative Received Power of the First Path (dashed blue) and the Relative Received Power of the Strongest Path (dotted red) in AK 311

4.6 LOS Measurements in AK 320

Room AK 320 is a research laboratory on the third floor of Atwater Kent Laboratories in WPI and is much like a typical office environment. AK 320 includes office desks for the students, file cabinets and metallic window frames and doors. In addition to the fluorescent lights, many utility pipes and metallic support beams hang from the ceiling.16 measurements were conducted with Δf and Δt set to 125KHz and 0.5 ns, respectively. Fig. 4-14 illustrates the schematic of the measurement site. All the points are within 5 meters of distance from transmitter, which is located in the center of the lab. Table 11 the shows the results of measurements and we see that for all the measured points the received first path is indeed the strongest path. Fig. 4-15 compares the complementary CDF of error with the actual distance .In this case we have an error in estimating distance as great as 2.3 meters even though we are in an LOS environment. This could be associated with the severe effect of multipath along with limited bandwidth of the system, which causes a large shift in the detected time of arrival with respect to actual first path. Here, $\overline{\mathbf{E}}_f = \overline{\mathbf{E}}_s$ = 0.4559 meters and $\mathbf{Var}(\mathbf{E}_f) = \mathbf{Var}(\mathbf{E}_s)$=0.3090 meters. Fig.4-16 shows the complementary CDFs of relative received power of the first path and the strongest path. In fact in this case, these two curves are identical and the measured path loss is between 36 dB and 49 dB.

Figure 4-14 Schematic of Measurement Site in AK 320

Table 11 Measurement Results in AK 320

Points	d (meters)	E_n	E_f (meters)	E_s (meters)	P_f (dB)	P_s (dB)
1	1.9939	-0.1338	0.2668	0.2668	-42.7487	-42.7487
2	1.2232	-0.1128	0.138	0.138	-37.2176	-37.2176
3	1.5290	-0.1844	0.2819	0.2819	-36.7212	-36.7212
4	2.2052	-0.0252	0.0555	0.0555	-41.1527	-41.1527
5	3.0118	0.1001	0.3014	0.3014	-45.1668	-45.1668
6	3.8682	-0.592	2.29	2.29	-44.082	-44.082
7	4.7474	-0.1393	0.6613	0.6613	-47.6028	-47.6028
8	5.0620	0.05	0.2529	0.2529	-48.4367	-48.4367
9	2.8194	-0.0145	0.0409	0.0409	-44.3506	-44.3506
10	3.5663	-0.1803	0.6431	0.6431	-39.495	-39.495
11	4.3785	-0.2353	1.0302	1.0302	-40.9571	-40.9571
12	4.0800	-0.0317	0.1295	0.1295	-44.3594	-44.3594
13	3.9755	-0.0588	0.2339	0.2339	-43.2243	-43.2243
14	4.0800	0.0418	0.1704	0.1704	-47.6069	-47.6069
15	3.1927	-0.1776	0.567	0.567	-40.4572	-40.4572
16	2.3289	-0.0994	0.2315	0.2315	-41.4455	-41.4455

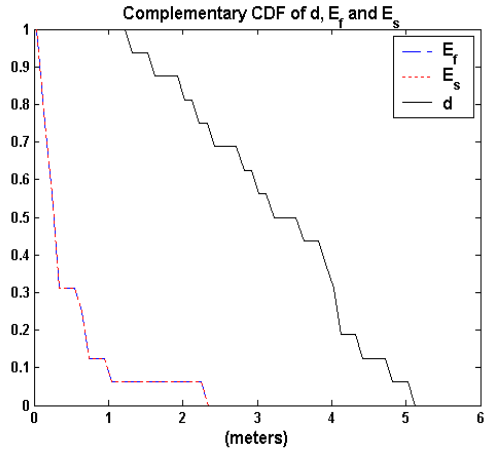

Figure 4-15 Complementary CDFs of the Actual Distance (solid black), the Absolute Value of Error Based on the TOA of the first path (dashed blue) and the Absolute Value of Error Based on the TOA of the the Strongest Path (dotted red) in AK 320

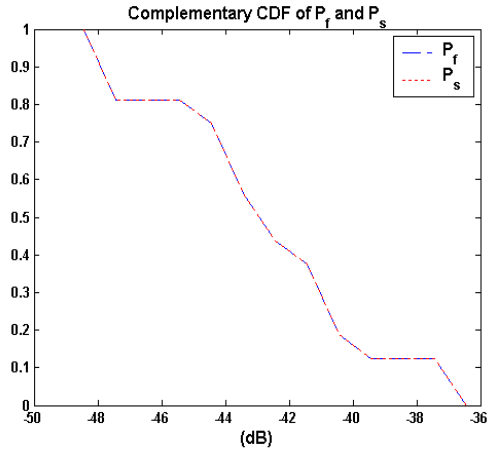

Figure 4-16 Complementary CDFs of the Relative Received Power of the First Path (dashed blue) and the Relative Received Power of the Strongest Path (dotted red) in AK 320

4.7 LOS Measurements in Norton Company (indoor to indoor)

Norton Company is a manufacturer of welding equipment and abrasives for grinding machines. The building selected for measurement is Plant 7 that is a large building with dimensions on the order of a few hundred meters. This building is

connected to a five-floor brick building and to another manufacturing floor through a long corridor. The remainder of Plant 7 is surrounded mainly by open areas and small buildings. The building is used for manufacturing abrasives and inside the building are huge ovens, grinding machines, transformers, cranes and other heavy machinery. The building includes a set of partitioned offices with brick external walls, metallic windows and doors attached to the main huge open manufacturing area with steel sheet walls of a height around seven meters and small metallic windows near the ceiling. In addition to the fluorescent lights, many utility pipes and metallic support beams hang from the ceiling [5]. A total of 15 measurements were conducted inside Norton Company with Δf and Δt set to 500KHz and 0.5 ns, respectively. Fig4-17 illustrates the schematic of the measurement site. Among these measurements, 10 represented the LOS scenarios and they are reflected in Table 12. From Table 12 we also see that for all the measurement points, the received first path is the same as the strongest path.

Fig.4-18 compares the complementary CDF of error with the actual distance. It is interesting to see that the error stays below a meter while the actual distance is as high as 38 meters. Here, $\overline{\mathbf{E}}_f = \overline{\mathbf{E}}_s$ = 0.2456 meters and $\mathbf{Var}(\mathbf{E}_f) = \mathbf{Var}(\mathbf{E}_s)$=0.0371 meters. Fig.4-19 shows the complementary CDFs of relative received power of the first path and the strongest path. In fact in this case, these two curves are identical and the measured path loss is between 50 dB and 80 dB.

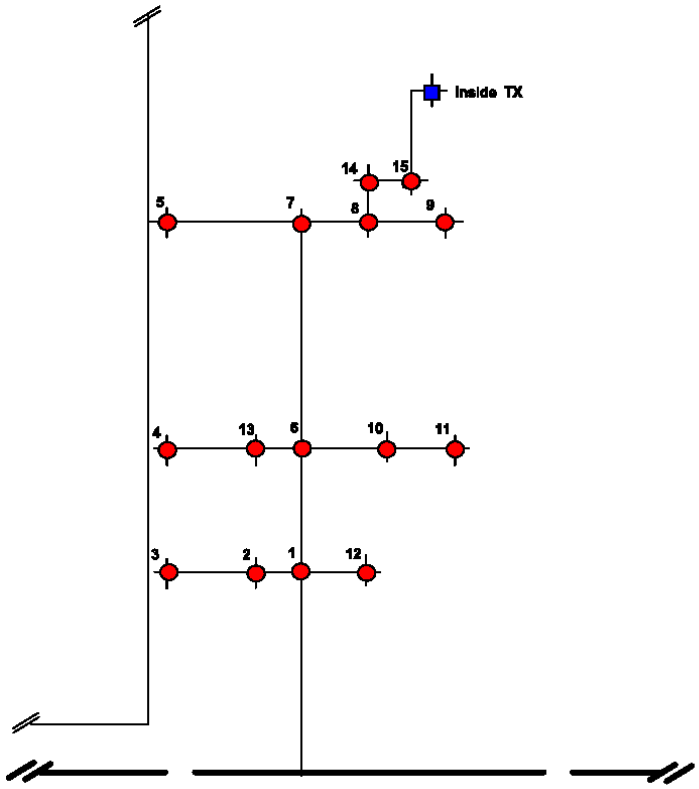

Figure 4-17 Schematic of Measurement Site in Norton Company (indoor to indoor)

Table 12 Measurement Results in Norton Company (indoor to indoor)

Points	d (meters)	E_n	E_f (meters)	E_s (meters)	P_f (dB)	P_s (dB)
2	35.685	0.0038	0.135	0.135	-76.4088	-76.4088
3	38.2165	0.003	0.1165	0.1165	-78.4364	-78.4364
7	12.932	0.0071	0.092	0.092	-58.8804	-58.8804
8	10.2175	0.0223	0.2275	0.2275	-55.2894	-55.2894
9	9.272	0.0617	0.572	0.572	-56.3235	-56.3235
10	24.583	-0.019	0.467	0.467	-62.1418	-62.1418
12	33.855	-0.0013	0.045	0.045	-68.2495	-68.2495
13	27.267	-0.0155	0.423	0.423	-72.0699	-72.0699
14	7.625	0.0046	0.035	0.035	-52.0726	-52.0726
15	6.283	0.0546	0.343	0.343	-51.1378	-51.1378

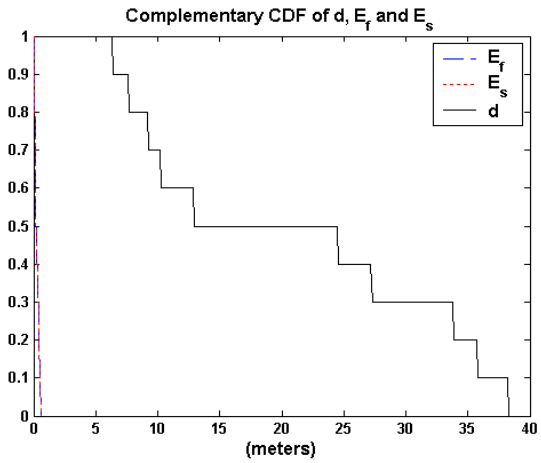

Figure 4-18 Complementary CDFs of the Actual Distance (solid black), the Absolute Value of Error Based on the TOA of the first path (dashed blue) and the Absolute Value of Error Based on the TOA of the Strongest Path (dotted red) in Norton Company (indoor to indoor)

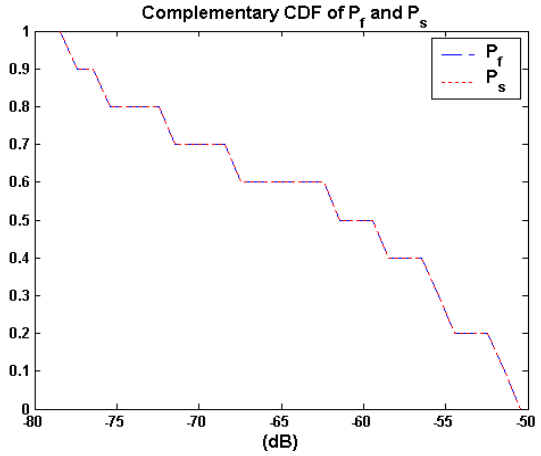

Figure 4-19 Complementary CDFs of the Relative Received Power of First Path (dashed blue) and the Relative Received Power of the Strongest Path (dotted red) in Norton Company (indoor to indoor)

4.8 OLOS measurements in Fuller Laboratories

Fuller Laboratories is a modern building that houses the Computer Science department at WPI and has been selected as the site for measurements applicable to office areas. The dimensions of this building are on the order of a few tens of meters. It is surrounded on two sides by older WPI buildings (the Atwater Kent Laboratories and the

Gordon Library) and by roads on the other two sides. One of the roads is an internal WPI campus driveway on the other side of which is the Salisbury Laboratories. The other road is a major city street with an open park on the other side. The external walls of Fuller Laboratories are made of brick with some aluminum siding on two sides, metallic window frames and doors. Within the building are several computer labs, department offices, offices of faculty and graduate students, lecture halls, and classrooms. The walls are made of sheetrock and in some offices, soft partitions divide the room into cubicles. Most of the rooms have furniture such as tables, chairs and desks as well as computers. Some conference rooms have glass walls mounted in metallic frames [5]. Three different scenarios are considered in this part of study: indoor to indoor, outdoor to indoor and outdoor to floor. For the indoor to indoor scenario, both transmitter and receiver were in the ground floor of Fuller laboratories. The second measurement scenario, outdoor to indoor, was conducted by positioning the transmitter outside of Fuller laboratories and moving the receiver about the ground floor. Fig. 4-20 (a) represents the schematic for these two cases. In the third scenario, outdoor to floor, the transmitter was placed outside the building and the receiver was moved among several locations of the first floor of the Fuller laboratories. The first floor was 4.15 meters higher than the ground floor. Fig.4-20 (b) represents the schematic of the third scenario. In the following sections we provide the statistics of the measurement results.

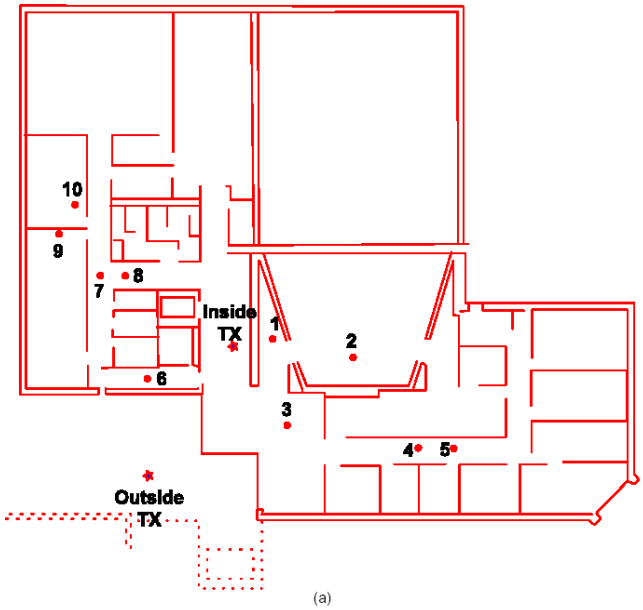

(a)

(b)

Figure 4-20 Schematic of Measurement Site in Fuller Laboratories. (a) shows indoor to indoor and outdoor to indoor cases.(b) shows outdoor to floor scenario.

4.8.1 Indoor to Indoor OLOS Measurements in Fuller Laboratories

As depicted in Fig.4-20(a), 10 indoor to indoor OLOS measurements were conducted in the ground floor of Fuller Laboratories. Parameters Δf and Δt were set to 1MHz and 0.5 ns, respectively. Table 13 shows the measurement results. It is interesting to see that for points 1 and 5, the first path is the strongest path though we are dealing with OLOS scenario. In fact in OLOS scenarios we may face with cases that DLOS path as well as other paths go through obstruction such that DLOS path becomes strongest path in the receiver side. Also the great amount of error (E_f) that we observe for points 4 and 5 is due to undetected direct path. (Refer to Appendix B for the channel profiles.) Fig.4-21 compares the complementary CDF of error with the actual distance. Distance error based on the TOA of the first path is up to 6.7 meters and distance error based on the TOA of the strongest path can reach even up to 18.3 meters though the actual distance is less than 17 meters. Here, $\overline{\mathbf{E}_f}$ = 2.5997 meters and $\mathbf{Var}(\mathbf{E}_f)$=4.0770 meters, while $\overline{\mathbf{E}_s}$ = 8.1530 meters and $\mathbf{Var}(\mathbf{E}_s)$=28.0056 meters. Fig. 4-19 shows the complementary CDFs of relative received power of the first path and the strongest path. In this case, path loss of the first path is between 50 dB and 100 dB while path loss of the strongest path is between 50 dB and 80 dB.

Table 13 Measurement Results in Fuller Laboratories (indoor to indoor)

Points	d (meters)	E_n	E_f (meters)	E_s (meters)	P_f (dB)	P_s (dB)
1	3.233	-0.4142	1.339	1.339	-51.7987	-51.7987
2	9.3635	-0.2572	2.4085	6.4585	-65.5664	-64.6287
3	7.564	0.0584	0.442	13.058	-61.8138	-58.534
4	16.5615	-0.3267	5.4105	12.6105	-71.9935	-71.4818
5	19.459	-0.345	6.713	6.713	-71.0931	-71.0931
6	7.564	0.1378	1.042	1.808	-74.8572	-61.7756
7	12.261	-0.0702	0.861	4.611	-81.926	-66.0755
8	10.431	-0.2292	2.391	8.241	-69.8979	-67.6659
9	16.226	-0.1785	2.896	18.346	-83.8552	-80.9002
10	16.9275	-0.1474	2.4945	8.3445	-97.7882	-80.2786

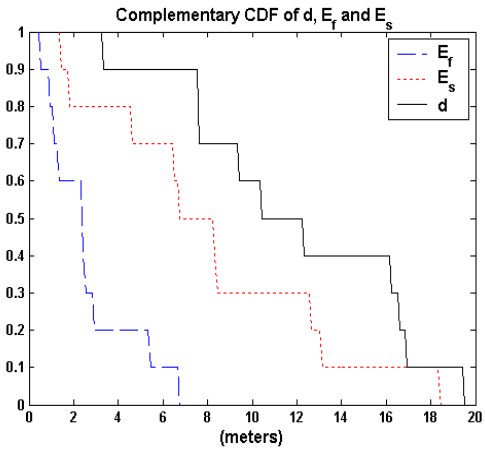

Figure 4-21 Complementary CDFs of the Actual Distance (solid black), the Absolute Value of Error Based on the TOA of the first path (dashed blue) and the Absolute Value of Error Based on the TOA of the Strongest Path (dotted red) in Fuller Laboratories (indoor to indoor)

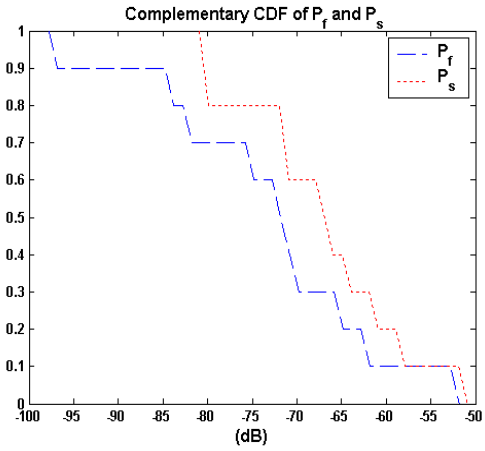

Figure 4-22 Complementary CDFs of the Relative Received Power of the First Path (dashed blue) and the Relative Received Power of the Strongest Path (dotted red) in Fuller Laboratories (indoor to indoor)

4.8.2 Outdoor to Indoor OLOS Measurements in Fuller Laboratories

As depicted in Fig.4-20 (a), 10 outdoor to indoor OLOS measurements were conducted within 26 meters of distance. Parameters Δf and Δt were set to 1MHz and 0.5 ns, respectively. Table 14 shows the measurement results. Again we see that for five

of the measurement points, the first path is the strongest path though we are dealing with the OLOS scenario. Also the great amount of error (E_f) that we observe for point 8 is due to an undetected direct path. (Refer to Appendix B for the channel profile.)

Fig. 4-23 compares the complementary CDF of error with the actual distance. Distance error based on the TOA of the first path is up to 6 meters and distance error based on the TOA of the strongest path can reach even up to 16 meters while the actual distance is less than 26 meters. This result is very close to what we saw in the Fuller indoor to indoor scenario. Here, $\overline{\mathbf{E}}_f$ = 2.0649 meters and $\mathbf{Var}(\mathbf{E}_f)$=4.5741 meters, while $\overline{\mathbf{E}}_s$ = 6.3540 meters and $\mathbf{Var}(\mathbf{E}_s)$=32.0586 meters. Fig 4-24 shows the complementary CDFs of relative received power of the first path and the strongest path. In this case, path loss of the first path is between 63 dB and 94 dB while path loss of the strongest path is between 63 dB and 85 dB.

Table 14 Measurement Results in Fuller Laboratories (outdoor to indoor)

Points	d (meters)	E_n	E_f (meters)	E_s (meters)	P_f (dB)	P_s (dB)
1	15.067	-0.1505	2.267	7.217	-81.5605	-77.6183
2	19.398	0.0059	0.114	6.186	-90.0337	-81.7509
3	12.0475	0.0966	1.1635	15.7865	-74.2543	-69.7866
4	22.387	0.018	0.403	0.403	-74.211	-74.211
5	25.2235	0.0095	0.2395	0.2395	-73.8911	-73.8911
6	8.0825	-0.0868	0.7015	0.7015	-63.0265	-63.0265
7	17.1105	0.0658	1.1265	9.3735	-92.5275	-78.379
8	16.7445	-0.3577	5.9895	14.9895	-99.5671	-84.4909
9	21.4415	-0.2492	5.3425	5.3425	-76.8553	-76.8553
10	23.3325	-0.1415	3.3015	3.3015	-85.9862	-85.9862

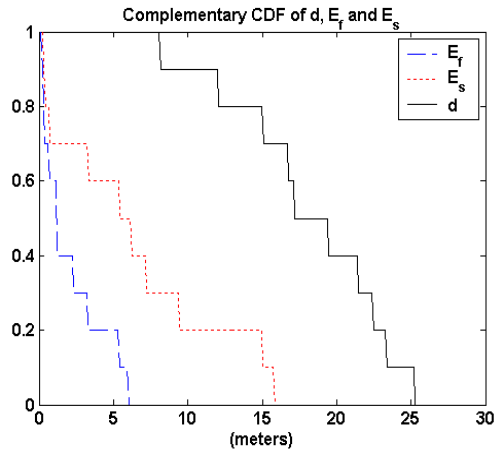

Figure 4-23 Complementary CDFs of the Actual Distance (solid black), the Absolute Value of Error Based on the TOA of the first path (dashed blue) and the Absolute Value of Error Based on the TOA of the Strongest Path (dotted red) in Fuller Laboratories (outdoor to indoor)

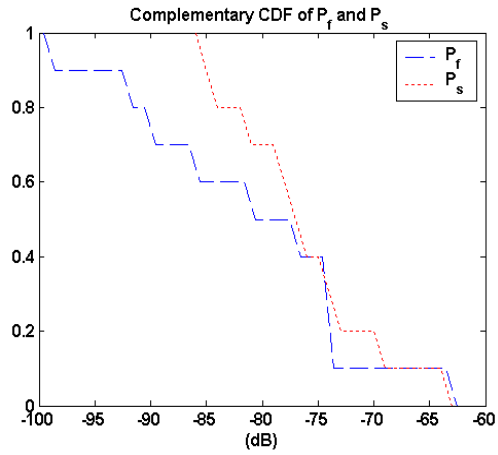

Figure 4-24 Complementary CDFs of the Relative Received Power of the First Path (dashed blue) and the Relative Received Power of the Strongest Path (dotted red) in Fuller Laboratories (outdoor to indoor)

4.8.3 Outdoor to Floor OLOS Measurements in Fuller Laboratories

As depicted in Fig.4-20 (b), 10 outdoor to floor OLOS measurements were conducted in Fuller Laboratories. Parameters Δf and Δt were set to 1MHz and 0.5 ns, respectively. Table 15 shows the measurement results. Again we see that for three of the measurement points, the first path is the strongest path. Also the great amount of error

(E_f) that we observe for points 8 and 10 is due to undetected direct path. (Refer to Appendix B for the channel profiles.) Fig. 4-25 compares the complementary CDF of error with the actual distance. Distance error based on the TOA of the first path is up to 7 meters and distance error based on the TOA of the strongest path can reach even up to 26 meters while the actual distance is less than 23 meters. Here, $\overline{\mathbf{E}}_f$ = 1.6559 meters and **Var**($\mathbf{E}_f$)=4.9193 meters, while $\overline{\mathbf{E}}_s$ = 8.4558 meters and **Var**($\mathbf{E}_s$)=64.7715 meters .We also observe that the complementary CDF of E_f for outdoor to floor and outdoor to indoor cases are very similar. Fig. 4-26 shows the complementary CDFs of relative received power of the first path and the strongest path. In this case, path loss of first path is between 69 dB and 94 dB while the path loss of the strongest path is between 69 dB and 89 dB. From Fig 4-.26, we observe that complementary CDFs of P_f and P_s in outdoor to floor are very similar to the ones in outdoor to indoor scenario.

Table 15 Measurement Results in Fuller Laboratories (outdoor to floor)

Points	d (meters)	E_n	E_f (meters)	E_s (meters)	P_f (dB)	P_s (dB)
1	10.126	0.0425	0.43	6.02	-79.8032	-75.4396
2	11.163	-0.097	1.083	1.083	-75.2069	-75.2069
3	13.8165	0.016	0.2205	10.5795	-83.8927	-80.8717
4	16.348	-0.006	0.098	11.198	-93.4766	-86.1604
5	12.9015	-0.0538	0.6945	4.4445	-75.7059	-71.5524
6	8.9365	0.0325	0.2905	0.2905	-69.0728	-69.0728
7	11.6815	-0.074	0.8645	0.8645	-73.6437	-73.6437
8	14.1825	-0.4769	6.7635	25.9635	-91.6157	-88.2587
9	19.093	-0.0813	1.553	16.403	-90.5938	-88.8687
10	22.2345	-0.2052	4.5615	7.7115	-89.6907	-86.4458

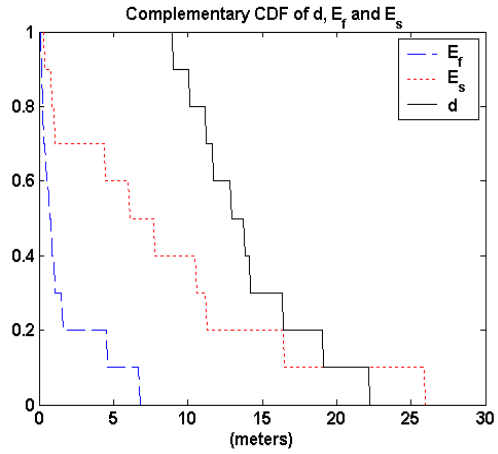

Figure 4-25 Complementary CDFs of the Actual Distance (solid black), the Absolute Value of Error Based on the TOA of the first path (dashed blue) and the Absolute Value of Error Based on the TOA of the Strongest Path (dotted red) in Fuller Laboratories (outdoor to floor)

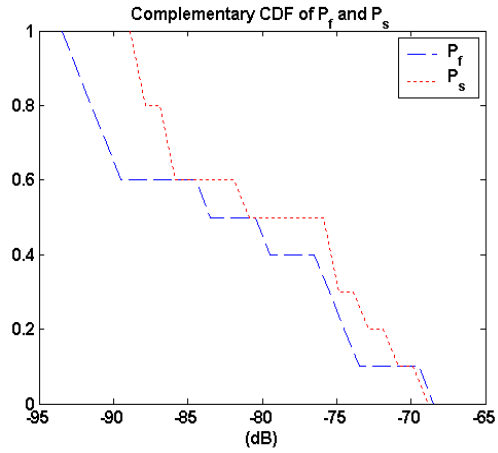

Figure 4-26 Complementary CDFs of Relative Received Power of the First Path (dashed blue) and the Relative Received Power of the Strongest Path (dotted red) in Fuller Laboratories (outdoor to floor)

4.9 OLOS measurements in the WPI Guest House

Schussler house on Schussler Road is a part of the residences available at WPI for visitors. This is a fairly big residential house with wooden exterior walls and sheetrock interior walls. The house is however very old and some portions of the external walls are made of stone. The house is located in a fairly open area with a few buildings of similar

features located nearby. Some trees and a parking lot are at other sides of the house. Inside, there are several rooms that are furnished (with couches, tables, chairs etc.). Some rooms have brick fireplaces. Rooms have dimensions on the order of a few meters [5]. Three different scenarios are considered in this part of study: indoor to indoor, outdoor to indoor and outdoor to floor. For the indoor to indoor scenario, both transmitter and receiver were positioned in the first floor of the Guest House. The second scenario, outdoor to indoor, was conducted by placing the transmitter outside of the Guest House and moving the receiver among various positions in the second floor. Fig. 4-27 (a) represents the schematic for these two cases.

Figure 4-27 Schematic of Measurement Site in WPI Guest House. (a) shows indoor to indoor and outdoor to indoor cases.(b) shows outdoor to floor scenario.

In the third scenario, outdoor to floor, the transmitter was placed outside the building and the receiver was moved among several locations on the second floor of the Guest House. Fig4-27 (b) represents the schematic of the third scenario. In the following sections we provide the statistics of the measurement results.

4.9.1 Indoor to Indoor OLOS Measurements in the Guest House

As depicted in Fig.4-27 (a), 10 indoor to indoor OLOS measurements were conducted in the first floor of Guest House. The actual distances are within 10 meters. Parameters Δf and Δt were set to 1MHz and 0.5 ns, respectively. Table 16 shows the measurement results. Except for point 9, in all other points the first path is the strongest path. Fig. 4-.28 compares the complementary CDF of error with the actual distance. Distance error based on the TOA of the first path is less than 0.6 meters and distance error based on the TOA of the strongest path can reach up to 1.5 meters. Here, $\overline{\mathbf{E}}_f$ = 0.3413 meters and $\mathbf{Var}(\mathbf{E}_f)$=0.0353 meters, while $\overline{\mathbf{E}}_s$ = 0.4159 meters and $\mathbf{Var}(\mathbf{E}_s)$=0.1590 meters. Fig 4-29 shows the complementary CDFs of relative received power of the first path and the strongest path. In this case, path losses of the first path and the strongest path are between 53 dB and 78 dB.

Table 16 Measurement Results in the Guest House (indoor to indoor)

Points	d (meters)	E_n	E_f (meters)	E_s (meters)	P_f (dB)	P_s (dB)
1	7.442	0.043	0.32	0.32	-60.1036	-60.1036
2	4.392	0.0615	0.27	0.27	-56.3898	-56.3898
3	4.27	-0.1059	0.452	0.452	-63.8965	-63.8965
4	4.636	0.1109	0.514	0.514	-64.033	-64.033
5	6.832	-0.0205	0.14	0.14	-64.5396	-64.5396
6	3.66	0.0787	0.288	0.288	-53.6255	-53.6255
7	8.1435	0.0149	0.1215	0.1215	-64.4703	-64.4703
8	9.272	-0.027	0.25	0.25	-73.9181	-73.9181
9	8.174	0.092	0.752	1.498	-77.0626	-76.4265
10	7.7165	-0.0396	0.3055	0.3055	-66.2802	-66.2802

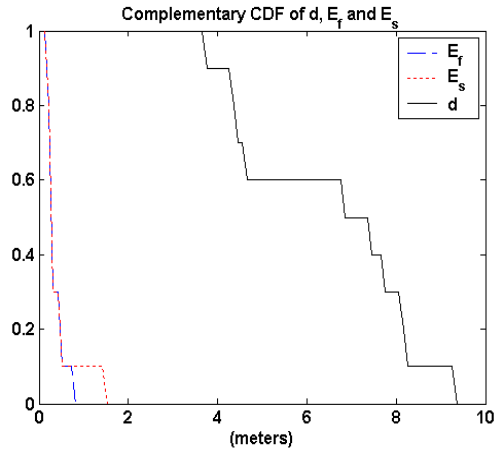

Figure 4-28 Complementary CDFs of the Actual Distance (solid black), the Absolute Value of Error Based on the TOA of the first path (dashed blue) and the Absolute Value of Error Based on the TOA of the Strongest Path (dotted red) in the Guest House (indoor to indoor)

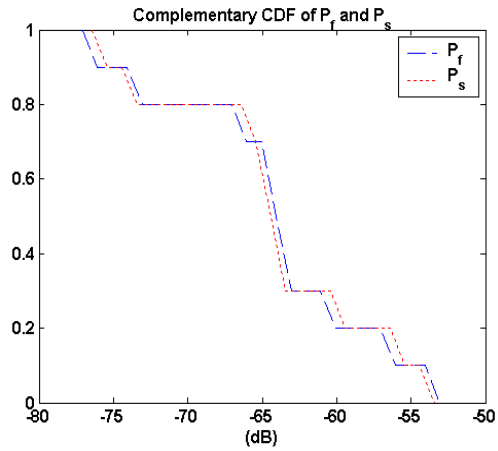

Figure 4-29 Complementary CDFs of the Relative Received Power of the First Path (dashed blue) and the Relative Received Power of the Strongest Path (dotted red) in the Guest House (indoor to indoor)

4.9.2 Outdoor to Indoor OLOS Measurements in the Guest House

As depicted in Fig.4-27 (a), 10 indoor to indoor OLOS measurements were conducted in the first floor of the Guest House. The actual distances are within 26 meters. Parameters, Δf and Δt were set to 1MHz and 0.5 ns, respectively. Table 17 shows the

measurement results. The great amount of error (E_f) that we observe for point 1 is due to an undetected path. (Refer to Appendix B for the channel profile.) Fig. 4-.30 compares the complementary CDF of error with the actual distance. Distance errors based on the TOA of the first path and the strongest path are within 6.6 meters. Here, $\overline{\mathbf{E}_f} =$ 1.5040 meters and $\mathbf{Var}(\mathbf{E}_f)$=4.0947 meters while, $\overline{\mathbf{E}_s} =$ 2.6290 meters and $\mathbf{Var}(\mathbf{E}_s)$=6.6309 meters. Fig 4-30 shows the complementary CDFs of relative received power of the first path and the strongest path. In this case, path losses of the first path and the strongest path are between 73 dB and 93 dB.

Table 17 Measurement Results in the Guest House (outdoor to indoor)

Points	d (meters)	E_n	E_f (meters)	E_s (meters)	P_f (dB)	P_s (dB)
1	25.742	-0.2556	6.58	6.58	-90.8854	-90.8854
2	24.8575	-0.0287	0.7145	4.1645	-90.8454	-89.5303
3	20.7095	-0.0175	0.3625	0.3625	-90.8008	-90.8008
4	17.5985	-0.1889	3.3235	3.3235	-84.4714	-84.4714
5	11.7425	-0.1175	1.3795	4.8295	-81.77	-80.3467
6	15.616	-0.0036	0.056	0.056	-79.8442	-79.8442
7	11.712	0.0205	0.24	0.24	-74.1006	-74.1006
8	12.688	-0.0224	0.284	0.284	-72.0208	-72.0208
9	14.518	-0.0485	0.704	0.704	-72.3745	-72.3745
10	16.226	-0.086	1.396	5.746	-92.6575	-89.1246

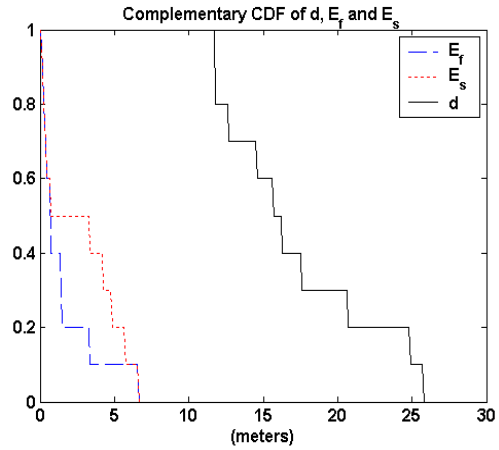

Figure 4-30 Complementary CDFs of the Actual Distance (solid black), the Absolute Value of Error Based on the TOA of the first path (dashed blue) and the Absolute Value of Error Based on the TOA of the Strongest Path (dotted red) in the Guest House (outdoor to indoor)

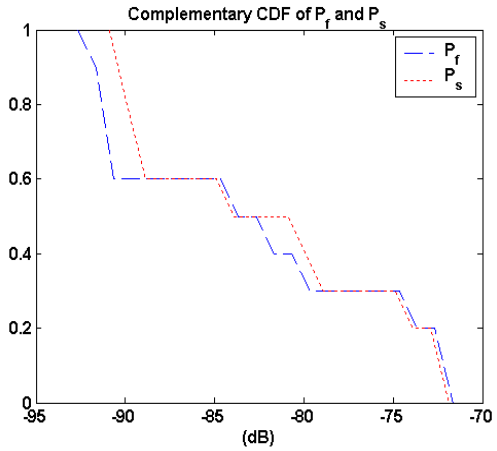

Figure 4-31 Complementary CDFs of the Relative Received Power of First Path (dashed blue) and the Relative Received Power of the Strongest Path (dotted red) in the Guest House (outdoor to indoor)

4.9.3 Outdoor to floor OLOS Measurements in the Guest House

As depicted in Fig.4-27 (b), 10 indoor to indoor OLOS measurements were conducted in the second floor of the Guest House. The actual distances are within 28 meters. Parameters Δf and Δt were set to 1MHz and 0.5 ns, respectively. Table 18 shows the measurement results. The great amount of error (E_f) that we observe for points 1,2 and 5 is due to an undetected path. (Refer to Appendix B for the channel profiles.) Fig. 4-32 compares the complementary CDF of error with the actual distance. Distance error based on the TOA of the first path is within 10 meters while distance error based on the TOA of the strongest path is within 27 meters. $\overline{\mathbf{E}}_f$ = 2.0621 meters and **Var**($\mathbf{E}_f$)=7.8246 meters. $\overline{\mathbf{E}}_s$ = 8.4047 meters and **Var**($\mathbf{E}_s$)=62.5752 meters. Fig 4-30 shows the complementary CDFs of relative received power of the first path and the strongest path. In this case, path losses of first path and strongest path are between 74 dB and 100 dB.

Table 18 Measurement Results in the Guest House (outdoor to floor)

Points	d (meters)	E_n	E_f (meters)	E_s (meters)	P_f (dB)	P_s (dB)
1	22.4175	-0.1474	3.3045	27.0045	-99.7021	-98.2415
2	27.206	-0.3369	9.166	9.166	-87.5189	-87.5189
3	21.106	0.0016	0.034	11.816	-95.8509	-81.3808
4	19.8555	-0.0008	0.0165	7.3665	-95.66	-95.1474
5	22.1125	-0.1564	3.4595	12.4595	-94.5386	-85.3802
6	17.5375	-0.0989	1.7345	1.7345	-85.3815	-85.3815
7	15.4635	-0.0329	0.5085	0.5085	-79.391	-79.391
8	13.3895	-0.1145	1.5325	4.0825	-77.3748	-76.814
9	12.2	0.0228	0.278	9.322	-81.3375	-75.0206
10	12.5355	-0.0468	0.5865	0.5865	-74.8114	-74.8114

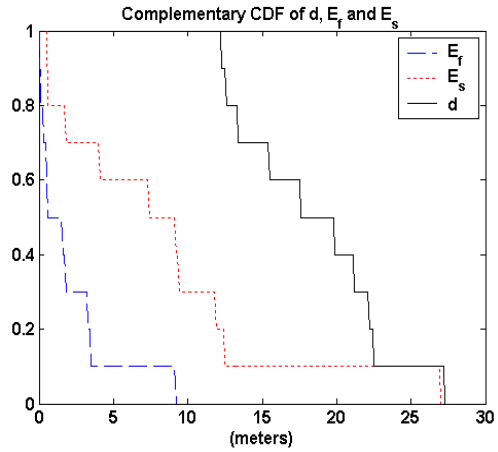

Figure 4-32 Complementary CDFs of the Actual Distance (solid black), the Absolute Value of Error Based on the TOA of the first path (dashed blue) and the Absolute Value of Error Based on the TOA of the Strongest Path (dotted red) in the Guest House (outdoor to floor)

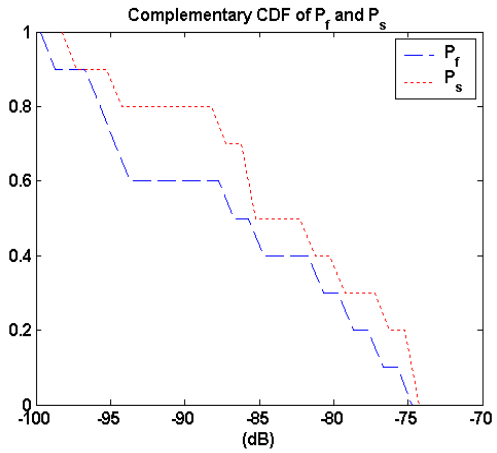

Figure 4-33 Complementary CDFs of the Relative Received Power of the First Path (dashed blue) and the Relative Received Power of the Strongest Path (dotted red) in the Guest House (outdoor to floor)

4.10 OLOS measurements in Norton Company

A general description of the Norton Company measurement site was given in section 4.7 .Two different scenarios are considered here: indoor to indoor and outdoor to indoor. For the first scenario, indoor to indoor, both transmitter and receiver were placed in the first floor of the Norton Company. Among 15 measurements that were conducted as indoor to indoor scenario, 5 of them represented OLOS scenarios. The second measurement scenario, which represents outdoor to indoor case, was conducted by placing the transmitter outside of the building and moving the receiver in the first floor. Fig. 4-34 represents the schematic for these two cases. In the following sections we provide the statistics of the measurement results.

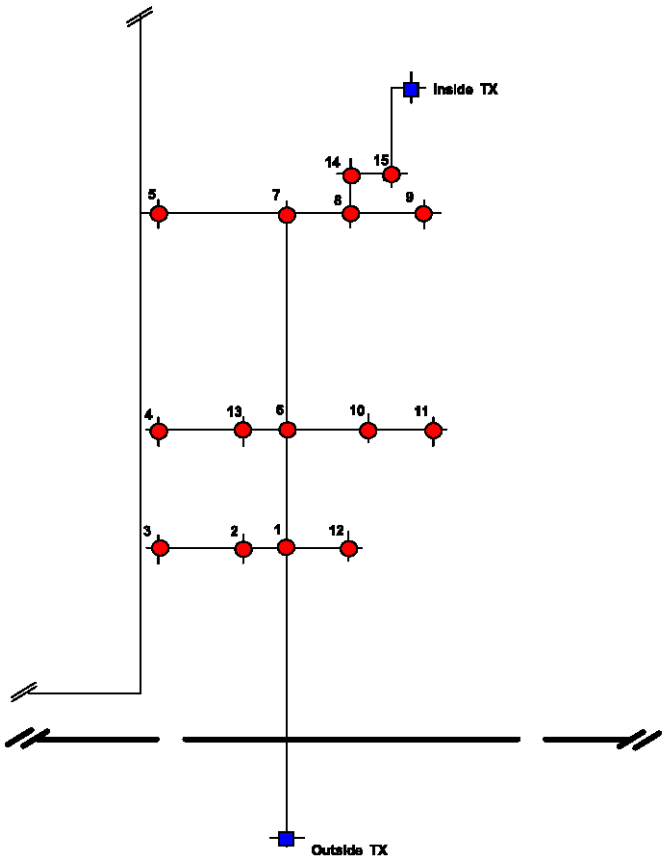

Figure 4-34 Schematic of Measurement Site in Norton Company (indoor to indoor and outdoor to indoor)

4.10.1 Indoor to Indoor OLOS Measurements in Norton Company

As depicted in Fig.4-34, 5 indoor to indoor OLOS measurements were conducted in the first floor of the Norton Company site. The actual distances are within 35 meters. Parameters Δf and Δt were set to 500 KHz and 0.5 ns, respectively. Table 19 shows the measurement results. Figure 4-35 compares the complementary CDF of error with the actual distance. Distance error based on the TOA of the first path is within 1 meter and distance error based on the TOA of the strongest path is 26 meters. Here, $\overline{\mathbf{E}}_f = 0.5727$ meters and $\mathbf{Var}(\mathbf{E}_f)=0.1184$ meters, while $\overline{\mathbf{E}}_s = 8.4573$ meters and $\mathbf{Var}(\mathbf{E}_s)=97.1483$ meters. This set of measurements clearly shows the difference between the accuracy

achieved by detecting the first path and that achieved by detecting the strongest path in OLOS scenarios. In fact, in order to detect the first path, the positioning system should be able to isolate the first path from the others and also have a large dynamic range to sense the first path. Fig 4-36 shows the complementary CDFs of relative received power of the first path and the strongest path. In this case path loss of the first path is between 75dB and 86 dB and the path loss of the strongest path is between 70 dB and 76 dB.

Table 19 Measurement Results in Norton Company (indoor to indoor)

Points	d (meters)	E_n	E_f (meters)	E_s (meters)	P_f (dB)	P_s (dB)
1	34.77	0.025	0.87	2.28	-83.017	-72.6899
4	30.5	0.0184	0.56	9.34	-85.7557	-75.9941
5	20.4655	0.0032	0.0655	25.2845	-75.6007	-74.0375
6	26.047	0.0175	0.457	2.693	-84.7635	-70.0916
11	24.461	0.0372	0.911	2.689	-87.1393	-70.0184

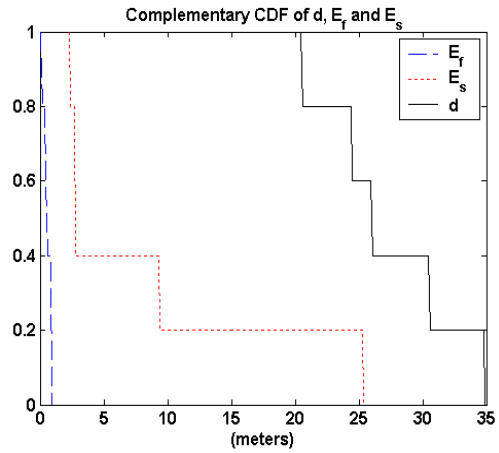

Figure 4-35 Complementary CDFs of the Actual Distance (solid black), the Absolute Value of Error Based on the TOA of the first path (dashed blue) and the Absolute Value of Error Based on the TOA of the Strongest Path (dotted red) in Norton Company (indoor to indoor)

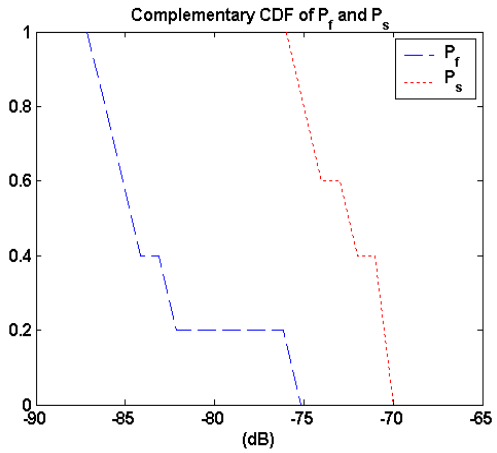

Figure 4-36 Complementary CDFs of the Relative Received Power of the First Path (dashed blue) and the Relative Received Power of the Strongest Path (dotted red) in Norton Company (indoor to indoor)

4.10.2 Outdoor to Indoor OLOS Measurements in Norton Company

As depicted in Fig.4-34, 15 outdoor to indoor OLOS measurements were conducted in the first floor of the Norton Company site. The actual distances are within 50 meters. Parameters Δf and Δt were set to 500 KHz and 0.5 ns, respectively. Table 20 shows the measurement results. The great amount of error (E_f) that we observe for points 12 and 13 is due to an undetected direct path. (Refer to Appendix B for the channel profiles.) Fig.4-37 compares the complementary CDF of error with the actual distance. Distance error based on the TOA of the first path is within 28 meters and distance error based on the TOA of the strongest path is within 31 meters. Here, $\overline{\mathbf{E}}_f = 3.1493$ meters and $\mathbf{Var}(\mathbf{E}_f) = 50.4488$ meters, while $\overline{\mathbf{E}}_s = 15.7195$ meters and $\mathbf{Var}(\mathbf{E}_s) = 77.2483$ meters Fig. 4-38 shows the complementary CDFs of relative received power of the first path and the strongest path. In this case path loss of the first path is between 74dB and 99 dB and the path loss of the strongest path is between 72 dB and 90 dB.

Table 20 Measurement Results in Norton Company (outdoor to indoor)

Points	d (meters)	E_n	E_f (meters)	E_s (meters)	P_f (dB)	P_s (dB)
1	21.35	0.0543	1.16	15.19	-78.9264	-73.4248
2	21.5635	0.0498	1.0735	30.5765	-75.6809	-72.1667
3	23.241	0.0151	0.351	17.949	-74.7484	-68.6131
4	31.842	0.0173	0.552	18.198	-79.5074	-74.0993
5	46.6345	-0.0087	0.4055	19.0055	-85.1134	-79.7569
6	30.5	0.0528	1.61	22.84	-82.9443	-80.2957
7	45.75	0.0079	0.36	10.29	-95.0679	-88.0824
8	45.9635	0.006	0.2735	24.0265	-98.4066	-86.0557
9	46.97	0.0368	1.73	1.73	-85.1587	-85.1587
10	31.11	0.0617	1.92	1.92	-77.9011	-77.9011
11	32.2995	0.0591	1.9095	22.0905	-88.317	-84.0201
12	21.838	0.3365	7.348	15.602	-98.1053	-79.0026
13	30.6525	0.9139	28.0125	4.5375	-93.3297	-75.5208
14	49.0135	0.0066	0.3235	7.6265	-95.7931	-89.9642
15	49.3795	-0.0043	0.2105	24.2105	-90.676	-85.6185

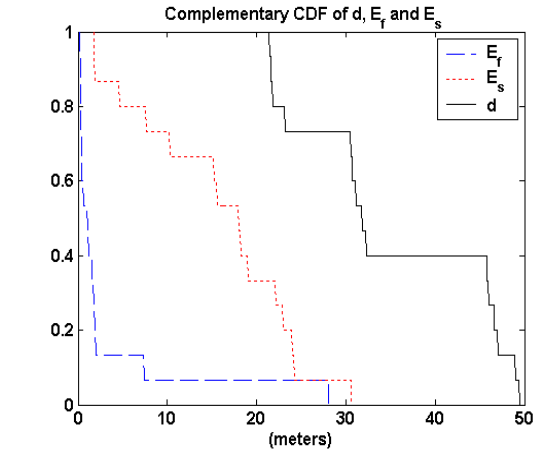

Figure 4-37 Complementary CDFs of the Actual Distance (solid black), the Absolute Value of Error Based on the TOA of the first path (dashed blue) and the Absolute Value of Error Based on the TOA of the Strongest Path (dotted red) in Norton Company (outdoor to indoor)

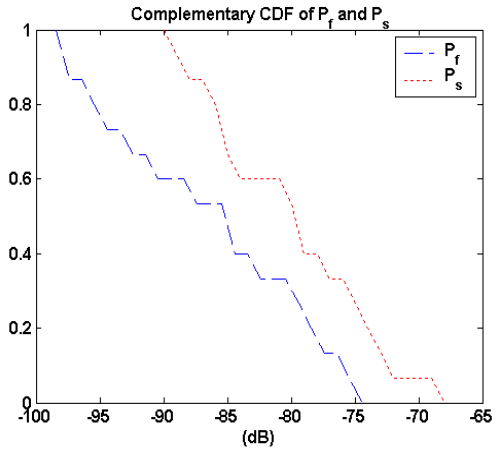

Figure 4-38 Complementary CDFs of the Relative Received Power of the First Path (dashed blue) and the Relative Received Power of the Strongest Path (dotted red) in Norton Company (outdoor to indoor)

4.11 Comparative Performance in LOS and OLOS Environments

Here, we combine all the LOS measurements in one group and all the OLOS measurements in another group. We compare the behavior of LOS vs. OLOS with respect to the absolute value of distance error based on the estimation of the TOA of the first path and the strongest path. Fig. 4-39 illustrates the complementary CDFs of distance error for LOS and OLOS based on estimation of the TOA of the first path. The distance error in LOS scenario is less than 2.5 meters while for the OLOS scenario it can reach up to 28 meters. Also the mean and variance of distance error for LOS scenario are $\overline{\mathbf{E}_f}$=0.33 and $\mathbf{Var}(\mathbf{E}_f)$=0.11 meters, respectively while for OLOS case the mean and variance of distance error are $\overline{\mathbf{E}_f}$ = 1.90 and $\mathbf{Var}(\mathbf{E}_f)$=12.67 meters, respectively.

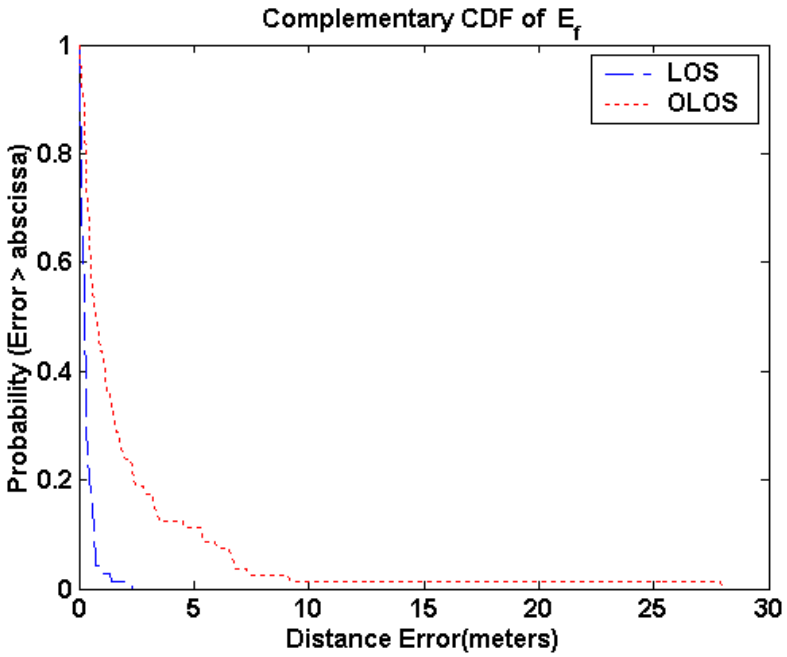

Figure 4-39 Comparison of Complementary CDFs of the Distance Error Based on the TOA of the First Path for LOS (dashed blue) and OLOS (dotted red)

Fig. 4-40 illustrates the complementary CDF of distance error for LOS and OLOS based on estimation of the TOA of the strongest path. The distance error in LOS scenario is less than 10 meters while for OLOS scenario it can reach up to 31 meters. Also, the mean and variance of distance error for the LOS scenario are $\overline{\mathbf{E}}_s$=0.70 and **Var**($\mathbf{E}_s$)=2.21 meters, respectively while for the OLOS case the mean and variance of distance error are $\overline{\mathbf{E}}_s$=7.78 and **Var**($\mathbf{E}_s$)=63.34 meters, respectively. By comparing the results illustrated in Fig 4.39 and Fig 4.40 we see that estimation based on the TOA of the first path gives better accuracy in both LOS and OLOS scenarios. In addition to that, the results associated to the LOS case are very close in both figures. In fact, the first path is always the strongest path in LOS scenarios except for the few measurement cases in which the antenna pattern changes due to surrounding objects such as metallic objects.

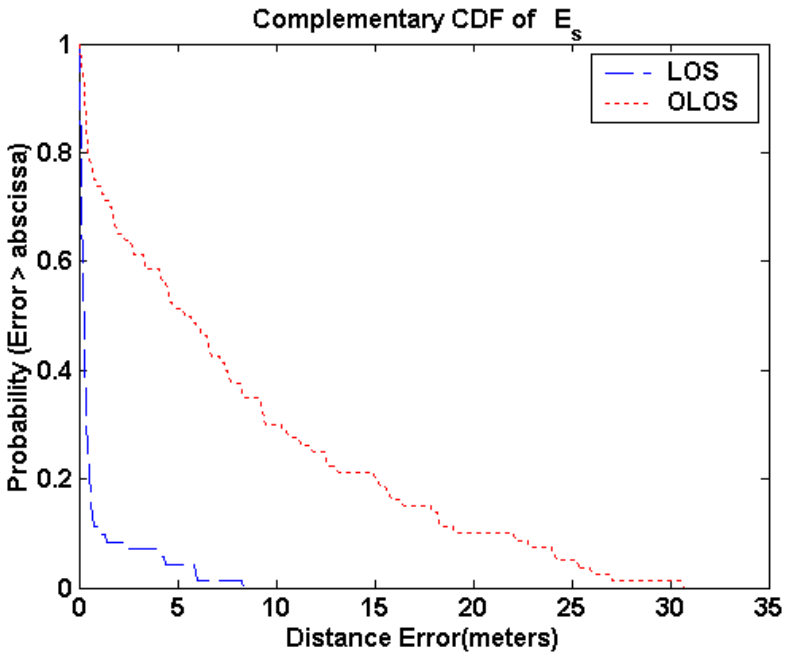

Figure 4-40 Comparison of Complementary CDF of the Distance Error Based on the TOA of the Strongest Path for LOS (dashed blue) and OLOS (dotted red)

In order to investigate the effect of multipath in OLOS cases we divide the OLOS scenarios into two categories. The first category contains all the UDP cases and the second one contains the remaining OLOS cases. We refer to the cases in the second category as the detected direct path (DDP). In fact the DDP category is the union of the following three scenarios:

1- The first path is detected and the first path is the strongest path.

2- The first path is detected but the first path in not the strongest path

3- Detected TOA of the first path corresponds to a combination of the TOAs of the DLOS path and the first other paths (NDDP).

Fig. 4-41 illustrates the complementary CDFs of distance error for LOS, DDP and UDP cases based on estimation of the TOA of the first path. The distance error in LOS

scenario is less than 2.5 meters while for DDP and UDP scenarios it can reach up to 5.5 and 28 meters, respectively. Also, the mean and variance of distance error for DDP scenario are $\overline{\mathbf{E}}_f$=0.9431 and $\mathbf{Var}(\mathbf{E}_f)$=0.9385 meters, respectively while for UDP case the mean and variance of distance error are $\overline{\mathbf{E}}_f = 7.9371$ and $\mathbf{Var}(\mathbf{E}_f)$=47.2678 meters, respectively. We observe that the behavior of DDP cases are relatively close to the behavior of LOS cases and the major cause of limiting the ranging accuracy of OLOS scenarios are in fact UDP cases. Fig. 4-42 illustrates the complementary CDFs of distance error for LOS, DDP and UDP cases based on estimation of the TOA of the strongest path. The distance error in LOS scenario is less than 10 meters while for DDP and UDP scenarios it can reach up to 31 and 27 meters, respectively. Also, the mean and variance of distance error for DDP scenario are $\overline{\mathbf{E}}_f$=6.94 and $\mathbf{Var}(\mathbf{E}_f)$=60.01 meters, respectively while for UDP case the mean and variance of distance error are $\overline{\mathbf{E}}_f = 13.03$ and $\mathbf{Var}(\mathbf{E}_f)$=57.04 meters, respectively. Again we see that the performance of OLOS scenarios improves as we exclude the UDP cases from them.

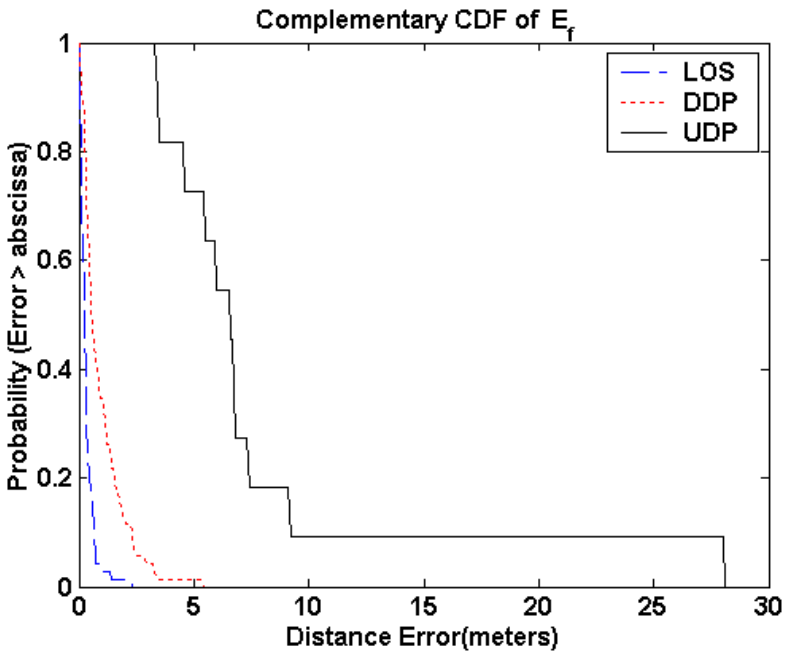

Figure 4-41 Comparison of Complementary CDFs of Distance Error Based on the TOA of the First Path for LOS (dashed blue), DDP (dotted red) and UDP (solid black)

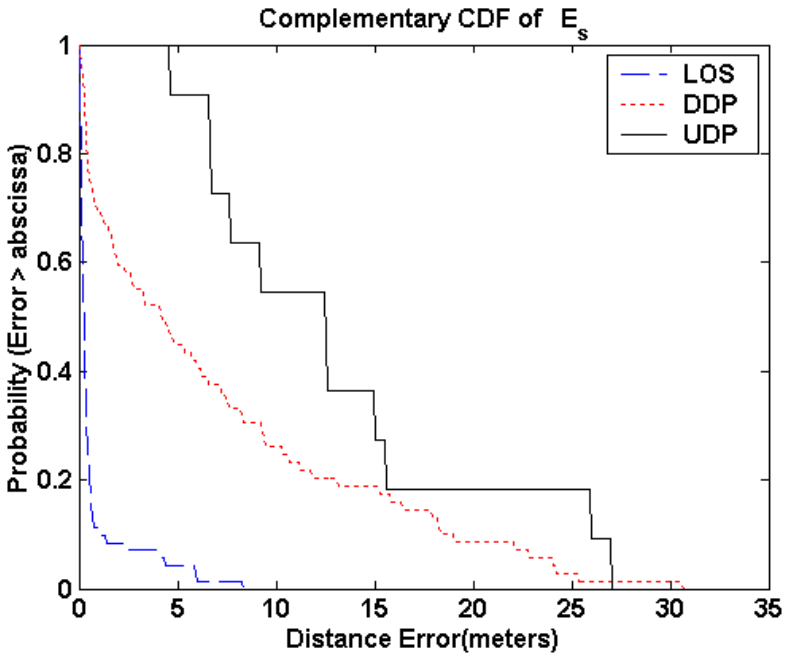

Figure 4-42 Comparison of Complementary CDFs of the Distance Error Based on the TOA of the Strongest Path for LOS (dashed blue), DDP (dotted red) and UDP (solid black)

4.12 Comparison of Distance Error with Gaussian Model

As described in Chapter 1, in order to evaluate the performance of indoor geolocation systems, new modeling is required. One of the recent models that has been developed by Alavi [10], suggests that normalized distance error for LOS scenario follows a Gaussian distribution with zero mean. The variance of the distribution depends on the environmental characteristics and the bandwidth.

In order to compare the measurement results with the model, we first generated 72 (the same number as LOS measurements) random points using a Gaussian distribution with the same mean and variance of the normalized error of the measurement results. Then we calculated the distance error (E_f) of the measurement results and the generated points from (4.1) and compared the complementary CDFs of distance error of the measurements and the generated points (Fig 4-43).

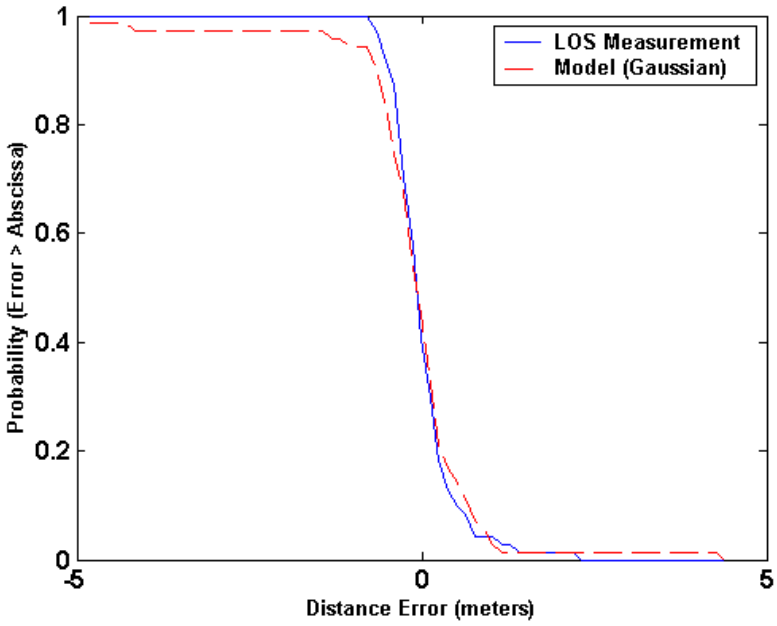

Figure 4-43 Comparison Between Complementary CDFs of the Distance Error for LOS Measurements and the Model

The criterion for the comparison is the average horizontal distance between the two curves, which we refer to as the fitting error. The fitting error between the two curves in Fig. 4-43 is 0.2323 meters, which shows that the model fits very well with the results.

Next, we repeat the same procedure with OLOS measurements. As shown in Fig. 4-44, the model is not very close to actual measurements and the fitting error is relatively large (1.9851 meters). But if we exclude the UDP cases from the OLOS measurements (as shown in Fig. 4-45) and repeat the procedure described above, we see that the model comes closer to the results of DDP measurements. In fact, the fitting error reduces from 1.9851 meters to1.0573 meters.

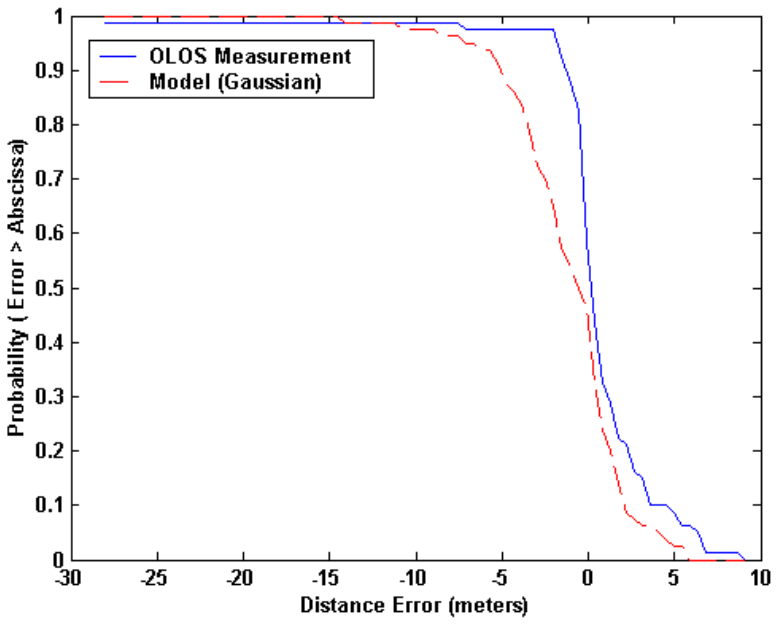

Figure 4-44 Comparison Between Complementary CDFs of the Distance Error for OLOS Measurements and the Model

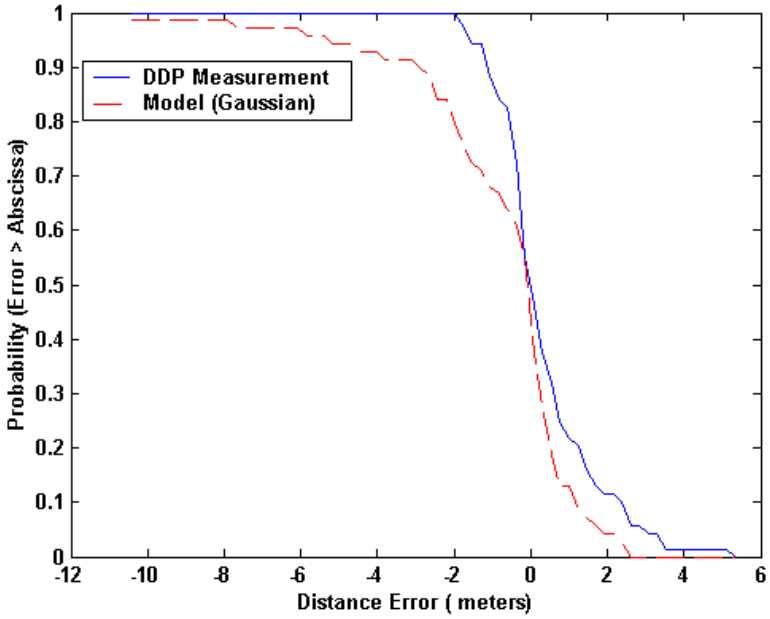

Figure 4-45 Comparison Between Complementary CDFs of the Distance Error for DDP Measurements and the Model

Chapter 5 Summary and Future Work

5.1 Summary

This work started with an analysis of the effect upon TOA measurement accuracy due to: sampling period in the frequency domain, sampling period in the time domain and the windowing filter used before transformation to the time domain. Then we presented some statistics for LOS and OLOS measurements in indoor environments to compare the characteristics of the measured TOA in these two important scenarios for indoor geolocation applications. Finally, we compared the measurement results with the ray tracing based model that had been developed previously by Alavi [10].

In Chapter 3, we first analyzed the effect of the sampling period in the frequency domain on the ranging accuracy. We showed that as long as the sampling period in the frequency domain is below a certain threshold, the distance error is relatively insensitive to changes in the sampling period in the frequency domain. Next, we analyzed the effect of sampling in the time domain and we found that distance error is lower bounded with the error due to quantization in time for a fixed multipath effect. We then compared the effect of four different filters (Rectangular, Bartlett, Hanning and Hamming windows) on the overall accuracy of the distance estimate and showed that the Hanning window provides the best performance among them.

In Chapter 4, we analyzed the results of measurements that were conducted in different sites. The statistics of distance error and relative received power were shown for each site. Then we compared the behavior of LOS and OLOS scenarios and observed a major difference in the behavior of these two cases due to multipath. According to our measurements, the distance error based on the TOA of the first path, E_f, was less than 2.5

meters in LOS cases while error could reach up to 28 meters for OLOS cases. Furthermore, we divided the OLOS cases into UDP and DDP categories. We observed that E_f is as big as 5.5 and 28 meters in DDP and UDP cases, respectively. Table 21 shows the mean and the variance of distance error in the four different scenarios.

Table 21 Mean and Variance of Distance Error for Different Scenarios

Case	Mean (E_f) (meters)	Var(E_f) (meters)
LOS	0.33	0.11
OLOS	1.90	12.67
DDP	0.94	0.93
UDP	7.93	47.26

We concluded that the main source of error in ranging accuracy for OLOS cases comes from the UDP subclass. In the final part of Chapter 4, we compared the results of measurements and the ray tracing based model that had been developed previously for indoor geolocation. The criterion for the comparison was the fitting error between complementary CDFs of the distance error generated from the model and the measurements. Table 22 shows the results of the comparison between the model and the measurements. We concluded that the model fits very well with the LOS measurements. We also observed that as we exclude the UDP subclass from the OLOS cases the results of the remaining OLOS measurements, DDP subclass, are relatively close to the model.

Table 22 Comparisons between the Measurement Results and the Model

Case	Fitting Error (meters)
Model vs. LOS Measurements	0.23
Model vs. OLOS Measurements	1.98
Model vs. DDP Measurements	1.05

5.2 Future work

For the future, there are several aspects of the indoor geolocation that can be investigated further. The effect of bandwidth on the accuracy of ranging should be studied. Developing a more advanced algorithm for detecting the first path is another worthwhile area of investigation. The behavior of the channel for higher and lower frequencies as well as other environments need further study as well. Also, new models should be developed to more accurately represent the behavior of OLOS scenarios.

Appendix A

Frequency and Time Response of the Radio Channel in Point 7, Generated with Different Sampling Periods in the Frequency Domain, Δf .

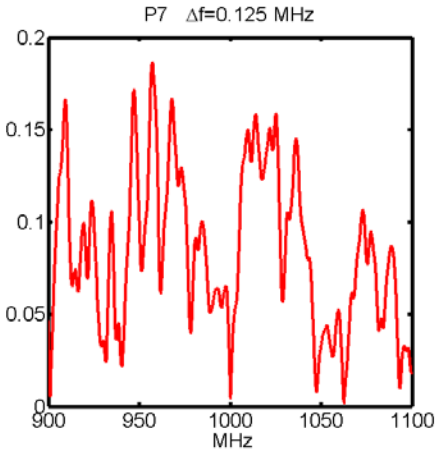

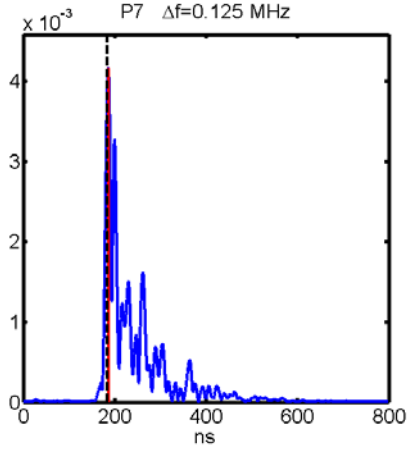

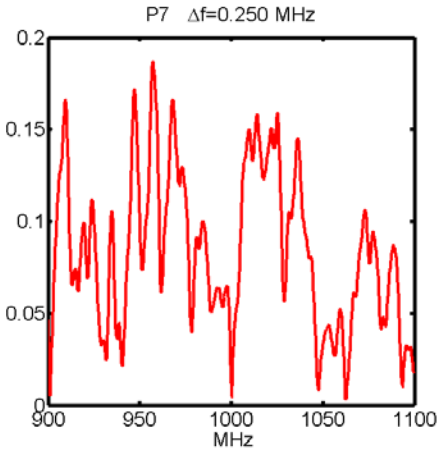

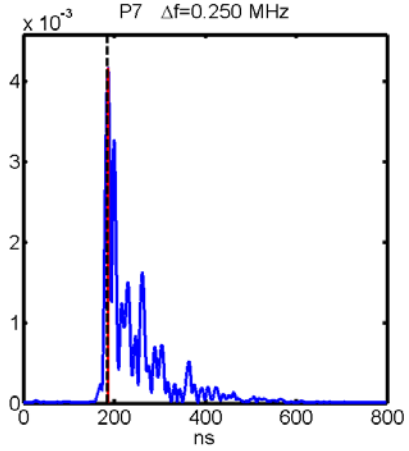

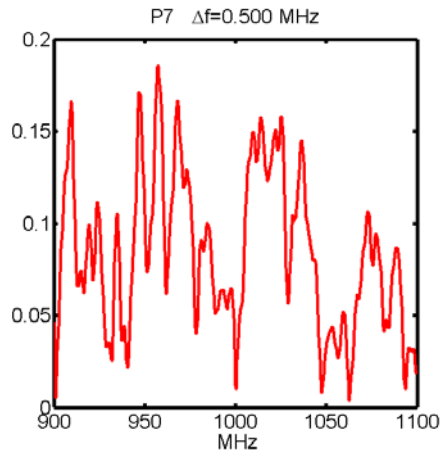
P7 Δf=0.500 MHz
0.2
0.15
0.1
0.05
0
900
950
1000
1050
1100
MHz

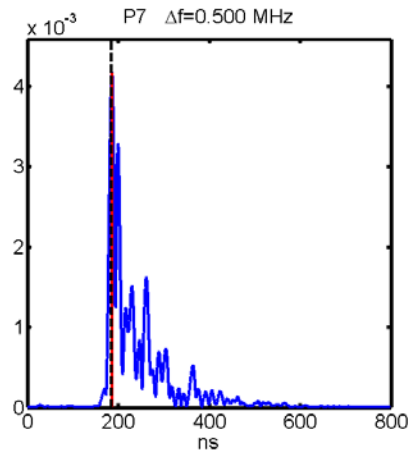
x 10^-3
P7 Δf=0.500 MHz
4
3
2
1
0
0
200
400
600
800
ns

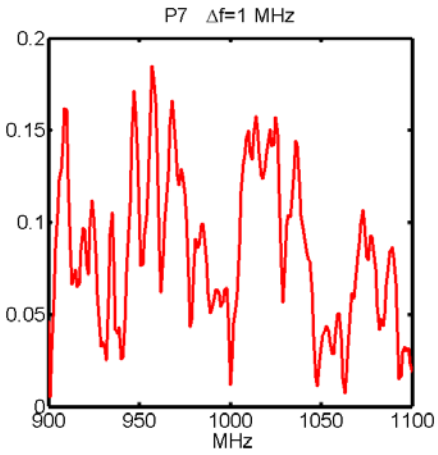
P7 Δf=1 MHz
0.2
0.15
0.1
0.05
0
900
950
1000
1050
1100
MHz

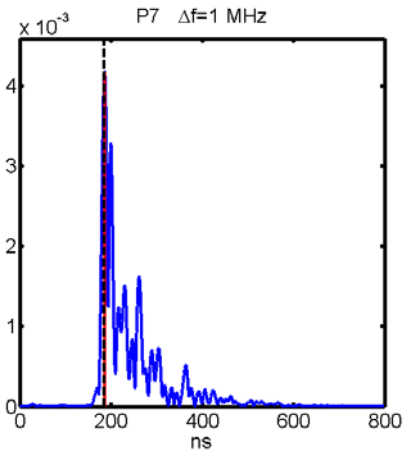
x 10^-3
P7 Δf=1 MHz
4
3
2
1
0
0
200
400
600
800
ns

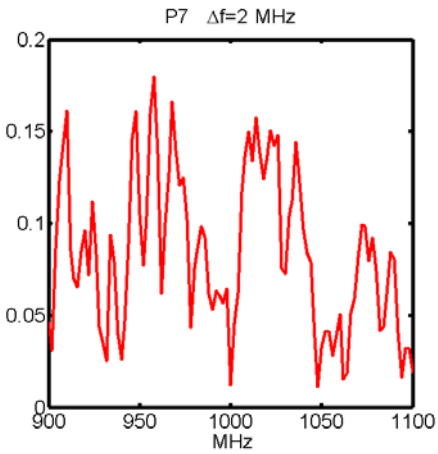
P7 Δf=2 MHz
0.2
0.15
0.1
0.05
0
900
950
1000
1050
1100
MHz

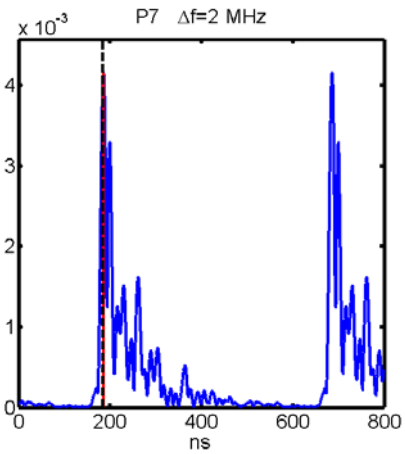
x 10^-3
P7 Δf=2 MHz
4
3
2
1
0
0
200
400
600
800
ns

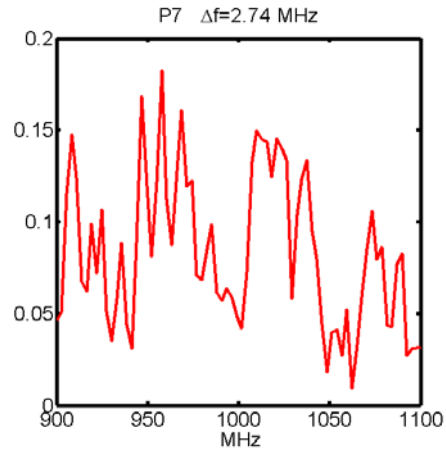
P7 Δf=2.74 MHz
0.2
0.15
0.1
0.05
0
900
950
1000
1050
1100
MHz

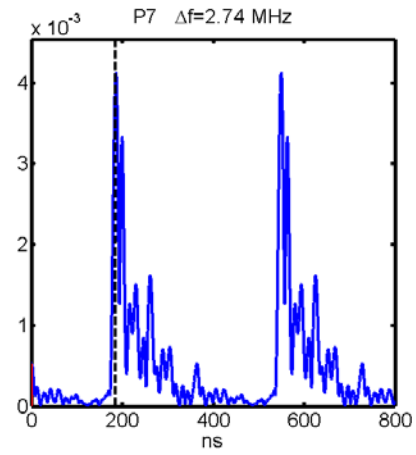
x 10^-3
P7 Δf=2.74 MHz
4
3
2
1
0
0
200
400
600
800
ns

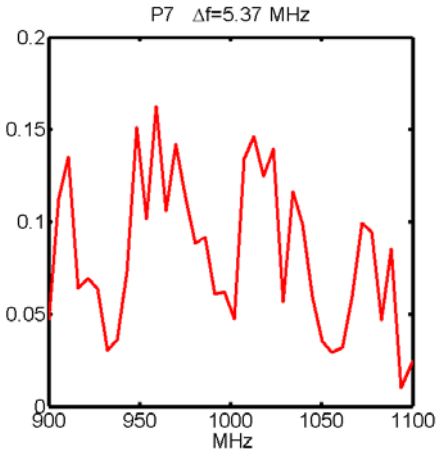
P7 Δf=5.37 MHz
0.2
0.15
0.1
0.05
0
900
950
1000
1050
1100
MHz

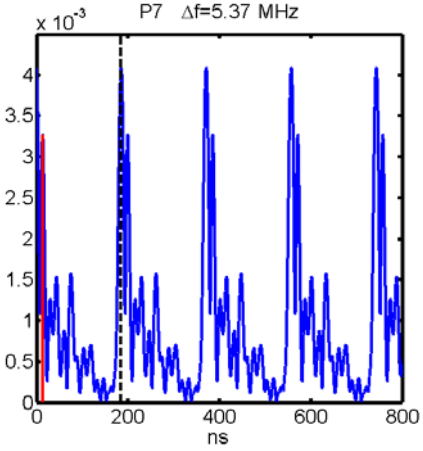
x 10^-3
P7 Δf=5.37 MHz
4
3.5
3
2.5
2
1.5
1
0.5
0
0
200
400
600
800
ns

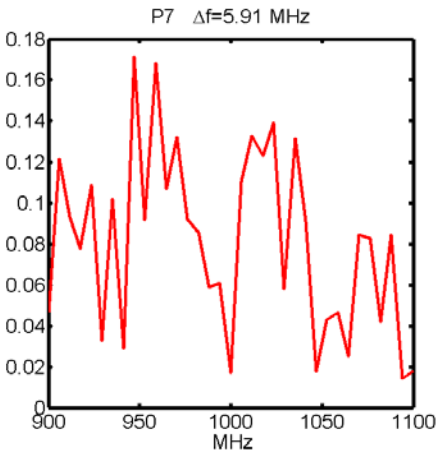
P7 Δf=5.91 MHz
0.18
0.16
0.14
0.12
0.1
0.08
0.06
0.04
0.02
0
900
950
1000
1050
1100
MHz

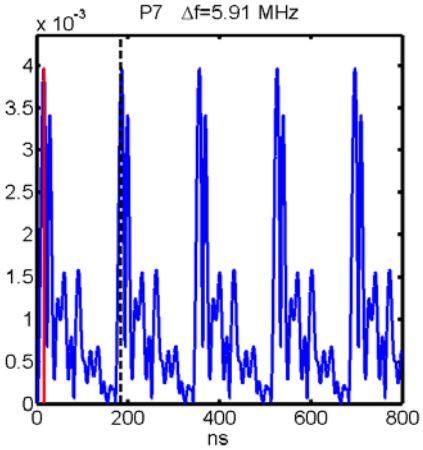
x 10^-3
P7 Δf=5.91 MHz
4
3.5
3
2.5
2
1.5
1
0.5
0
0
200
400
600
800
ns

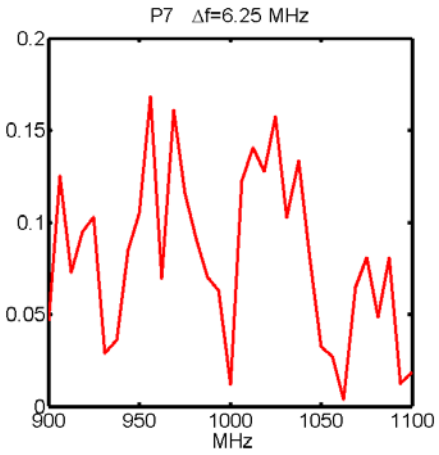
P7 Δf=6.25 MHz
0.2
0.15
0.1
0.05
0
900
950
1000
1050
1100
MHz

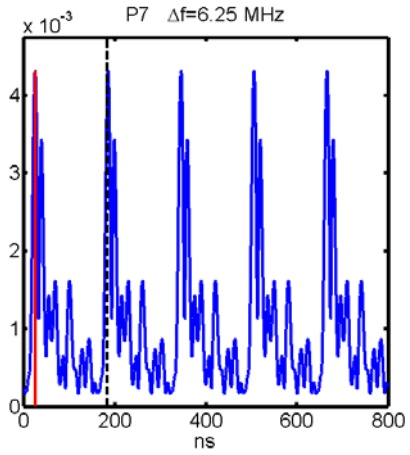
x 10^-3
P7 Δf=6.25 MHz
4
3
2
1
0
0
200
400
600
800
ns

Appendix B

Channel Impulse Response of OLOS Measurements with Undetected Direct Path (UDP)

Since each profile is independent, it was necessary to adopt a good naming convention, which could satisfy the diversity of sites, positions and conditions.

Each profile name can be decomposed as follows:

Site Position number Condition

where each component can take on the following strings:

Table 23 Measurement database filename strings description

Site	Position	Condition
"h" for House	1" through "10" for House	"ii" for indoor-to-indoor
"f" for Fuller	1" through "10" for Fuller	"oi" for outdoor-to-indoor
"n" for Norton	1" through "15" for Norton	"of" for outdoor-to-floor

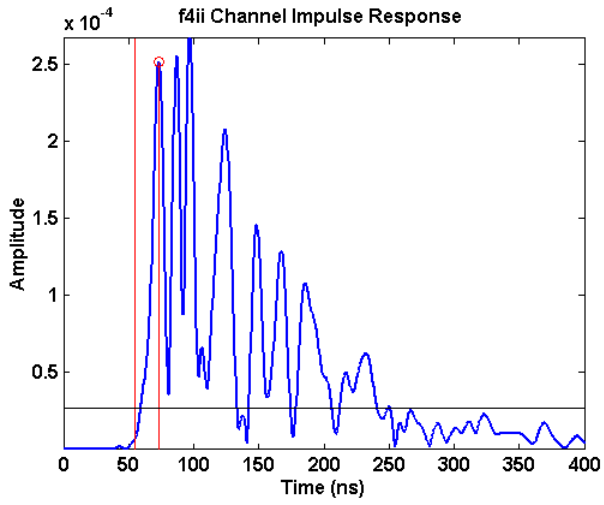

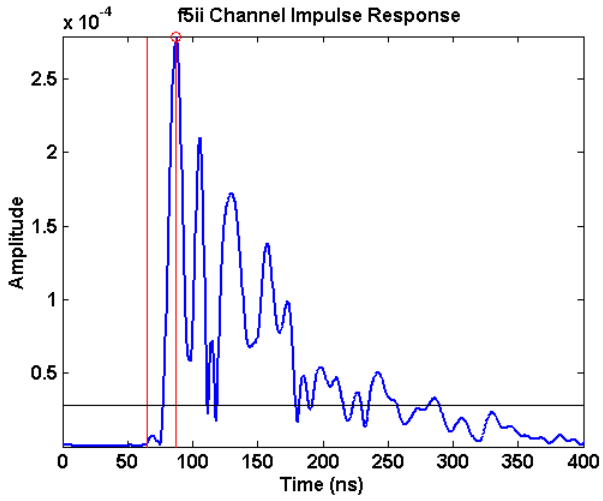
f5ii Channel Impulse Response
x 10^-4
Amplitude
Time (ns)

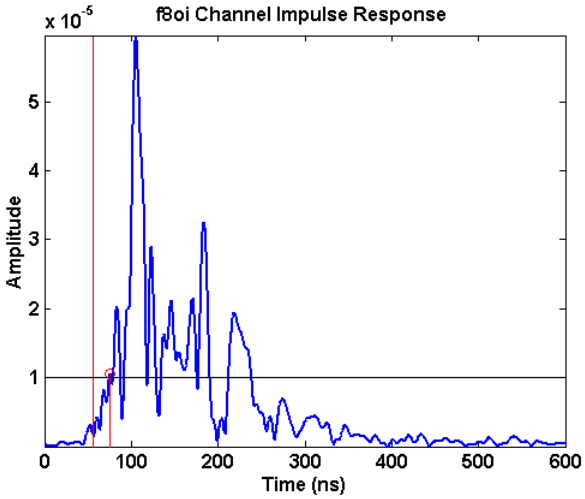
f8oi Channel Impulse Response
x 10^-5
Amplitude
Time (ns)

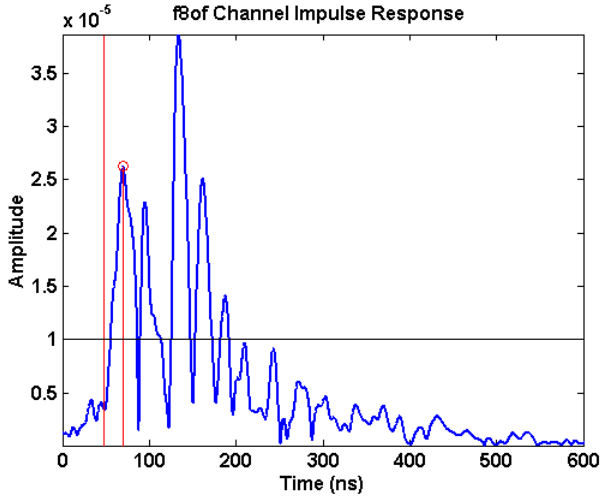
f8of Channel Impulse Response
x 10^-5
Amplitude
Time (ns)

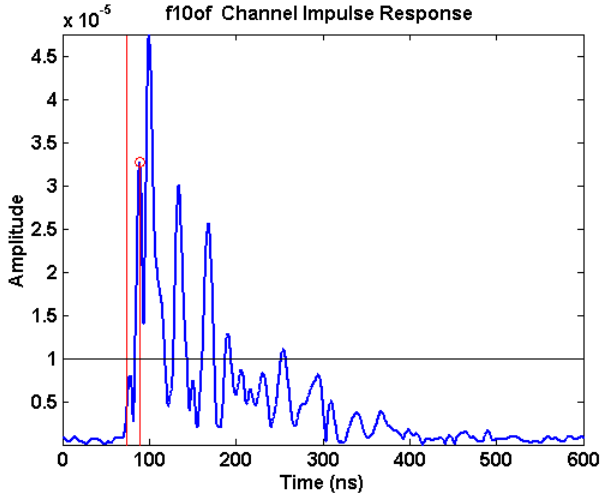
f10of Channel Impulse Response
x 10^-5
Amplitude
Time (ns)

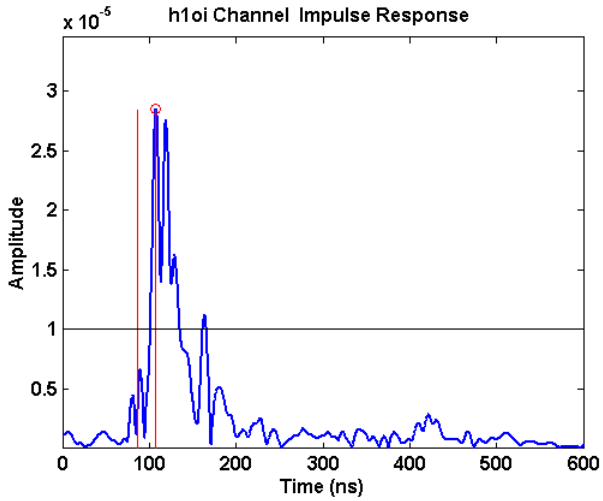
h1oi Channel Impulse Response
x 10^-5
Amplitude
Time (ns)

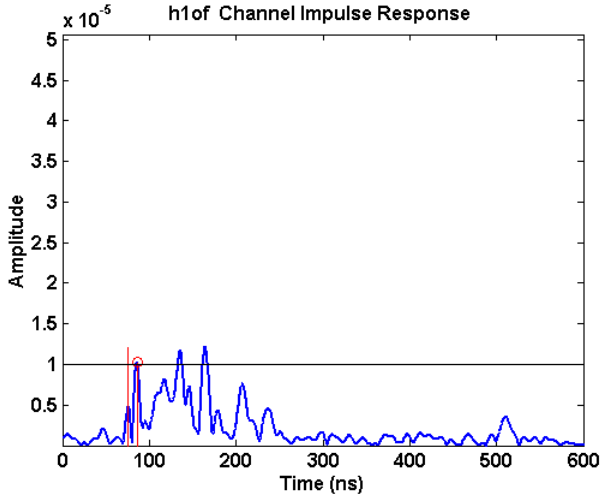
h1of Channel Impulse Response
x 10^-5
Amplitude
Time (ns)

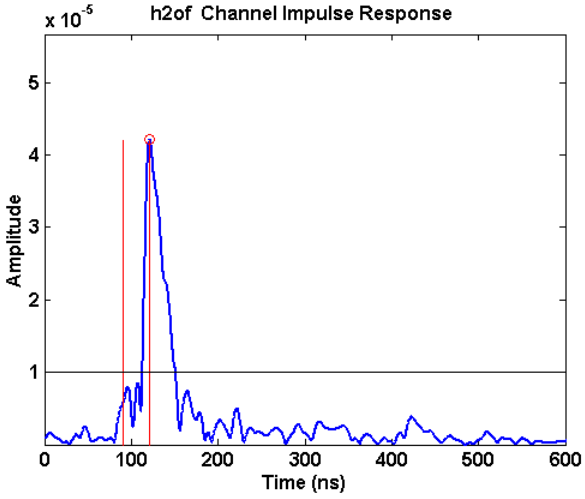
h2of Channel Impulse Response
x 10^-5
Amplitude
Time (ns)

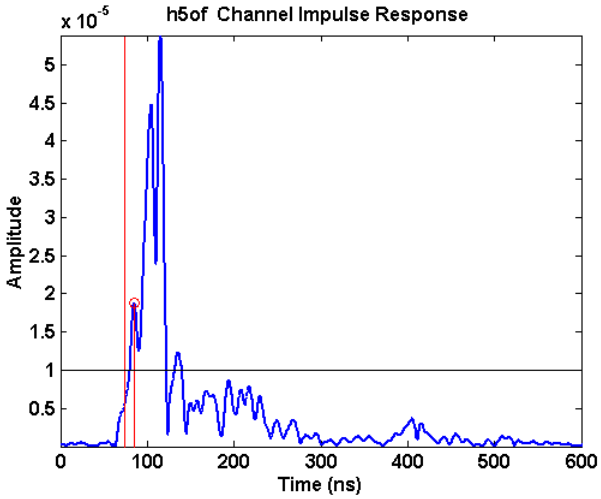
h5of Channel Impulse Response
x 10^-5
Amplitude
Time (ns)

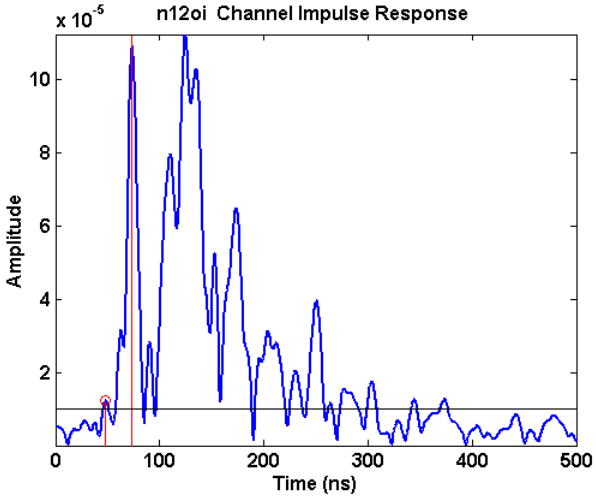
n12oi Channel Impulse Response
x 10^-5
Amplitude
Time (ns)

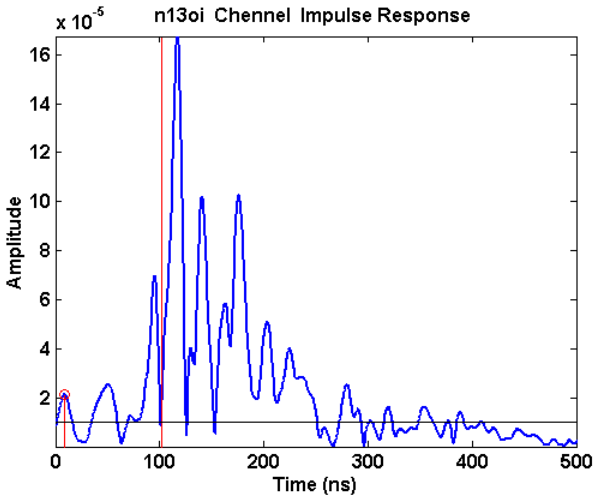
x 10^-5
n13oi Chennel Impulse Response
Amplitude
Time (ns)
16
14
12
10
8
6
4
2
0
100
200
300
400
500

References

[1] K. Pahlavan and P. Krishnamurthy, "Principles of Wireless Networks", Prentice Hall PTR, 2002.

[2] K.Pahlavan, Xinrong Li and J.P. Makela, " Indoor Geolocation Science and Technology", IEEE Communication Magazine, vol.40, no.2, February 2002.

[3] J. Beneat, K. Pahlavan and P. Krishnamurthy, "Radio Channel Characterization for Geolocation at 1GHz, 500 MHz, 90 MHz and 60 MHz in SUO/SAS", MILCOM, November 1999.

[4] S.J. Howard and K. Pahlavan" Measurement and Analysis of the Indoor Radio Channel in the Frequency Domain "IEEE Trans. Instr. Meas., no 39,1990,pp.751-55

[5] J. Beneat, P. Krishnamurthy, M. Marku and K. Pahlavan, "Short Range Geolocation and Telecommunication Channel Measurement and Modeling at 1GHz, 500MHz, 90MHz and 60 MHz ", DARPA SUO SAS report, January 1999

[6] A.V. Oppenheim and R.W. Shafer, "Discrete –Time Signal Processing" Prentice-Hall, Inc., 1989,pp. 447-451.

[7] S.J. Howard "Frequency Domain Characteristics and Auto-Regressive Modeling of the Indoor Radio Channel" Ph.D. Dissertation 1991

[8] S. Tekinay, E. Chao, and R. Richton, "Performance benchmarking for wireless location systems," IEEE Communications Magazine, April 1998.

[9] K. Pahlavan and A. Levesque, "Wireless Information Networks", John Wiley and Sons, 1995.

[10] B. Alavi and K. Pahlavan " Modeling of The Distance Error for Indoor Geolocation, WCNC 2003